# The Roles of Constituent Minerals and Residual Bitumen in the Filtration of Alberta Oil Sands Tailings

by

Dong Wang

A thesis submitted in partial fulfillment of the requirements for the degree of

Doctor of Philosophy

in

Materials Engineering

Department of Chemical and Materials Engineering

University of Alberta

**Abstract**

The dewatering of Alberta oil sands tailings is one of the most challenging problems faced by the oil sands industry. Despite significant efforts in the past several decades, the industry still lacks viable technologies that can quickly dewater and reclaim the oil sands tailings and eliminate their environmental impact.

Pressure filtration of mine tailings has been gaining popularity in the past ten years or so due to the needs to quickly recycle process water and to eliminate the risks of impounding large volumes of unconsolidated wet tailings. However, despite its success in treating mine tailings, the pressure filtration of Alberta oil sands tailings is laden with low filtration rates, low filter cake solid contents, and high and uneconomical reagent dosages. It has been unclear why the Alberta oil sands tailings filtered so differently from typical mine tailings. The work reported in this thesis is the first such effort to address this issue to systematically investigate the roles of the constituent minerals and residual bitumen in the filtration of Alberta oil sands tailings.

Three different types of minerals, including non-clay minerals (rutile, quartz), non-swelling clays (kaolinite, illite), and swelling clays (illite–smectite, montmorillonite) were selected as model solids for the study. The dewatering of each mineral slurry was studied using filtration and capillary suction time measurements. It was found that the filtration did not depend on mineral particle size but rather, on the type of minerals. The presence of the swelling clays, even in small quantities, significantly affected the filterability of other minerals. It was thus deduced that swelling clays in the oil sands tailings were the main reason for the poor filterability. It was further revealed that the filtration behaviors of the different minerals could be explained through the concept of the "effective volume fraction of the solids", which accounts for the volume taken by the solid particles and their surrounding electrical double

layers. Swelling clays had a high effective solid volume fraction in the aqueous slurry due to their high specific surface areas. Any methods to lower their specific surface area and/or reduce their electrical double layer thickness could help improve filtration.

The residual bitumen in the Alberta oil sands tailings can be present in three different forms, i.e., the bulk free bitumen, the bitumen-in-water emulsion, and the bitumen adsorbed on mineral surfaces. The effects of the different forms of the residual bitumen were investigated in this work. It was found that the bulk bitumen and emulsified bitumen had negligible effects on the filtration of oil sands tailings, while the effects of the adsorbed bitumen were more complex.

To investigate the effect of adsorbed bitumen on filtration performance, the model minerals were treated in bitumen-toluene solutions at different bitumen concentrations. Bitumen-coated quartz was compared with silanized quartz to decouple the effects of surface hydrophobicity and adsorbed bitumen layer on filtration. It was found that the filtration rate of silanized quartz increased linearly with increasing contact angle. Similarly, when the minerals were treated at a low bitumen-in-toluene concentration, the contact angle and filtration rate of all tested minerals were increased. However, at high bitumen-in-toluene concentration, the filtration rates were reduced drastically despite the high contact angle. CHNS elemental analyses and X-ray photoelectron spectroscopy surface composition and depth profile analyses showed that the minerals had higher C, N, S contents and thicker and patchy bitumen layer when they were treated at higher bitumen-in-toluene concentration. It was hypothesized that under the pressure gradient during filtration, the thick and patchy bitumen coating layers could interpenetrate when the mineral particles were pressed together, to form an inter-locked film to close off the pores in the filter cakes. It was concluded that a thin layer of bitumen coating helped improve

filtration due to the induced hydrophobicity, but a thick and patchy bitumen coating impeded filtration.

The findings from this work, i.e., that the filtration of the Alberta oil sands tailings seemed to be controlled by the specific surface area and the thickness of the electrical double layer of the clay minerals, and by the thickness of the bitumen coating on the clay minerals, were expected to guide the development of suitable filtration treatment strategies for the Alberta oil sands tailings.

## Preface

The main contents of this thesis have been published or submitted to scientific and technical journals. Below is a statement of my contributions to co-authored papers.

Chapter 3 has been published as "Wang D, Tao H, Wang K, Tan X, Liu Q, 2022. The filterability of different types of minerals and the role of swelling clays in the filtration of oil sands tailings. Fuel. 316, 123395." I was responsible for designing and performing the experiments, analyzing the data, and writing the paper draft. Tao H contributed to the experiment design, data analysis and deeply involed in particle size and X-ray fluorescence experiments. Wang K and Tan X were involved in the experimental design. Liu Q was the supervisory author and contributed to experiment design, data interpretation, and manuscript editing and composition. All the authors contributed to the discussion and commented on the manuscript.

Chapter 4 has been submitted to Journal of Petroleum Science and Engineering as "Wang D, Tao H, Wang K, Tan X, Liu Q, 2022. The role of bitumen in the filtration of oil sands tailings." and is under review. I was responsible for designing and performing the experiments, analyzing the data, and writing the paper draft. Tao H contributed to experiment design, data analysis and was deeply involved in the pressure filtration experiments. Wang K and Tan X were involved in the experiment design. Liu Q was the supervisory author and contributed to experiment design, data interpretation, and manuscript editing and composition. All the authors contributed to the discussion and commented on the manuscript.

Chapter 5 has been published as “Wang D, Tao H, Wang DW, Wang K, Tan X, Liu Q, 2022. Effects of mineral surface silanization and bitumen coating on its filtration from an aqueous slurry. Fuel, 325, 124921.” I was responsible for designing and performing the experiments, analyzing the data, and writing the paper draft. Tao H, Wang K, Wang DW, and Tan X were involved in the experiment design. Liu Q was the supervisory author and contributed to experiment design, data interpretation, and manuscript editing and composition. All the authors contributed to the discussion and commented on the manuscript.

**Acknowledgments**

I would like to express my deepest gratitude to my supervisor Dr. Qi Liu and advisor Dr. Xiaoli Tan for their patient guidance throughout my PhD journey. Dr. Liu is knowledgeable, encouraging, considerate, and very responsible for students. Each time I encountered frustrations with my projects or experienced stressful moments in life, Dr. Liu's guidance and encouragement could always navigate me out of struggles. It is my luck and honor to have Dr. Liu as my supervisor. Dr. Liu shaped my attitude towards work and life. Dr. Tan provided not only solid help and suggestions with the lab work but also many valuable and sincere advice to my life, encouraging me, and guiding me when I was confused. Without Drs. Liu and Tan's kind and patient guidance, I would not be able to finish my PhD degree. I can never thank them enough for their great help. I really appreciated the free and enjoyable environment in Dr. Liu's group during my PhD study, which I will memorize for my whole life.

I am thankful to my supervisory committee members: Dr. Hongbo Zeng and Dr. Neda Nazemifard. Their suggestions and advice provide valuable information for this research.

Strong support was provided by the Institute for Oil Sands Innovation (IOSI) at the University of Alberta for my PhD project. Most of my research work was conducted in the IOSI laboratories. Special thanks go to Lisa Brandt, Brittany Mackinnon, Ni Yang for their technical support and training.

I must express my gratitude to my colleagues, Dr. Hongbiao Tao and Dr. Kaipeng Wang. Dr. Tao offered much assistance of this project and taught me a lot. Dr. Wang provided helpful discussions about the project. Thanks to my colleagues, Daowei Wang, Hanyu Zhang, Xuyang Liu, Xianfeng Sun, Menatalla Ahmed et al. for their support and encouragement during the

whole PhD journey. We stay together as a family. Thanks to my friends: Jinghan Cui, Yi Zhang, Yuanyuan Hong, Shuo Yang.

I would like to acknowledge the financial support from Imperial Oil Limited, Alberta Innovates, and Canada's Oil Sands Innovation Alliance (COSIA) through the Institute for Oil Sands Innovation (IOSI) (IOSI2017-04), and Natural Sciences and Engineering Research Council of Canada (NSERC CRDPJ532050-18). I appreciate the technical advice and discussion from Dr. Weibing Gan (Teck), Dr. Simon Yuan (Syncrude), Dr. Abu Junaid (CNRL), and Dr. Givemore Sakuhuni (Imperial Oil).

Finally, I would like to express my heartfelt thanks to my husband Rui Yang, my sister Jing Wang and other families for their endless support and love. Thank you for always standing behind me and letting me grow on my own path.

## Table of Contents

## List of Tables

## List of Figures

# CHAPTER 1 Introduction

## 1.1. Background

### 1.1.1. Alberta oil sands tailings

Alberta's oil sands deposit is the fourth-largest oil reserve on the Earth, containing more than 165 billion barrels of proven bitumen in the ground [1], and is a key driver of Canada's economy. The bitumen extraction from oil sands involves the use of warm water, followed by bitumen flotation. This hot water extraction operation was first proposed by Dr. Karl Clark in 1920s, which formed the basis of the current commercial warm-water technology to recover bitumen from the surface-mined oil sands [2]. One of the most difficult challenges in the efficient and responsible utilization of oil sands is the tailings produced from the warm-water extraction operations. In this process, a large volume of slow-settling tailings is produced and discharged to tailings ponds. In the first several months, the tailings separate into three distinct layers: the water released forms the top layer, which can be recycled back to the extraction process; the coarse sands settle quickly to the bottom; the middle layer of the tailings contains 20-30 wt% of fine solids, known as fluid fine tailings (FFT), which consist of clay, fine silt, coarse silt and fine sand particles suspended in water. After several years, this middle layer settles to form a stable, viscous, and gel-like suspension commonly called mature fine tailings (MFT). On average, approximately 2 barrels of MFT and 13 barrels of coarse tailings are generated to produce one barrel of bitumen [3]. By 2016 the accumulated MFT had reached about 800 million cubic meters in the tailings ponds, and the total area of tailings ponds had reached over 250 square kilometers [4]. Unlike conventional hard rock mining tailings, the Alberta oil sands tailings could take decades or even centuries to naturally dewater to be

reclaimed, and it is impossible to reclaim the oil sands tailings in a timely fashion to meet regulatory requirements without significant intervention.

### 1.1.2. Environmental impact of the oil sands tailings ponds

The tailings ponds contain the wastes of oil sands extraction and bitumen upgrading, which is a mixture of sand, silt, clay, water, hydrocarbons, and other contaminants [5]. Research revealed that the tailings ponds are seeping into local groundwater, and the leach chemicals from these ponds poison wildlife, harm the health of local communities, and pose the ever-growing threat of polluting the local water resources [5–8]. Furthermore, the emitted pollutants from the tailing ponds were reported to include carbon dioxide, volatile organic compounds, reduced sulfur compounds, and methane [9]. Those emissions were considered to associate with a wide range of human health concerns, such as eye irritation, respiratory symptoms, cough, and congestion [10,11]. Due to a lack of viable tailings dewatering technologies, the tailings problem is getting worse. The total volume of fluid tailings has now surpassed 1.73 trillion liters and continues to increase. The total public liability for tailings ponds cleanup cost was anticipated to be 60.5 billion [12]. Much more intensive research is needed to develop treatment technologies to reclaim the oil sands tailings to meet regulatory requirements.

### 1.1.3. Current technology of oil sands tailings treatment

The oil sands industry has examined a number of dewatering methods to accelerate the solid-liquid separation of the oil sands tailings over the last several decades. The composite tailings (CT) technology began to be used commercially in 2000 by Syncrude in response to the challenge of fine tailings management [13,14]. Other technologies such as the thickened tailings technology (paste technology) and the new emerging technologies (in-line thickening with thin lift, centrifugation, filtration, etc.) have been proposed and tested [15]. Most of those

technologies involve the use of polymer flocculants to accelerate solid-liquid separation. The addition of polymer flocculants to the oil sands tailings enhanced the permeability and settling rate of oil sands tailings and promoted the recovery of process water. However, the results of treatment are generally not satisfactory as high dosages of expensive high molecular weight polymers are required to achieve a reasonable water release rate, and large desposal areas (called Dedicated Deposition Areas, or DDA) and high capital expenditures are needed. Even with the polymer amendment, the MFT still retains a considerable amount of water after gravity settling or centrifugation and remains in a viscous fluid state, ruling out the possibility of reclamation.

Despite the significant efforts, there is no available commercial technology nor "perfect" polymers that can solve the challenges of dewatering and consolidating oil sands tailings. If the oil sands tailings could be sufficiently dewatered so that it changed from the fluid state to the solid state, then it could be converted into a reclaimed firm terrain, and the tailings disposal problem would be solved. For this to be possible, it is generally recognized that the oil sands tailings need to be dewatered to >= 75 wt% solids [16]. However, after chemical amendment and gravity settling or centrifugation, it is only possible to achieve about 50-55 wt% solids. Using pressure filtration, the solid content can reach about 65 wt% with high dosage coagulant or flocculant treatment [17]. Therefore, the key requirement is to separate water from the fine solids in the oil sands tailings to achieve the required solid contents. However, the question "why is such a liquid-solid separation so difficult" does not seem easy to answer. The solids are composed of fine minerals/clays, and the liquid phase is composed of water, residual bitumen, and dissolved species. Loerke et al. found that ultrafine fractions from MFT, dubbed "middle layer" after centrifugating the MFT at 17,300 RCF, could make the kaolinite slurry

unfilterable [18]. It was considered that the middle layer contained most of the residual bitumen, and the difficult filtration of the "middle layer" doped kaolinite slurry was caused by the residual bitumen introduced to the kaolinite. This observation is meaningful, but there are still many questions that have not been answered. For example, was the low filterability caused by the ultrafine minerals or residual bitumen or both in the "middle layer" of MFT? What was the effect of different types of minerals in the oil sands on the filtration rates? What was the effect of particle size on the filtration rate? How did the residual bitumen affect the filtration process? Therefore, the effects of bitumen and constituent minerals in the Alberta oil sands on the filtration dewatering of the oil sands tailings still needs further clarification.

### 1.2. Research Objectives

The ultimate objective of any oil sands tailings dewatering study is to separate the solids and water in the oil sands tailings to reach a solid content of >= 75 wt% (or <= 25 wt% water as this is the so-called plastic limit below which the tailings can be reclaimed). Barring thermal drying, nearly all reported research so far did not achieve 75 wt% solids in the dewatered tailings, even in the laboratories, and the question of why the oil sands tailings was so difficult to filter was unanswered. The main objective of this research is to find the reason or reasons for the difficulties in filtering the Alberta oil sands tailings. Vacuum filtration and pressure filtration will be used as the mechanical solid-water separation technique to study the roles of the types of minerals, residual bitumen, mineral surface hydrophobicity, and chemical aids, on the filtration process. More specifically, the research objectives are:

(1) Investigate the filterability of different types of minerals with the objective to identify the ones that are more difficult to filter than the others.

(2) Investigate the role of residual bitumen in the filtration of oil sands tailings. All possible forms of the residual bitumen will be investigated, including bulk "free" bitumen, bitumen-in-water emulsion, and bitumen adsorbed on mineral surface.

(3) Investigate the effects of mineral surface hydrophobicity on the filtration by comparing the silanized minerals to bitumen coating treated minerals to decouple the effects of surface hydrophobicity and adsorbed bitumen layer thickness in the filtration process.

### 1.3. Organization of the Thesis

Chapter 1 includes a brief introduction of the background of the Alberta oil sands tailings, the challenges of the tailings treatment and a summary of the current treatment technologies, and provides the research objectives.

Chapter 2 reviews the relevant literature about the reasons of the difficult dewatering of oil sands tailings.

Chapter 3 investigates the filterability of different types of minerals, leading to the observation that swelling clays are the most difficult to filter. It was postulated that the filtration of the different minerals could be explained by the "effective volume fractions" of the solid phases of the mineral slurries.

Chapter 4 reports the roles of the three forms of residual bitumen, bulk bitumen, bitumen-in-water emulsion droplets (emulsified bitumen), and bitumen adsorbed on mineral surfaces (adsorbed bitumen) in the filtration of oil sands tailings. It led to the conclusion that both bulk bitumen and emulsified bitumen only marginally affected filtration, while adsorbed bitumen showed drastically different effects from significantly promoting filtration to significantly impeding filtration, depending on the amount of bitumen adsorbed on the mineral surface.

Chapter 5 compares the filtration behaviors of minerals that were rendered hydrophobic either by bitumen coating or by surface silanization treatment. This was an attempt to explain the observed wide swings of the adsorbed bitumen on the filtration behaviors of the bitumen-coated minerals.

Chapter 6 summarizes the major conclusions and original contribution of this work to solid-liquid separation by filtration, and presents possible directions for future research.

**References**


[1] Alberta Energy Regulator. Alberta Energy Regulator 2016/17 Annual Report. 2017. https://doi.org/https://static.aer.ca/prd/documents/reports/AER2016-17AnnualReport.pdf.

[2] Masliyah JH, Czarnecki J, Xu Z. Handbook on Theory and Practiceon Bitumen Recovery from Athabasca Oil Sands. 2011. https://doi.org/https://doi.org/10.7939/r3-nr43-8t34.

[3] Hande AB. Accelerated Dewatering and Drying Treatment of Oil Sands Tailings by Electrical Resonant Auto-Transformer 2014:59–61.

[4] Alberta Environment and Parks. OSIP - Data Library 2015. http://osip.alberta.ca/library/Dataset/Details/542 (accessed April 4, 2015).

[5] Fennell J, Arciszewski TJ. Current knowledge of seepage from oil sands tailings ponds and its environmental influence in northeastern Alberta. Sci Total Environ J 2019. https://doi.org/10.1016/j.scitotenv.2019.05.407.

[6] Finkel ML. The impact of oil sands on the environment and health. Curr Opin Environ

Sci Heal 2018;3:52–5. https://doi.org/10.1016/J.COESH.2018.05.002.

[7] Environmental defence. One trillion litres of toxic waste and growing: Alberta's tailings ponds. n.d. https://doi.org/https://d36rd3gki5z3d3.cloudfront.net/wp-content/uploads/2017/06/AlbertaTailingsPondsReportFINAL.pdf?x78791.

[8] Timoney K. Environmental and Health Impacts of Canada's Oil Sands Industry 2010. https://doi.org/http://www.youtube.com/watch?v=nReBw5IzaCM.

[9] Small CC, Cho S, Hashisho Z, Ulrich AC. Emissions from oil sands tailings ponds: Review of tailings pond parameters and emission estimates. J Pet Sci Eng 2015;127:490–501. https://doi.org/10.1016/J.PETROL.2014.11.020.

[10] Taylor BEng T, Jamieson W, Grant A. Fugitive Emissions from Tailings Facilities in the Athabasca Oil Sands Region Summary of national emissions database, current scientific knowledge, and regulatory frameworks ENVS 4405: Air Quality. 2021. https://doi.org/https://www.canada.ca/content/dam/eccc/documents/pdf/npri-/academic challenge/Fugitive%20Emissions%20from%20Tailings%20Facilities%20in%20the%20Athabasca%20Oil%20Sands%20Region.pdf.

[11] Government of Alberta P. Annual Emissions Inventory Report Standard and Guidance Document: 2018 and 2019 Emissions Inventory Years. 2018. https://doi.org/https://open.alberta.ca/dataset/7f234172-a595-47b0-b8f9-4b3739bbcfda/resource/6c1cc270-ba68-4fff-8b12-f2b8eb6dfe73/download/aeir-standard-aug2018.pdf.

[12] Environmental defence. Report: Alberta's Tailings Ponds： One Trillion Litres of Toxic Waste and Growing 2022.

https://doi.org/https://environmentaldefence.ca/report/albertas-tailings-ponds/.

[13] Proskin S, Sego D, Alostaz M. Oil Sands MFT Properties and Freeze-Thaw Effects. J Cold Reg Eng 2012;26:29–54. https://doi.org/10.1061/(asce)cr.1943-5495.0000034.

[14] Matthews JG, Shaw WH, MacKinnon MD, Cuddy RG. Development of Composite Tailings Technology at Syncrude. Int J Surf Mining, Reclam Environ 2002;16:24–39. https://doi.org/10.1076/ijsm.16.1.24.3407.

[15] Sobkowicz J. Oil Sands Tailings Technology Deployment Roadmap. vol. 2. 2012.

[16] Revington, Adrian Peter et al. Process for flocculating and dewatering oil sands mature fine tailings. 9,909,07, 2018.

[17] Zhu Y, Tan X, Liu Q. Dual polymer flocculants for mature fine tailings dewatering. Can J Chem Eng 2017;95:3–10. https://doi.org/10.1002/cjce.22628.

[18] Loerke R, Tan X, Liu Q. Dewatering of Oil Sands Mature Fine Tailings by Dual Polymer Flocculation and Pressure Plate Filtration. Energy and Fuels 2017;31:6986–95. https://doi.org/10.1021/acs.energyfuels.7b00938.

# CHAPTER 2 Literature Review

## 2.1. Oil Sands Tailings Mineralogy

The Alberta oil sands contain various minerals, including quartz, clay minerals (kaolinite, illite, chlorite, and interstratified illite-smectite), carbonate minerals (calcite, siderite), K-feldspar, titanium dioxide minerals, and pyrite, etc. [1–5]. Quartz is the dominant mineral [5]. Kaolinite, illite, and interstratified illite-smectite were found to be the primary fine clay minerals in the oil sands ores [6]. It was difficult to identify swelling clays directly from the peaks of X-ray powder diffraction (XRD) patterns. The presence of smectite was confirmed by comparison of XRD patterns produced from air-dried and ethylene-glycol treated oil sands ore samples, and the estimated content of swelling clays was 2-6% in the oil sands [7]. Illite-smectite is the most common interstratified clay with an expandability of 10%, and its particle size was generally less than 0.2 μm [1,8]. The properties and behaviors of different minerals on the dewatering of oil sands tailings were rarely investigated. The carbonate minerals could dissolve by adjusting the solution pH with the addition of carbon dioxide ($CO_2$). The water chemistry and turbidity were changed by the interaction of $CO_2$ and carbonate minerals, which were considered a promising treatment for the fast settling of oil sands tailings [9]. However, carbonate minerals with a particle size < 250 μm was reported to be easy to filter both by pressure and vacuum filtration [10]. The clay minerals have been recognized to be detrimental for the separation of bitumen from oil sands in the bitumen extraction process, and the low dewatering and consolidation rates of oil sands tailings were believed to be driven by the fine clay minerals [11,12]. The aggregation of the clay minerals in the presence of coagulating cations in the process water was indicated to be the main reason for the high water holding capacity of MFT, and the thixotropic gel structure, formed by fine clays and residual bitumen, could provide a

viscous supporting medium for the coarse fraction of the tailings [12–15]. Therefore, the clay minerals were considered as the main reason for the slow dewatering of oil sands tailings.

Clay minerals are composed of two basic units, a silicon-oxygen tetrahedral sheet and an alu minum-oxygen-hydroxyl octahedral sheet [16]. It has been suggested that the relative sizes of two sheets control the clay minerals' morphology, and different arrangements determine the types of clay minerals [17,18]. Kaolinite is made up of alternating $SiO_4$ tetrahedral and $Al_2O_6$ octahedral sheets connected by sharing the apex oxygen atoms of the tetrahedral sheet. Each layer is held together by hydrogen bonds and charge-compensation ions, mainly potassium ions [18]. As a result, the compensation ions in the two-layer kaolinite are not easy to exchange with other cations, so that kaolinite has a low cation exchange capacity of 3-5 meq/100g [18], and is a non-swelling clay. The silicon ($Si^{4+}$) in the tetrahedral sheet could be substituted by aluminum ($Al^{3+}$), and the aluminum in the octahedral sheet could be substituted by magnesium ($Mg^{2+}$). The process of higher valance cations substituted by lower valance cations of similar sizes was referred to as isomorphic substitution [18,19], which causes the existence of a permanent negative charge on the basal surfaces of the clay minerals.

Illite and montmorillonite are three-layer clay minerals, composed of two opposing tetrahedral sheets sandwiching an octahedral sheet [20]. Different three-layer clay minerals have different compensation ions and the location, also different degrees of isomorphic substitution. The isomorphic substitution of illite mainly occurs in the tetrahedral sheet and the compensating ions, mainly potassium, bound the sheets together. For example, the significant substitution in the tetrahedral sheet makes illite to possess a higher cation exchange capacity (10-40 meq/100g) than kaolinite [18]. The isomorphic substitutions exist in both tetrahedral and octahedral layers of montmorillonite. The degree of substitution in the tetrahedral sheet is similar to that of illite.

However, the substitution in the octahedral sheet could delocalize the permanent charge in the octahedral sheet, and the compensation ions leave the octahedral sheet and attach on the tetrahedral sheet. The interlayer binding of sheets is weakened by the movement of those compensation ions, and the ions become available for ion exchange, leading to a high cation exchange capacity of 80-100 meq/100g [18,21,22]. Montmorillonite exhibits swelling characteristics and is classified as a swelling clay mineral. The aforementioned clay minerals (kaolinite, illite, montmorillonite) take pseudo-hexagonal plates and stacks shape and the schmematic structure was shown in Figure 2-1.

Due to their different morphologies, structures and chemical properties, the clay minerals would have different filtration behaviors. However, we are unaware of studies comparing the filtration behaviors of individual clay minerals reported in the open literature.

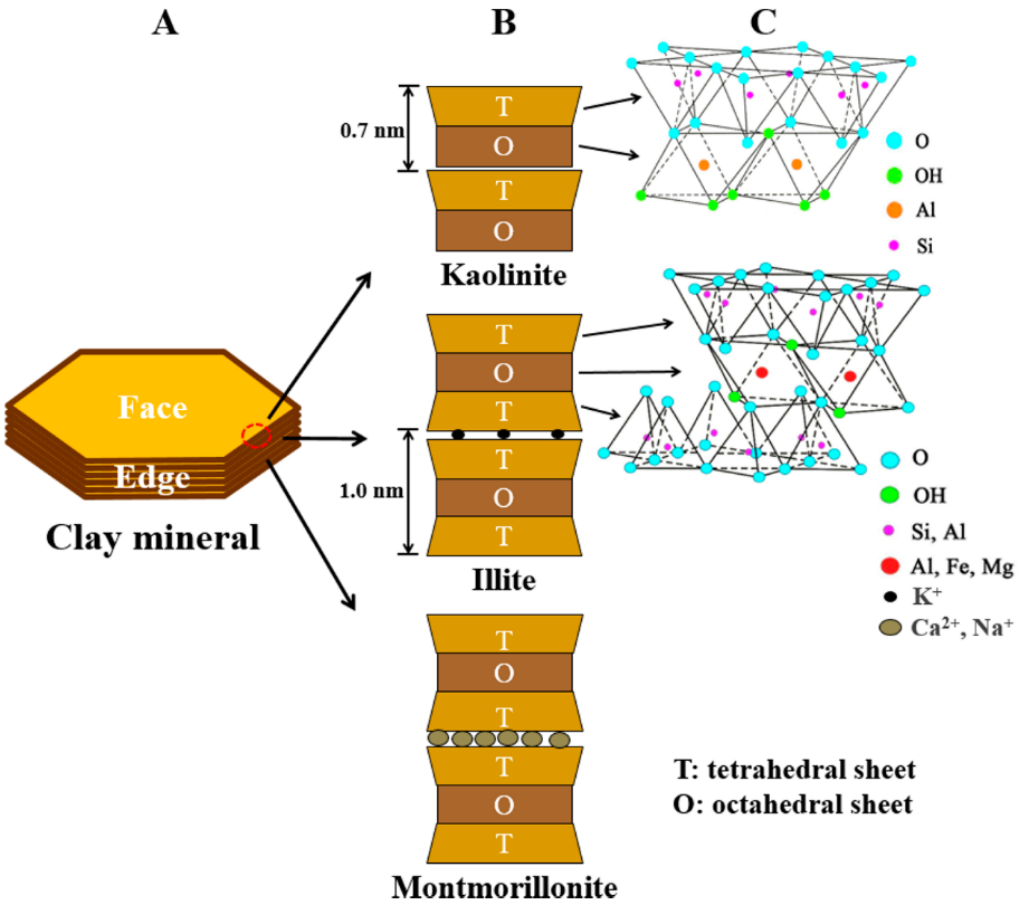


Figure 2-1 Schematic of (A) clay mineral structure with face and edge surfaces and (B, C) crystalline structures of kaolinite, illite, montmorillonite with interchangeable cations [23].

## 2.2. The Dewatering of Aqueous Mineral Slurries

The presence of fine minerals and clays in oil sands tailings is widely accepted as the main reason for its poor dewatering behavior. However, it is not clear how the fine minerals and clays affect the different dewatering processes and what types of minerals and clays are mainly responsible to the slow dewatering.

### 2.2.1. Particle size effect

In a study of the filtration of a coal slurry, it was observed that the filterability decreased as the particle size decreased [24]. This is understandable as the slurry containing large proportions of small particles had a low porosity, which would result in decreased permeability and a slow filtration rate. Figure 2-2 shows the particle size distribution of coarse and fine oil sand tailings, obtained by laser diffraction and sieve-hydrometer methods [25]. The smaller than 44 μm particles in the oil sands are usually called fines, which account for 17% of the solids in the whole tailings. For the typical mature fine tailings, about 95% of the solids are fines, i.e., less than 44 μm, and 30-50% of the fines are clay fraction that are smaller than 2 μm in diameter [26].

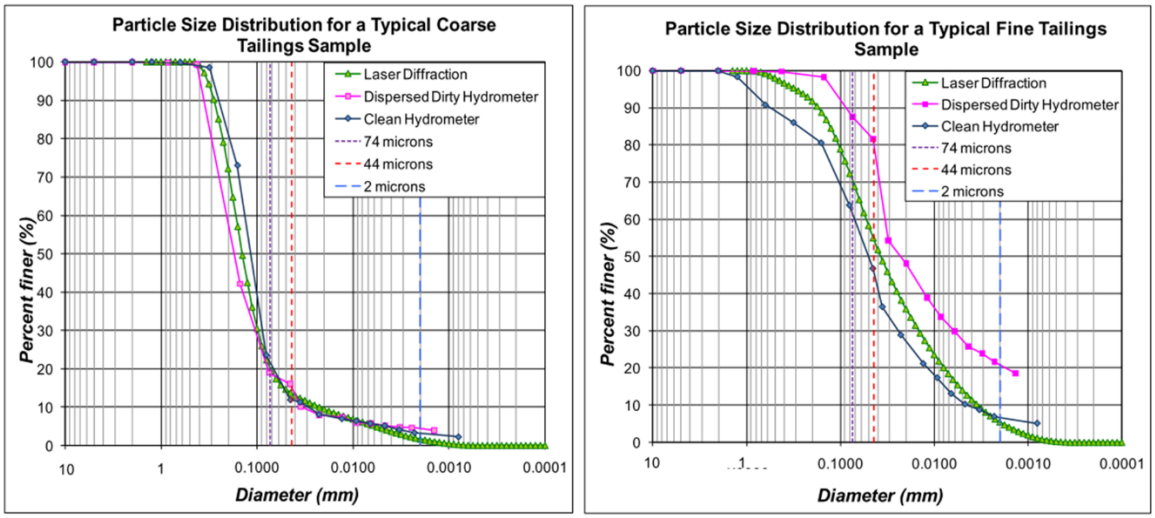


Figure 2-2 Particle size distribution of coarse and fine oil sands tailings measured by different methods [25].

High-resolution transmission electron microscopy (TEM) and X-ray diffraction (XRD) studies of kaolinite and illite in the 0.2-2 μm size fractions showed that the fundamental particle thickness was about 6 nm (TEM) and 19 nm (XRD), and this explained the observed large specific surface areas of the clay minerals in the oil sands tailings [27]. The specific surface area was directly related to the water holding capacity, and the smaller the particles, the larger the specific surface area. The high water holding capacity was also attributed to the porous gel network structure of the mature fine tailings formed by ultrafine clays, which could trap water, coarse solids, and free or emulsified bitumen [28].

Tu et al. considered that the < 0.3 μm ultrafine solids were responsible for the gel formation of oil sands tailings. The gelation of ultrafines isolated from oil sands samples was investigated by a $^{2}H$ NMR method. Results showed that the start of sludging occurs when the ultrafines contents exceeded 1.5 wt% [29]. The 20-200 nm fraction isolated from oil sands was amorphous and characterized by large specific surface area, high adsorption capacity, and large

cations exchange capacity [30]. Mercier et al. used a combined XRD analysis and laser diffraction method to quantitatively estimate the contents of illite and kaolinite in the oil sands and suggested that the amount of ultrafine illite with a high specific surface area was critical for the assessment of processability for the oil sands and was assumed to have a drastic negative impact on bitumen recovery. Furthermore, the amount of ultrafine illite and kaolinite closely matched the concentration required to cause gelation in the bitumen recovery process [31].

The foregoing discussion shows that the fine and ultrafine particle fractions in the oil sands tailings contribute significantly to water holding capacity, specific surface area, and gel formation, all of which could have detrimental effects on filtration.

### 2.2.2. The dewatering of different types of minerals

Using X-ray diffraction (XRD) method, many studies have indicated that kaolinite, illite, and chlorite are the dominant non-swelling clay minerals in the oil sands tailings. In XRD patterns, the signals of swelling clays such as smectite would be lost in the background due to their extremely fine particle size and/or low concentration. As a result, the regular powder XRD method is not able to detect smectite in oil sands tailings [32]. The presence of swelling clays is detected by their expandable property, i.e., the swelling clays were identified by comparing the XRD patterns of oil sands samples prepared by air-dried and ethylene glycol treated samples. Changes in the shape, positions, and relative intensities of reflections after ethylene glycol treatment revealed the presence of interstratified illite-smectite, kaolinite-smectite, and montmorillonite [1,7,33].

What are the roles of the different minerals in oil sands tailings dewatering? Some researchers considered that the presence of clays, mainly kaolinite and montmorillonite, contributed to the exceptional stability of the oil sands tailings [34] and adversely affected bitumen extraction

from oil sands [35]. Omotoso et al. compared the calculated and measured specific surface areas of MFT [33]. They found that the calculated specific surface areas based on the contributions of clay minerals corresponded well to the specific surface area measured by the methylene blue adsorption method, as shown in Table 2-1. The calculated specific surface area was based on the following equation [33],

$$\text{Calculated specific surface area SSA} = (SSA_{kaolinite} \times wt.\%_{kaolinite} + SSA_{kaolinite\text{-}smectite} \times wt.\%_{kaolinite\text{-}smectite}) + (SSA_{illite} \times wt.\%_{illite} + SSA_{illite\text{-}smectite} \times wt.\%_{illite\text{-}smectite}) \quad 2.1$$

In their studies, the specific surface area (SSA) of the individual mineral was calculated by the crystallite size, and wt% of minerals in the MFT was determined by quantitative XRD analysis. The high specific surface area of the mature fine tailings can be attributed to kaolinite and illite interstratified by smectite. But interstratified kaolinite and illite were always overlooked in many studies because of the relative low concentrations and the inability of detection by routine powder XRD.

Table 2-1 Measured and calculated specific surface area of the clay fractions in MFT [33].

| Sample | Fraction (μm) | Measured specific surface area ($m^2/g$) | Calculated specific surface area ($m^2/g$) |
|---|---|---|---|
| MFT | < 0.25 | 197 | 194 |
| | < 0.2 > 0.25 | 108 | 97 |

The surface properties of oil sands were also reported to be controlled by the type and quantity of clay minerals, mainly interstratified clay minerals. The cation exchange capacity, specific surface area, total specific surface area, and negative layer charge density all increased with increasing concentrations of the interstratified illite-smectite [36]. Basnayaka et al. [36] investigated the roles of bentonite and kaolin in the filtration of a pyritic gold ore. They showed

that montmorillonite, which is the main constituent mineral in bentonite, had a more detrimental effect on the specific cake resistance, filter medium resistance, and final cake moisture content than kaolinite [37].

It was reported that the dewatering problem of some mineral sludges was especially acute/serious when certain kinds of clay minerals were present in the mine wastes. For example, the phosphate slimes, which were produced from the mining of phosphate rocks, was slow-settling, had high water retaining capacity, and trapped process water[38]. The red muds, coal slimes, and steel mill sludges also presented similar problems. The dewatering of slimes was reported to be controlled by the presence of swelling clays [39]. The difficulty in dewatering phosphatic clay slurry was believed to be resulted from the presence of montmorillonite and attapulgite, originating from their unique properties of swelling, morphology, cation exchange capacity, and charged surface, which were responsible for the colloidal behavior and the remarkable stability of the phosphatic clay suspensions [40]. Saponite, a three-layer clay mineral of the smectite group, was identified to be responsible for forming the colloidally stable state of the diamond mine slimes [41]. The mineralogical analysis of oil sands tailings shows that montmorillonite was present in their oil sands tailings sludge sample (about 0.9 wt%), and that montmorillonite was found to impose high viscosity on the drilling muds even at low solids content [42].

The gel strengths of oil sands tailings were similar to a 5 wt% montmorillonite slurry as a function of rest time after stirring [43]. Also, the viscosity of the two slurries displayed some similarities at pH above 8 (the pH of the oil sands tailings was 8.4). But the montmorillonite was not thought to present in sufficient amount to control the stability and dewatering performance of the oil sands tailings. In fact, freeze-thaw dewatering tests showed that the 5

wt% montmorillonite slurry behaved very differently from oil sands slime at different pH. The montmorillonite retained most of the water during thawing irrespective of pH, while the oil sands slime lost the greatest amount of water at lower and higher pH compared with the original pH [43]. It was assumed that changing pH in the oil tailings slimes could destroy the gel-like structure and release water. Also, the flocculation performance of anionic Percol 727 polymer on a Syncrude fine tailings was determined at different pH of the slurry [44], and it was found that the swelling clays behaved differently at different pH.

### 2.3. The Role of Bitumen in Oil Sands Tailings Dewatering

The dewatering of oil sands tailings is more difficult than other mine tailings, which have similar particle sizes but without the presence of bitumen. The majority of the research conducted so far has focused on the fine solids in the MFT, but the role of bitumen has not received sufficient attention. Bitumen is insoluble in water and only partially soluble in most organic solvents, and can create challenging problems in tailings dewatering. The presence of bitumen may exert an extra effect on the suspension of MFT so that the conventional methods of the two-phase solid-liquid separation may not work well.

#### 2.3.1. The composition of Alberta oil sands bitumen

Bitumen composition is described by SARA, a common acronym of saturate, aromatic, resin and asphaltene [45], classified according to their solubility in n-pentane and chromatographic separation. The specific class fraction of Alberta oil sands bitumen is listed in Table 2-2. Bitumen is highly viscous because of its high content of asphaltenes [46]. Asphaltene is the generic term used to describe bitumen or petroleum compounds that is soluble in toluene but insoluble in n-alkane, such as n-heptane or n-pentane. Asphaltenes have the highest molar mass compared with the other three sub-fractions of bitumen, and the majority of polar compounds

are contained in the asphaltenes [47]. Asphaltene's propensity to precipitate and to adsorb on any solid surfaces has been extensively studied, and has been considered the root cause for many problems encountered in the oil sands industry [48]. But interestingly, it has not been extensively studied in oil sands tailings dewatering.

Table 2-2 Class fraction of bitumen [49].

| Bitumen | Amount of fraction, wt% | | | |
|---|---|---|---|---|
| | Saturates | Aromatics | Resins | Asphaltenes |
| Athabasca | 10.3 | 5.3 | 62.3 | 22.2 |
| Cold Lake | 12.3 | 6.7 | 54.6 | 38.8 |

### 2.3.2. The adsorption of oil sands bitumen and asphaltene

Some organic materials in the oil sands bitumen may adsorb on clay surfaces through chemical bonds. From the structure and composition perspective, asphaltenes contain acid-base pairs of oxygen- and nitrogen-containing functional groups, contributing to negative and positive charges, metal porphyrins or chelating metal structures. The intramolecular forces are a combination of acid-base interactions, hydrogen bonding, π-π stacking, hydrophobic pockets by van der Waals forces, and coordination stacking [50]. The combination of those forces can be quite strong and can facilitate asphaltene-asphaltene interaction as well as asphaltene-substrate adsorption.

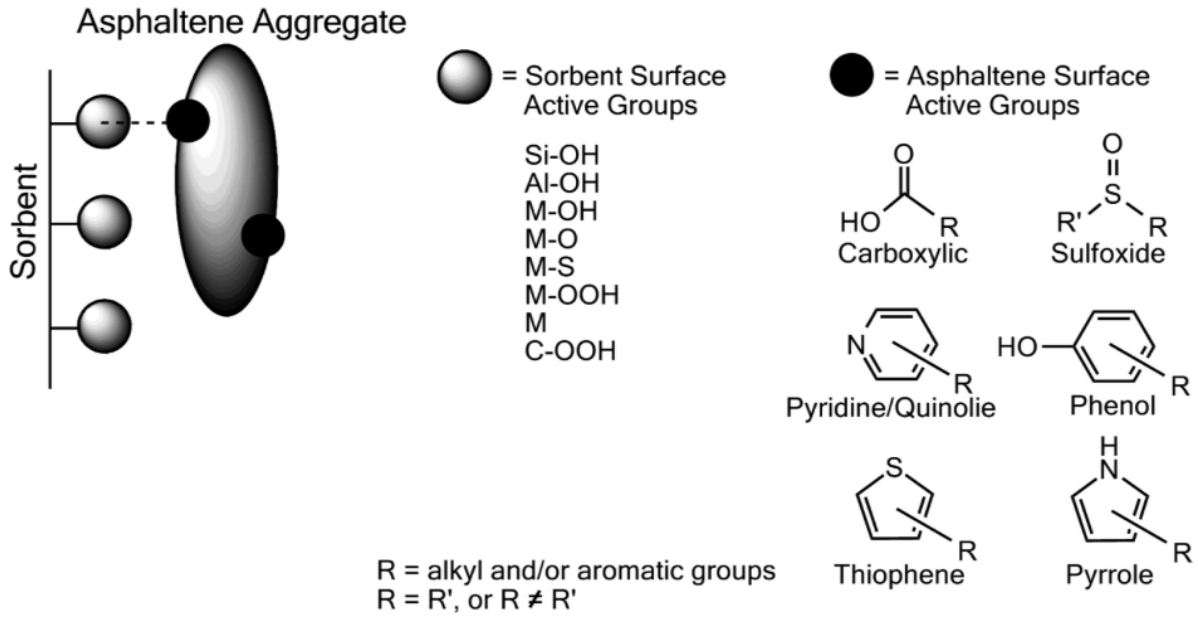


Figure 2-3 The adsorption interaction of an asphaltene aggregate at a sorbent surface through respective active sites [48].

Figure 2-3 shows a representation of the interaction between sorbent surface and asphaltene surface active sites by the different functional groups. In the middle of the figure are shown the possible sorbent surface active groups and at the right side are the asphaltene surface active groups. The asphaltene aggregates could have a strong interaction with the sorbent. Asphaltenes contain a mixture of acids and bases with ionized groups in aqueous solutions, and the polar functional groups as well as the aromatic backbone give rise to significant electrostatic interactions. Adams [48] claimed that these asphaltene aggregates can interact with other asphaltene molecules or other oil sands components, such as clays.

The oil sands tailings solids were indeed found to be associated with toluene-insoluble organic components. The clay minerals could interact with the bitumen components, owing to the high surface area and charge density [2]. The adsorption of asphaltene on different clay minerals

was investigated by the Langmuir adsorption isotherms and $N_2$ adsorption [51]. Due to asphaltene adsorption, the inner surfaces per unit volume of minerals decreased, thus the specific surface areas significantly decreased, suggesting that the asphaltene clogs the pores of clay minerals [51]. Bensebaa et al. [52] detected 40-60 at% organic carbon on the surfaces of mineral solids extracted from bitumen froth by X-ray photoelectron spectroscopy. Their ToF-SIMS spectroscopy results showed that the surface layer of organic materials was patchy rather than continuous on solids surface, and the particle surfaces were not completely covered by organic matters. The patchy-distributed structure of organics on the clay minerals surface was studied by the PeakForce quantitative nanomechanical mapping (QNM) mode of atomic force microscopy (AFM), and the inhomogeneous spatial distribution of adhesion forces showed that the organics on the minerals surface were distributed in a patchy fashion [53]. The fine solids extracted from bitumen froth were found to have a 17±6% surface organic coverage [53]. The amount of toluene insoluble organics on minerals in the fine fractions was higher than in the coarse fraction, and the authors claimed that the organics were mainly associated with the clay minerals [8]. By means of density fractionation, combined with elemental composition and $^{13}C$ NMR analysis, the aromatic carbon was found to be the predominant type of carbon on the fine solids that were associated with bitumen [54].

The organic materials adsorbed on mineral surfaces, which could not be washed off by toluene, was found to be deformable through studies by QNM-AFM [53]. The organic coating thickness was difficult to quantify unequivocally on the unsmooth clay surface. Chen et al. [53] measured the adhesion force of separated organics at different thicknesses with the AFM tip and extrapolated the linear fit of the separated organics (Figure 2-4 ) to estimate the average thickness of the organic coating, which was about 1.4 nm, based on its average adhesion force.

Even with toluene wash, some organics could not be washed off. The minerals in the oil sands tailings could be partially coated with bitumen.

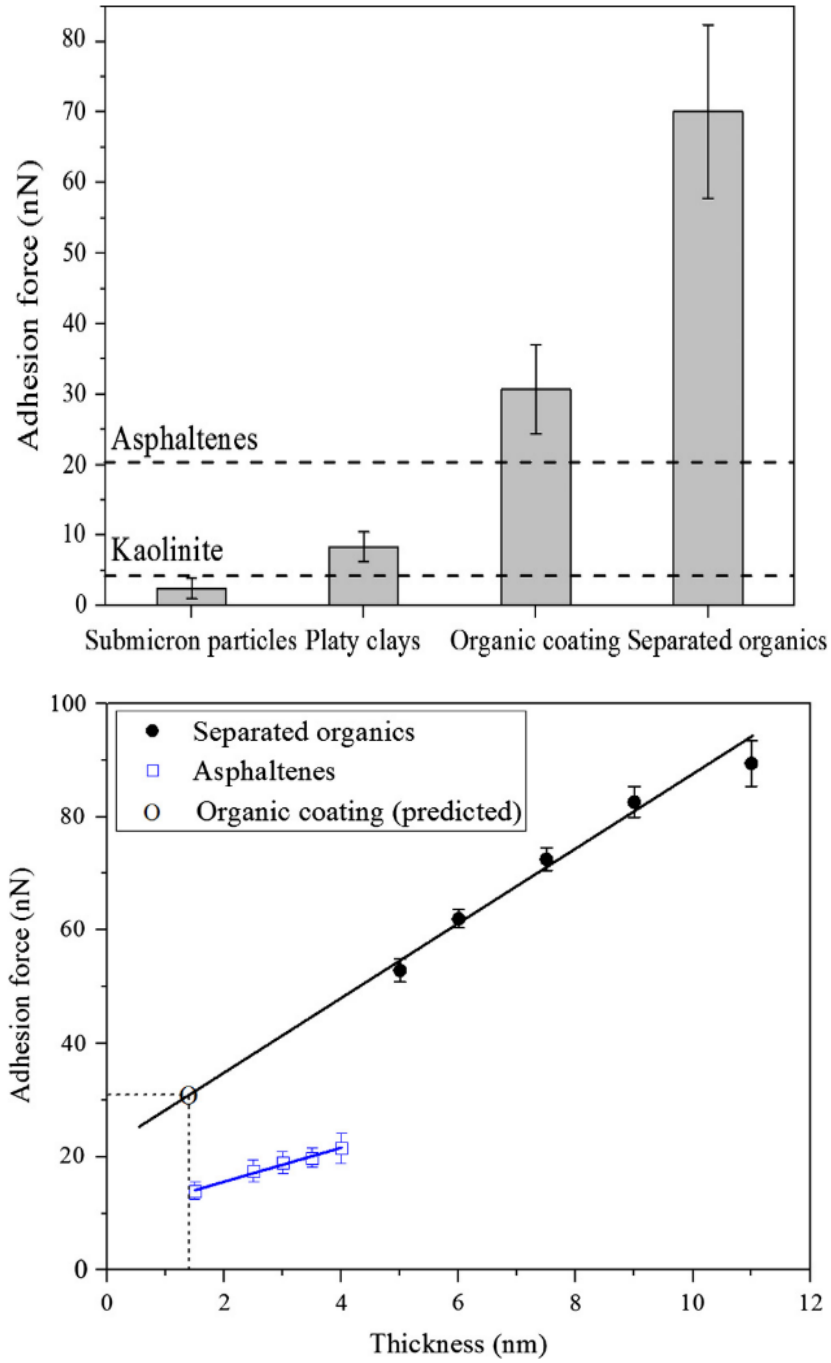


Figure 2-4 Tip-sample adhesion of different components (top) and as a function of the thickness (bottom) of the organic materials [53].

Although many researchers have investigated the interaction mechanisms between bitumen and minerals surface, a good understanding is still elusive. Chen et al. [23] summarized the interaction forces at bitumen-clay interfaces , including hydrogen bonding, chemical bonding, acid-base interaction, cation bridging, physical entanglement, etc., as indicated in Figure 2-5. These bonding forces were believed to be crucial for bitumen coating on the mineral surface. From the preceding review, we can assume that the asphaltene aggregates could also interact with the functional groups of chemicals and polymer flocculants introduced in the dewatering process.

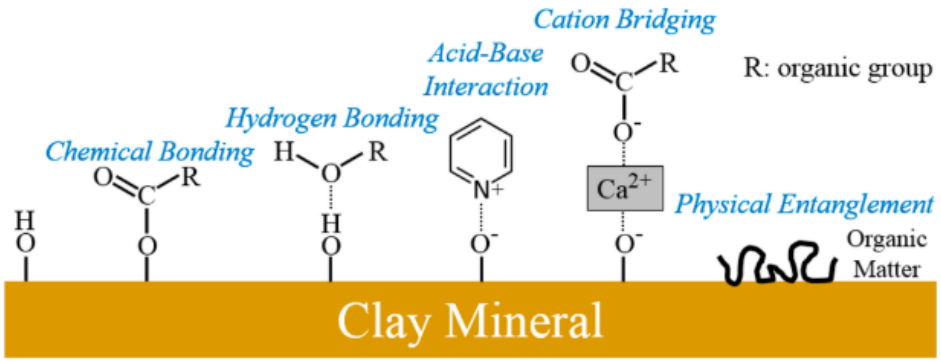


Figure 2-5 The possible interaction mechanisms at bitumen-clay interfaces[23].

However, literature indicated that bitumen may exist in the form of bitumen-in-water emulsions in oil sands slurry. Since water interacts strongly with hydrophilic solid surfaces, water molecules near the surface could form a solid like hydration film [55]. This behavior could decrease the amount of adsorption sites for asphaltene molecules.

Tan and Liu [56] subjected an MFT sample to strong centrifugal forces, and noticed that the MFT was separated into three layers: clear water layer on the top, a bitumen-in-water emulsion in the middle layer that contained about 10 wt% solids, and a clean sand layer at the bottom. The middle layer could disperse in water but could not disperse in toluene, which was the basis

of the bitumen-in-water emulsion claim. However, it was unclear if the bitumen-in-water emulsion was made of free bitumen droplets or bitumen coated on ultrafine clay surfaces. It was possible that both types of bitumen existed in the middle layer.

### 2.3.3. The effect of bitumen on tailings dewatering and consolidation

The oil sands tailings slurry settles quickly when discharged to tailings ponds originally at a solid content of about 5 wt%. The sedimentation slows down as the solid content increases and becomes extremely slow when the solid content reaches about 30 wt%, corresponding to the solid content of MFT [57]. The residual bitumen in the oil sands tailings slurry may exist in three forms: bulk "free" bitumen, bitumen-in-water emulsions droplets, and bitumen adsorbed on clay surface. These different forms of bitumen may have different effects on tailings dewatering.

#### 2.3.3.1. The effect of bitumen on hydraulic conductivity

Scott et al. [57] studied the property of clay minerals in the presence of "free" bitumen based on the data of void ratio to permeability and effective stress relationship [the word 'free" was inserted by the present author]. They proposed a model for bitumen and particle interaction, as shown in Figure 2-6. As can be seen, bitumen mostly adheres to the edges of clay particles, which connects the particles to form agglomerates, while the Brownian motion collisions of bitumen help the agglomerates formation. This may block water channels and make it difficult to release the interstitial water. Azizov et al. [58] employed a microfluidic method to study the transportation of oil droplets in the porous media and found that the size of oil droplets was critical to the pore-clogging. The large droplets could entirely clog the pores, and the oil droplets that are smaller than the pores could flow through the pores with little to no retention. Additionally, the polydisperse emulsions experiment showed that the large oil droplets could

facilitate the retention of the small droplets, which meant that all size oil droplets were retained due to the existence of large oil droplets. Therefore, the presence of "free" bitumen could have a retardation effect on the permeability and compressibility of tailings sediments.

Scott et al. [57] also reported that as the water content in sediments decreased, its hydraulic conductivity decreased by many orders of magnitude. Therefore the hydraulic conductivity could potentially decrease more in the presence of bitumen which blocked the water channels. Thus removing the residual bitumen from the MFT would increase the hydraulic conductivity and the rate of consolidation. By the same reasoning, it could be assumed that immobilizing residual bitumen in MFT may have the similar beneficial effect.

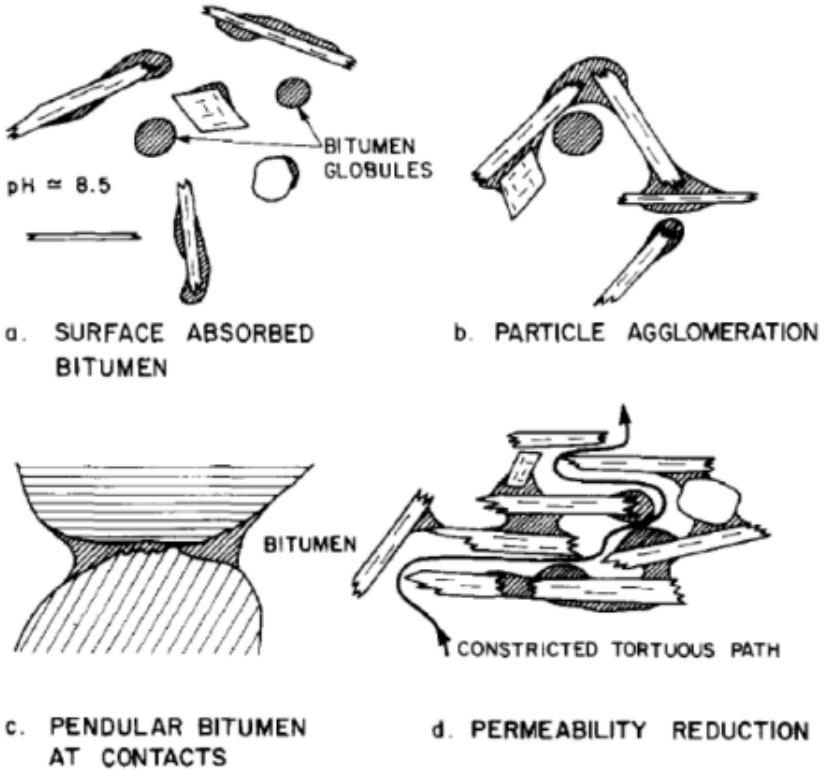


Figure 2-6 Effect of bitumen on particle settling and sediment permeability [57].

#### 2.3.3.2. The effect of bitumen on settling rate

Klein et al. [59] studied the settling rate of polymer flocculated MFT at different bitumen contents and observed an interesting phenomenon: only in a certain range could the removal of bitumen from the MFT improve the settling rate. When the bitumen content was further reduced, the settling rate of MFT decreased dramatically and became even lower than the original MFT without removing bitumen. They attributed the observation to the selective removal of hydrophobic solids during the bitumen removal process which was accomplished by Denver flotation.

It is known that bitumen could adsorb on clays causing them to agglomerate, which would benefit settling. On the other hand, the presence of bitumen could also cause gel formation, which would hinder settling. Therefore, there may be a critical bitumen content that kept the clay agglomeration and gel formation in a balanced state. Below this critical concentration, there was not enough bitumen to cause clay agglomeration but it was sufficient for gel formation, hence the settling rate was decreased.

#### 2.3.3.2 The effect of bitumen on filtration

The oil sands mature fine tailings showed a gel-like structure, which was considered to have caused their extremely slow dewatering. Suthaker and Scott [60] mentioned that the gel structure controlled the hydraulic conductivity to a certain degree. The ultrafine clays were always considered to be the primary reason for the formation of gel-like structure in MFT which increased the water-holding ability of MFT [63, 64]. However, the often neglected point was that bitumen could also play a vital role in the gel-formation of MFT. This point was mentioned by Scott et al. [57] who demonstrated that the gel strength was positively related to the content of residual bitumen. Chalaturnyk et al. [61] proposed that the asphaltic acids

contained in bitumen were soluble in water because of the addition of NaOH during bitumen extraction and they acted as a clay dispersant, which can reduce the interfacial and surface tension of the clay suspension. The presence of both a bitumen phase and extremely well dispersed ultrafine clays were all the necessary components to form a gel structure, and this gel was probably a clay-bound organic structure [57].

The dewatering of MFT has been extensively studied in the past several decades. In most of the reported studies, the fine clays in the MFT are regarded as the main reason for the poor dewatering performance. Researchers have been looking for chemical additives such as different polymers that have the desired interactions with the solid particles rather than the residue bitumen. However, even with the addition of high dosages of expensive high molecular weight polymers, the dewatering performance is generally unsatisfactory. When the solid content reaches 50 wt%, it becomes very difficult to continuously remove water from the oil sands tailings. At 50 wt% solids, the MFT contains 50 wt% (or about 70 vol%) water (assume the density of the clays is 2.6 g/cm$^3$). It is puzzling why such a high volume fraction of water is not readily removable. Reis et al. [63] and Vajihinejad et al. [64] considered that the added polymer flocculants may promote gel formation: The amide groups on the polyacrylamide (PAM) backbone contribute to strong hydrogen bonds with water, and together with the ionic species in the slurry, they promote the formation of a gel-like structure. Gumfekar et al. thought that the presence of bitumen on the mineral surfaces limited the adsorption of conventional water-soluble flocculants [65]. So most of the added polymers were not useful for the dewatering process of oil sands tailings. Kotlyar et al. [66] proposed that the ultrafine clays which were coated with toluene-insoluble-organic material were responsible for the presence of intractable water and associated salts in bitumen froth. The nature of organic matter on the

surfaces of the particles was such that it had a high propensity to form coke [52], and the coke could play a role in the dewatering process, such as foul and/or block the filter medium.

Zhu et al. [67] used a dual polymer system, an anionic polyacrylamide (trade name A3335) and a cationic polyDADMAC (Alcomer 7115) to filter a MFT sample. The dewatering performance was evaluated by capillary suction time (CST), solids content in the filter cake, specific resistance to filtration (SRF), and net water release (NWR). The results demonstrated that the dual polymer system performed better than the single polymer. The SEM images at different treatment conditions (Figure 2-7) show that a more organized porous structure was produced, the pore size was enlarged and obvious water channels could be observed when treating the MFT with the dual polymer system.

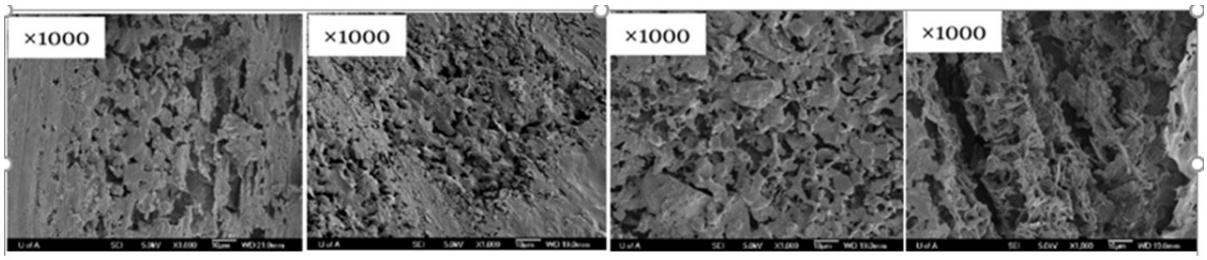


Figure 2-7 Cryo-SEM images of (A) untreated MFT, (B) MFT treated with 1 kg/t A3335, (C) MFT treated with 4 kg/t Alcomer 7115, (D) MFT treated with 4 kg/t Alcomer and 1 kg/t A3335 [67].

In her MSc thesis work, Loerke [68] compared the pressure filtration of three slurries: an MFT sample with 35.6 wt% solids and 2.7 wt% bitumen; a kaolinite slurry containing 35.6 wt% kaolinite, and a kaolinite/bitumen sample which was kaolinite mixed with centrifuged MFT middle layer at 35.6 wt% solids and 2.7 wt% bitumen.

The capillary suction time (CST) and cake solid content after pressure filtration at 6 bar that Loerke observed are compared in Figure 2-8 [69]. As can be seen, the kaolinite slurry had a much lower CST (159 s) than kaolinite/bitumen (1600 s) and MFT (3075 s). After treatment with low dosages of polymers (50 g/t A3335 and 150 g/t Alcomer 7115), there was an across the board decrease in CST, and the CST for kaolinite (50 s) was still lower than those of kaolinite/bitumen slurry (1080 s) and MFT (1220 s). When treated with high polymer dosages (1000 g/t A3335 and 3000 g/t Alcomer 7115), the three slurries had similar CST. The CST results of the slurries showed that kaolinite slurry released the water relatively easily. But after blending in 2.7 wt% bitumen, the kaolinite/bitumen slurry behaved like the MFT. Therefore, bitumen was considered to be responsible for the inferior dewatering performance of the kaolinite/bitumen slurry. It was therefore logical to assume that the residual bitumen in MFT was also the culprit for its slow dewatering behavior. This became especially clear when one noticed that the particle size of the kaolinite sample used in Loerke's work was an order of magnitude smaller than that of the MFT.

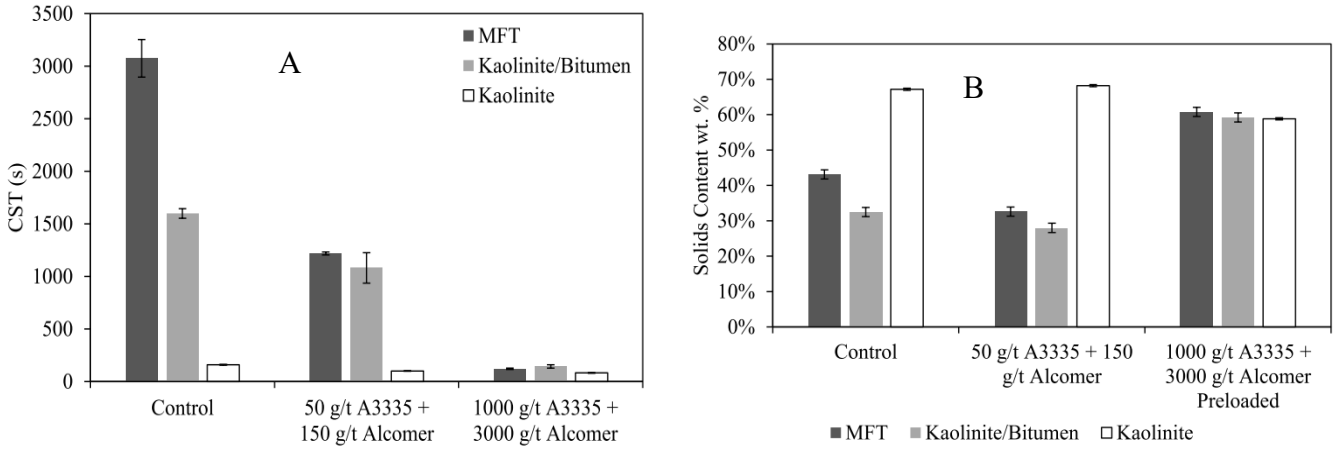


Figure 2-8 Comparison of CST (A) and solid content in pressure filtration cake (B) between dual polymer treated and untreated kaolinite, kaolinite/bitumen, and MFT [69].

Figure 2-8B shows that the solid content in the pressure filtration cake followed the opposite trend as CST. The filter cake after the pressure filtration of pure kaolinite slurry could reach about 70 wt% solids. The low dosages of dual polymers did not make much difference. However, when bitumen was blended to the kaolinite (to 2.7 wt%), the filtration behavior of the mixture was similar to MFT. The low dosages of the dual polymers could only generate a cake containing the similar wt% solids as the filter feed. At the high dosages of the dual polymers, the kaolinite/bitumen slurry reached a cake of about 60 wt% solids, which was similar to MFT.

One interesting observation was the appearances of the filter cloth after the filtration tests, as shown in Figure 2-9. As can be seen, there was a noticeable "smearing" of the filter cloth with bitumen when the kaolinite/bitumen slurry was filtered without treatment with polymers (bottom row in Figure 2-9). After treatment with high dosages of polymers (1000 g/t A3335 and 3000 g/t Alcomer 7115), the filter cloth was clean without bitumen smearing. It seemed that the added polymers primarily interacted with bitumen but not kaolinite, which significantly improved the filtration. Without the polymer treatment, the kaolinite/bitumen slurry was not filterable and the filter clothes were severely smeared with bitumen. This observation contradicted the report of Gumfekar at el. [65] which seemed to indicate that the bitumen-coating on clay surface would block the adsorption of added polymer flocculants.

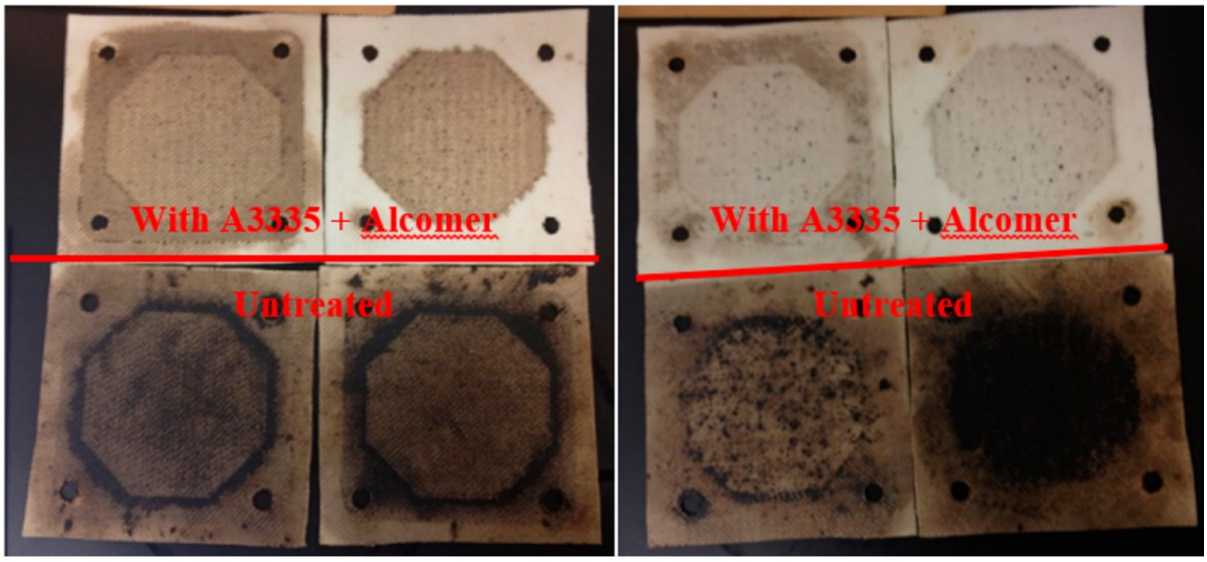


Figure 2-9 Visual comparison between filter cloths. The top row images show the filter cloths from the kaolinite/bitumen slurry treated with 1000 g/t A3335 + 3000 g/t Alcomer 7115. The bottom row images show filter cloths from the untreated kaolinite/bitumen slurry. (A) inside surface, and (B) outside surface [69].

### 2.4. The Effect of Particle Hydrophobicity on Filtration

The residual bitumen in the oil sands tailings can be free in the form of bulk bitumen and bitumen-in-water emulsion, or adsorbed on the solid surface. Bitumen is hydrophobic hydrocarbon material and its contact angle has been reported to be larger than 90° [55,70]. The adsorbed organic matter on the mineral surface influence the wettability of solids [71]. When sufficient amount of asphaltene aggregates adsorb on clay surface, they could change the clay surface from hydrophilic to hydrophobic. So the surface of originally hydrophilic minerals may be altered and become hydrophobic. The question is: are hydrophobic particles easier to filter?

Zhou et al. [55] described the interactions of water with hydrophilic and hydrophobic solid surfaces, as shown in Figure 2-10. Water molecules randomly orientate on the hydrophobic solid surface and have a high mobility because of the weak attraction between the water dipoles and solid surfaces. Therefore the surface water films can be easily removed. Recent research indicated that the more hydrophobic the solid surface, the lower the film drainage resistance and the faster the water flow at the solid surface [72]. From the dynamic viewpoint, water is purely diffusive on the hydrophobic surfaces, with no surface binding and trapping (if smooth). On the other hand, on the hydrophilic surfaces, the binding of water with the solid surface helps to form a water layer of ordered structures which are rigid and difficult to remove. Transient binding of water with the hydrophilic surface can cause the apparent surface viscosity to increase [73], hindering water flow and water film removal. Fleys [74] showed that the confinement in hydrophobic pores enhanced the water transportation rate than the hydrophilic pores.

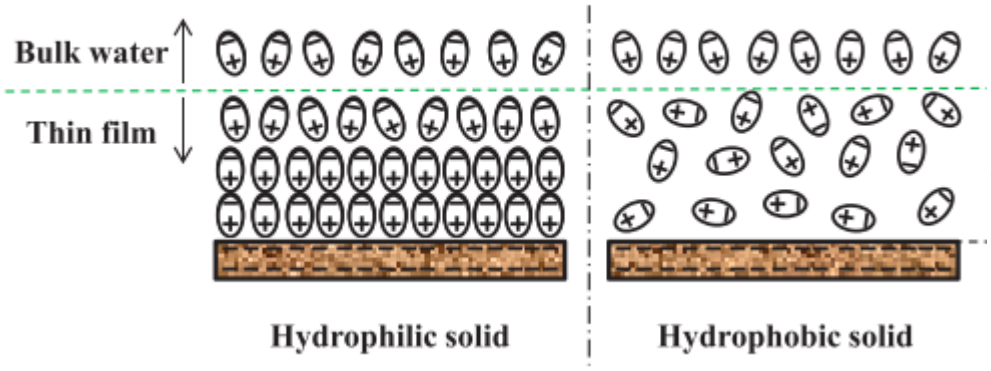


Figure 2-10 The schematics of water dipole orientation on the hydrophilic and hydrophobic solid surface [55].

Researchers have devoted significant effort to look for the optimum polymer flocculants or chemicals that can lead to efficient dewatering and consolidation of MFT to eliminate tailings ponds. Hripko et al. [75] found that hydrophobically modified polyacrylamide copolymers dewatered MFT more effectively than polyacrylamide only. They demonstrated that grafting more than 30 wt% hydrophobic chains to PAM effectively improved the dewatering performance, evaluated by CST and initial settling rate (ISR). Li et al. [62] and Zhang et al. [76] used temperature sensitive poly(n-isopropyl acrylamide) (PNIPAM) and copolymer poly(AEMA-st-NIPAm) to flocculate and dewater a MFT sample by changing the temperature to alter the hydrophilicity and hydrophobicity of the polymers. They reported that these polymers work better than commercial PAM, judging by the measured supernatant clarity and sediment solid contents. Also, pH-sensitive, temperature-responsive, or $CO_2$-switchable polymer flocculants were used to dewater MFT [77]. The basic principle of these polymers are the same (i.e., the hydrophobicity and hydrophilicity can be changed by a change in pH, temperature, or the presence/absence of $CO_2$) and the dewatering performance improved compared with PAM. Gumfekar et al. [77] and Hripko et al. [75] concentrated on the hydrophobicity alteration of polymer flocculants such as hydrophobically modified polyacrylamide copolymers, degradable polymer flocculants, and hydrolytically-degradable polymer [78] in the past several years. The degradable polymers increased the hydrophobicity of the polymer through hydrolysis without the need of an external trigger. The resulting polymers caused a drop of CST by 85% when used to treat dilute MFT.

On the other hand, there were also reports that hydrophobicity of particles had little effect on dewatering. Chen et al. [79] studied the filterability of kaolinite with different degrees of asphaltene surface coverage. The hydrophobicity of kaolinite particles increased (contact angle

increasing from 15-102°) with the increase of asphaltene surface coverage (0-41%). But the filtration time had not significantly changed with the increasing surface coverage of asphaltene. Condie and Veal [80] reported that a change of surface tension of filtrate and water-air-coal three-phase contact angle had a minor effect on the reduction of cake moisture when the coal sample was dewatered by vacuum filtration. Hripko et al. [75] studied the role of hydrophobic particles on the stability of oil sands tailings and found that the settling performance improved after removing bitumen and hydrophobic solid particles. These contradict the review results described in the previous paragraph. Therefore, the effect of particle surface hydrophobicity on dewatering, and the effect of bitumen on particle surface hydrophobicity still need to be studied under well-controlled conditions to decouple these effects.

**References**


[1] Osacky M, Geramian M, Ivey DG, Liu Q, Etsell TH. Mineralogical and chemical composition of petrologic end members of Alberta oil sands. Fuel 2013;113:148–57. https://doi.org/10.1016/j.fuel.2013.05.099.

[2] Ignasiak TM. Separation and characterization of clay from Athabasca asphaltene 1983;62:353–62.

[3] Botha L, Soares JBP. The Influence of Tailings Composition on Flocculation. Can J Chem Eng 2015;93:1514–23. https://doi.org/10.1002/cjce.22241.

[4] Kaminsky HAW, Etsell TH, Ivey DG, Omotoso O. Distribution of clay minerals in the process streams produced by the extraction of bitumen from athabasca oil sands. Can J Chem Eng 2009;87:85–93. https://doi.org/10.1002/cjce.20133.

[5] Cloutis EA, Gaffey MJ, Moslow TF. Characterization of minerals in oil sands by

reflectance spectroscopy 1994.

[6] Omotosoa O, Mikulaa R, Urquhartb S, Sulimmab H, Stephensc P. Characterization of Clays from Poorly Processing Oil Sands using Synchrotron Techniques. Clay Sci 2006;12:88–93.

[7] Gupta SK, Gartley MG. XRD analysis of illite-smectite interstratification in clays from oil sands ores. Adv. X-ray Anal., vol. 62, 1999, p. 22–31.

[8] Osacky M, Geramian M, Dyar MD, Sklute EC, Valter M, Ivey DG, et al. Characterisation of petrologic end members of oil sands from the athabasca region, Alberta, Canada. Can J Chem Eng 2013;91:1402–15. https://doi.org/10.1002/cjce.21860.

[9] Poon HY, Cossey HL, Balaberda A lynne, Ulrich AC. The role of carbonate mineral dissolution in turbidity reduction in an oil sands end pit lake. Chemosphere 2021;271:129876. https://doi.org/10.1016/j.chemosphere.2021.129876.

[10] Liu X, Yan W, Stenby EH, Thormann E. Release of Crude Oil from Silica and Calcium Carbonate Surfaces: On the Alternation of Surface and Molecular Forces by High- and Low-Salinity Aqueous Salt Solutions. Energy and Fuels 2016;30:3986–93. https://doi.org/10.1021/acs.energyfuels.6b00569.

[11] COSIA. Tailings clay chanllenge. 2017. https://doi.org/https://cosia.ca/sites/default/files/attachments/COSIA%20Challenge%20Tailings%20-%20Tailings%20Clay%20Challenge_0.pdf.

[12] Mohammad Ali Hooshiar Fard. Characterization of Clay Minerals in the Athabasca Oil

Sands in Water Extraction and Nonaqueous Solvent Extraction Processes. University of Alberta, 2011.

[13] Kotlyar LS. Effect of Particle Size on the Flocculation Behaviour of Ultra-Fine Clays in Salt Solutions. Clay Miner 1998;33:103–7. https://doi.org/10.1180/claymin.1998.033.1.10.

[14] Kotlyar LS, Deslandes Y, Sparks BD, Kodama H, Schutte R. Characterization of colloidal solids from Athabasca fine tails. Clays Clay Miner 1993;41:341–5. https://doi.org/10.1346/CCMN.1993.0410309.

[15] Kotylar LS, Sparks BD, Schutte R. Effect of salt on the flocculation behavior of nano particles in oil sands fine tailings. Clays Clay Miner 1996;44:121–31. https://doi.org/10.1346/CCMN.1996.0440111.

[16] Schoonheydt RA, Johnston CT. Chapter 3 Surface and Interface Chemistry of Clay Minerals. Handb. Clay Sci. Clay Sci., vol. 1, 2006, p. 87–113. https://doi.org/10.1016/S1572-4352(05)01003-2.

[17] Many CM. Chapter 15 - trioctahedral 1:1 clay minerals. Chem. Clay Miner., 1962, p. 159–67.

[18] Masliyah JH, Czarnecki J, Xu Z. Handbook on Theory and Practiceon Bitumen Recovery from Athabasca Oil Sands. 2011. https://doi.org/https://doi.org/10.7939/r3-nr43-8t34.

[19] Brigatti MF, Galan E, Theng BKG. Chapter 2 Structures and Mineralogy of Clay Minerals. Handb. Clay Sci., vol. 1, 2006, p. 19–86. https://doi.org/10.1016/S1572-

4352(05)01002-0.

[20] Środoń J. Chapter 12.2 Identification and Quantitative Analysis of Clay Minerals. Handb. Clay Sci. Clay Sci., vol. 1, 2006, p. 765–87. https://doi.org/10.1016/S1572-4352(05)01028-7.

[21] Geramian M, Osacky M, Ivey DG, Liu Q, Etsell TH. Effect of Swelling Clay Minerals (Montmorillonite and Illite-Smectite) on Nonaqueous Bitumen Extraction from Alberta Oil Sands. Energy and Fuels 2016;30:8083–90. https://doi.org/10.1021/acs.energyfuels.6b01026.

[22] Pham Thi，Hang, G. W. Brindley. Methylene Blue Absorption by Montmorillonites. Determinations of Surface Areas and Exchange Capacities with Different Initial Cation Saturations (Clay-Organic Studies XIX). Isr J Chem 1970;8:409–15. https://doi.org/10.1002/ijch.197000047.

[23] Chen Q, Liu Q. Bitumen Coating on Oil Sands Clay Minerals: A Review. Energy and Fuels 2019;33:5933–43. https://doi.org/10.1021/acs.energyfuels.9b00852.

[24] Kuh SE, Kim DS. Effects of surface chemical and electrochemical factors on the dewatering characteristics of fine particle slurry. J Environ Sci Heal - Part A Toxic/Hazardous Subst Environ Eng 2004;39:2157–82. https://doi.org/10.1081/ESE-120039382.

[25] Senft D, Masala S, Nik Klohn Crippen Berger R, Scott Martens C, Esposito G, Eaton T. Comparison of particle size distributions obtained by laser diffraction and sieve-hydrometer methods for oil sand tailings. Geotech. Conf., 2011.

[26] Beier N, Wilson W, Dunmola A, Sego D. Impact of flocculation-based dewatering on the shear strength of oil sands fine tailings. Can Geotech J 2013;50:1001–7. https://doi.org/10.1139/cgj-2012-0262.

[27] Kaminsky H, Etsell T, Ivey DG, Omotoso O. Fundamental particle size of clay minerals in athabasca oil sands tailings. Clay Sci 2006;12:217–22. https://doi.org/10.11362/jcssjclayscience1960.

[28] Kotlyar LS, Sparks BD, Woods J, Capes CE, Schutte R. Biwetted ultrafine solids and structure formation in oil sands fine tailings. Fuel 1995;74:1146–9. https://doi.org/10.1016/0016-2361(95)00064-C.

[29] Tu Y, O'Carroll JB, Kotlyar LS, Sparks BD, Ng S, Chung KH, et al. Recovery of bitumen from oilsands: gelation of ultra-fine clay in the primary separation vessel. Fuel 2005;84:653–60. https://doi.org/10.1016/J.FUEL.2004.03.020.

[30] Majid A, Argue S, Boyko V, Pleizier G, L'Ecuyer P, Tunney J, et al. Characterization of sol-gel-derived nano-particles separated from oil sands fine tailings. Colloids Surfaces A Physicochem Eng Asp 2003;224:33–44. https://doi.org/10.1016/S0927-7757(03)00266-8.

[31] Mercier PHJ, Patarachao B, Kung J, Kingston DM, Woods JR, Sparks BD, et al. X-ray Diffraction (XRD)-Derived Processability Markers for Oil Sands Based on Clay Mineralogy and Crystallite Thickness Distributions. Energy and Fuels 2008;22:3174–93. https://doi.org/10.1021/EF8002203.

[32] Murray H. Structure and composition of the clay minerals and their physical and chemical. Clay Miner., 1997, p. 7–31.

[33] Omotoso OE, Mikula RJ. High surface areas caused by smectitic interstratification of kaolinite and illite in Athabasca oil sands. Appl Clay Sci 2004;25:37–47. https://doi.org/10.1016/j.clay.2003.08.002.

[34] Rao SR. Flocculation and dewatering of Alberta oil sands tailings. Int J Miner Process 1980;7:245–53. https://doi.org/10.1016/0301-7516(80)90020-4.

[35] Liu J, Xu Z, Masliyah J. Role of fine clays in bitumen extraction from oil sands. AIChE J 2004;50:1917–27. https://doi.org/10.1002/aic.10174.

[36] Osacky M, Geramian M, Liu Q, Ivey DG, Etsell TH. Surface properties of petrologic end-members from alberta oil sands and their relationship with mineralogical and chemical composition. Energy and Fuels 2014;28:934–44. https://doi.org/10.1021/ef402150z.

[37] Basnayaka L, Subasinghe N, Albijanic B. Influence of clays on fine particle filtration. Appl Clay Sci 2018;156:45–52. https://doi.org/10.1016/J.CLAY.2018.01.008.

[38] Ottley DJ. Gravity Concentration In Modern Mineral Processing. 1986. https://doi.org/10.1007/978-94-009-4476-3_11.

[39] Wright HJL, Kitchener JA. The problem of dewatering clay slurries: Factors controlling filtrability. J Colloid Interface Sci 1976;56:57–63. https://doi.org/10.1016/0021-9797(76)90146-6.

[40] D.R., Nagaraj, P., Somasundaran, L., McAllister. Subsidence of suspensions of phosphatic slime and its major constituents. Int J Miner Process 1977;4:111–29. https://doi.org/https://doi.org/10.1016/0301-7516(77)90020-5.

[41] J.V., O'Gorman, J.A., Kitchener. The flocculation and de-watering of kimberlite clay slimes. Int J Miner Process 1974;1:33–49. https://doi.org/https://doi.org/10.1016/0301-7516(74)90025-8.

[42] Camp FW. Processing athabasca tar sands — tailings disposal. Can J Chem Eng 1977;55:581–91. https://doi.org/10.1002/cjce.5450550516.

[43] Kessick MA. Structure and properties of oil sands clay tailings. J Can Pet Technol 1979:49–52. https://doi.org/10.2118/79-01-01.

[44] Sworska A, Laskowski JS, Cymerman G. Flocculation of the Syncrude fine tailings Part I. Effect of pH, polymer dosage and Mg2+ and Ca2+ cations. Int J Miner Process 2000;60:143–52. https://doi.org/10.1016/S0301-7516(00)00012-0.

[45] Babu DR, Cormack DE. Effect of low-temperature oxidation on the composition of Athabasca bitumen. Fuel 1984;63:858–61. https://doi.org/10.1016/0016-2361(84)90080-2.

[46] Meyer R. The Petroleum System- Status of Research and Methods. 2003.

[47] Gray MR. Upgrading oilsands bitumen and heavy oil. 2015.

[48] Adams JJ. Asphaltene adsorption, a literature review. Energy and Fuels 2014;28:2831–56. https://doi.org/10.1021/ef500282p.

[49] Gray MR, Jokuty P, Yeniova H, Nazarewycz L, Wanke SE, Achia U, et al. The relationship between chemical structure and reactivity of alberta bitumens and heavy oils. Can J Chem Eng 1991;69:833–43. https://doi.org/10.1002/CJCE.5450690404.

[50] Gray MR, Tykwinski RR, Stryker JM, Tan X. Supramolecular assembly model for

aggregation of petroleum asphaltenes. Energy and Fuels 2011;25:3125–34. https://doi.org/10.1021/ef200654p.

[51] Pernyeszi T, Patzkó Á, Berkesi O, Dékány I. Asphaltene adsorption on clays and crude oil reservoir rocks. Colloids Surfaces A Physicochem Eng Asp 1998;137:373–84. https://doi.org/10.1016/S0927-7757(98)00214-3.

[52] Bensebaa F, Kotlyar LS, Sparks BD, Chung KH. Organic coated solids in Athabasca bitumen: Characterization and process implications. Can J Chem Eng 2000;78:610–6. https://doi.org/10.1002/cjce.5450780402.

[53] Chen Q, Liu J, Thundat T, Gray MR, Liu Q. Spatially resolved organic coating on clay minerals in bitumen froth revealed by atomic force microscopy adhesion mapping. Fuel 2017;191:283–9. https://doi.org/10.1016/j.fuel.2016.11.091.

[54] Kotlyar LS, Ripmeester JA, Sparks BD, Montgomery DS. Characterization of oil sands solids closely associated with Athabasca bitumen. Fuel 1988;67:808–14. https://doi.org/10.1016/0016-2361(88)90155-X.

[55] Zhou J, Li H, Zhao L, Chow R. Role of Mineral Flotation Technology in Improving Bitumen Extraction from Mined Athabasca Oil Sands: I. Flotation Chemistry of Water-Based Oil Sand Extraction †. Can J Chem Eng 2018;96:1986–99. https://doi.org/10.1002/cjce.23139.

[56] Xiaoli Tan QL. Two-stage chemicals treatment for tailings slurry dewatering. Final Proj Rep 2016.

[57] Scott J., Dusseault MB, Carrier WD. Behaviour of the clay/bitumen/water sludge system

from oil sands extraction plants. Appl Clay Sci 1985;1:207–18. https://doi.org/10.1016/0169-1317(85)90574-5.

[58] Azizov I, Dudek M, Øye G. Studying droplet retention in porous media by novel microfluidic methods. Chem Eng Sci 2022;248:117152. https://doi.org/10.1016/J.CES.2021.117152.

[59] Klein C, Harbottle D, Alagha L, Xu Z. Impact of fugitive bitumen on polymer-based flocculation of mature fine tailings. Can J Chem Eng 2013;91:1427–32. https://doi.org/10.1002/cjce.21863.

[60] Suthaker NN, Scott. JD. Measurement of hydraulic conductivity in petroleum sand tailings slurries. Can Geotech J 1996;33:642–53.

[61] Chalaturnyk RJ, Scott JD, Özüm B. Management of oil sands tailings. Pet Sci Technol 2002;20:1025–46. https://doi.org/10.1081/LFT-120003695.

[62] Li H, Zhou J, Chow R, Adegoroye A, Najafi AS. Enhancing treatment and geotechnical stability of oil sands fine tailings using thermo-sensitive poly(n-isopropyl acrylamide). Can J Chem Eng 2015;93:1780–6. https://doi.org/10.1002/CJCE.22276.

[63] Reis LG, Oliveira RS, Palhares TN, Spinelli LS, Lucas EF, Vedoy DRL, et al. Using acrylamide/propylene oxide copolymers to dewater and densify mature fine tailings. Miner Eng 2016;95:29–39. https://doi.org/10.1016/j.mineng.2016.06.005.

[64] Vajihinejad V, Guillermo R, Soares JBP. Dewatering Oil Sands Mature Fine Tailings (MFTs) with Poly(acrylamide-co-diallyldimethylammonium chloride): Effect of Average Molecular Weight and Copolymer Composition. Ind Eng Chem Res

2017;56:1256–66. https://doi.org/10.1021/acs.iecr.6b04348.

[65] Gumfekar SP, Vajihinejad V, Soares JBP. Advanced Polymer Flocculants for Solid–Liquid Separation in Oil Sands Tailings. Macromol Rapid Commun 2019;40:1–18. https://doi.org/10.1002/marc.201800644.

[66] Kotlyar LS, Sparks BD, Woods JR, Raymond S, Le Page Y, Shelfantook W. Distribution and types of solids associated with bitumen. Pet Sci Technol 1998;16:1–19. https://doi.org/10.1080/10916469808949769.

[67] Zhu Y. Cationic and Anionic Dual Polymer Pairs for Mature Fine Tailings Flocculation and Dewatering 2015.

[68] Loerke RS. Pressure Filtration of Mature Fine Tailings. University of Alberta, 2016.

[69] Loerke R, Tan X, Liu Q. Dewatering of Oil Sands Mature Fine Tailings by Dual Polymer Flocculation and Pressure Plate Filtration. Energy and Fuels 2017;31:6986–95. https://doi.org/10.1021/acs.energyfuels.7b00938.

[70] Salou M, Si B, Jada A. Study of the stability of bitumen emulsions by application of DLVO theory 1998;142:9–16.

[71] Darcovich K, Kotlyar LS, Tse WC, Ripmeester JA, Capes CE, Sparks BD. Wettability Study of Organic-Rich Solids Separated from Athabasca Oil Sands. Energy and Fuels 1989;3:386–91. https://doi.org/10.1021/ef00015a023.

[72] Ivanova NO, Xu Z, Liu Q, Masliyah JH. Surface forces in unconventional oil processing. Curr Opin Colloid Interface Sci 2017;27:63–73. https://doi.org/10.1016/j.cocis.2016.09.013.

[73] Sendner C, Horinek D, Bocquet L, Netz RR. Interfacial Water at Hydrophobic and Hydrophilic Surfaces : Slip , Viscosity , and Diffusion 2009;25:10768–81. https://doi.org/10.1021/la901314b.

[74] Fleys M. Water behavior in hydrophobic porous materials. Comparison between Silicalite and Dealuminated zeolite Y by Molecular Dynamic Simulations. Worcester Polytechnic Institute, 2003.

[75] Hripko R, Vajihinejad V, LopesMotta F, Soares JBP. Enhanced Flocculation of Oil Sands Mature Fine Tailings Using Hydrophobically Modified Polyacrylamide Copolymers. Glob Challenges 2018;2:1700135. https://doi.org/10.1002/gch2.201700135.

[76] Zhang D, Thundat T, Narain R. Flocculation and dewatering of mature fine tailings using temperature-responsive cationic polymers. Langmuir 2017;33:5900–9. https://doi.org/10.1021/acs.langmuir.7b01160.

[77] Gumfekar SP, Rooney TR, Hutchinson RA, Soares JBP. Dewatering Oil Sands Tailings with Degradable Polymer Flocculants. ACS Appl Mater Interfaces 2017;9:36290–300. https://doi.org/10.1021/acsami.7b10302.

[78] Younes GR, Proper AR, Rooney TR, Hutchinson RA, Gumfekar SP, Soares JBP. Structure Modifications of Hydrolytically-Degradable Polymer Flocculant for Improved Water Recovery from Mature Fine Tailings. Ind Eng Chem Res 2018;57:10809–22. https://doi.org/10.1021/acs.iecr.8b02783.

[79] Chen Q. Organically-Modified Clay Minerals in Oil Sands: Characterization and Effect of Hydrothermal Treatment. University of Alberta, 2017.

[80] Condie DJ, Veal CJ. Modeling the Vacuum Filtration of Fine Coal : Part 2. Filtaration&Separation 1997;2:957–63.

# CHAPTER 3 The Filterability of Different Types of Minerals and the Role of Swelling Clays in the Filtration of Oil Sands Tailings

## 3.1 Introduction

With 165.4 billion barrels of proven reserve, Canada's oil sands resource in the province of Alberta is the third largest crude oil reserve after Venezuela and Saudi Arabia [1]. The surface mining and bitumen extraction from the oil sands is the largest earth-moving operation in the world. Bitumen extraction by warm water is the current commercial technology to recover bitumen from the surface-mined oil sands [2]. After removing bitumen, the waste stream is discharged into tailings ponds to settle. While the coarse sands settle quickly, the fine clays and residual bitumen settle extremely slowly, form so-called mature fine tailings (MFT) that contain 30-40 wt% fine solids and 1-3 wt% residual bitumen, and take several decades to release the trapped process water. The long impoundment time has caused a rapid increase in the tailings pond area as a result of the increasing oil sands production, reaching 178 $km^2$ in 2010, and nearly 250 $km^2$ by 2015, about twice the size of the city of Vancouver, BC [3]. The tailings contain toxic and harmful chemicals that pose risks to the waterfowl. Other problems such as fugitive carbon emission and groundwater pollution by the tailings ponds have also been ongoing concerns [4]. The oil sands industry is facing increasing pressure from both the public and the regulators for the environmental impacts it causes.

Many of the mineral slurries, including oil sands tailings and other mine tailings, are found to be slow to settle and difficult to consolidate [5–7]. Mineralogical analysis showed that the solid phase in oil sands MFT contained quartz, kaolinite, illite, K-feldspar, minor amount of montmorillonite, interstratified illite-smectite and kaolinite-smectite [8,9,18,19]. Most researchers considered the presence of clays in tailings to be the reason for the challenging

dewatering problem [10–13]. For example, a fresh coal mine tailings contained almost 28% fine particles with size less than 4 μm [14], and more than 34% of a copper mine tailings solids were reported to be less than 1 μm in size [15]. Typically, the 30-40% clay minerals in the oil sands MFT were thought to be responsible for the difficult dewatering due to their fine particle size [6,16–18]. Indeed, the particle size of minerals was reported to affect the viscosity of oil sands slurry, and the fine solids in MFT showed high gelling tendency at a low weight fraction [16]. Some specific mineral types, such as illite and kaolinite interstratified with swelling clays, were reported to contribute to the high surface area of MFT [19,20]. Research shows that montmorillonite can form stable gels even at very low concentrations, and the montmorillonite in the tailings was expected to contribute to the water-retaining properties and hamper dewatering of oil sands tailings [21]. However, there has been no controlled experiments and analyses of the effects of different types of minerals in the oil sands tailings on their dewatering behavior. The mainstream methods are to test different polymer flocculants and/or coagulants followed by some form of mechanical treatments. These somewhat blind trials have not been able to identify effective amendment chemicals, leading to the perception that there is no "silver bullet" for oil sands tailings treatment.

The composition of the solid phase in oil sands MFT is complicated, and it is impractical to segregate the different minerals and treat them separately. Kaolinite or quartz suspensions were often used as model minerals to represent the oil sands tailings, and their filterability was found to be much higher than MFT at the same solid concentration [22,23]. However, when an ultrafine fraction from MFT, dubbed "middle layer" after centrifuging the MFT at 17300 RCF for 3 hours, was added to the kaolinite slurry to reach the same bitumen content as MFT, the kaolinite slurry became unfilterable unless 10 times more of the polymer flocculants were

added [22]. This was attributed to the residual bitumen introduced to the kaolinite slurry by the "middle layer".

We recently found that when the centrifuged MFT middle layer was washed repeatedly with toluene to remove the bitumen, its detrimental effect on kaolinite slurry filtration remained and only changed slightly. Therefore, it was inferred that the fine solids contained in the middle layer may be the more important determining factor for MFT filtration. The solids in the middle layer were analyzed by X-ray diffraction which revealed quartz, kaolinite, and montmorillonite as the main constituent minerals. In order to decouple the roles of residual bitumen and these ultrafine minerals, this chapter focuses on the effects of different types of minerals on filtration, and the effects of residual bitumen on filtration are reported in Chapters 4 and 5.

The clay minerals are divided into non-swelling and swelling clays. The interlayer exchangeable cations in the swelling clays have a tendency to hydrate, forcing clay layers apart, and the interlayer would expand by the adsorption of a suitable solvent [24–26]. In this work, rutile, quartz, kaolinite, illite, illite-smectite, and montmorillonite were chosen as model minerals to investigate the filterability of the non-clay minerals (quartz, rutile), non-swelling clays (kaolinite, illite), and swelling clays (illite-smectite, montmorillonite). Sub-micron rutile was chosen to test the effect of particle size on filterability, and the other five minerals were chosen because they were commonly found in the oil sands tailings [27,28].

## 3.2. Materials and Methods

### 3.2.1. Materials

High purity rutile ($TiO_2$, US Research Nanomaterials) and quartz ($SiO_2$ Min-U-Sil 15 from US Silica) were used as non-clay minerals; kaolinite (BASF ASP 600) and illite (Ward's Sciences, USA) were used as non-swelling clays; illite-smectite (from Slovakia), obtained from the clay

mineral repository of the Clay Minerals Society, and montmorillonite (Ward's Sciences, USA) were used as representative swelling clays. While the other minerals were received in powder form, illite and illite-smectite were received as rock pieces. They were crushed with a hammer, ground manually with an agate mortar and pestle, followed by grinding in a Fritsch Pulverisette 6 mechanical agate mortar/pestle mill (Fritsch GmbH, Germany). The mechanical mortar/pestle grinding was performed in 1 hour batches of 10 g samples each batch to obtain the desired particle size of the illite and illite-smectite minerals. The ground samples in each batch were combined and homogenized prior to use.

A mature fine tailings (MFT) sample was collected in 2017 from the tailings ponds of an oil sands operator in northern Alberta, Canada. The MFT sample was treated by the Dean-Stark procedure and was found to contain 31.8 wt% minerals, 3.1 wt% bitumen, and 65.1 wt% water. The MFT sample after Dean-Stark treatment was used for characterization of the solid phase. Sodium hydroxide (NaOH) and hydrochloric acid (HCl) of analytical grade were purchased from Fisher Scientific and used to adjust the pH of the mineral slurry. Hydrochloric acid was also used to treat montmorillonite sample. Methylene blue (M.W. 373.9 g/mol) was purchased from Sigma-Aldrich and used as the titrant in the methylene blue index (MBI) measurement. Sodium bicarbonate and sulfuric acid were used in the methylene blue titration tests.

### 3.2.2. Vacuum filtration test

The assembled vacuum filtration setup is schematically shown in Figure 3-1. An aliquot of 20 mL mineral slurry, at different solids contents, was used in each filtration test. The filtrate was collected by a plastic tube with graduation markers by which the filtration rate was monitored. Each filtration test was run for 30 mins. The initial negative pressure was set at 1 mbar, but the effective working pressure varied from 30 to 50 mbar depending on the sample being filtered.

The P2 grade paper (Fisher Scientific) with a pore size of 1−5 μm was used as the filter medium, and the total filter area was 9.6 $cm^2$.

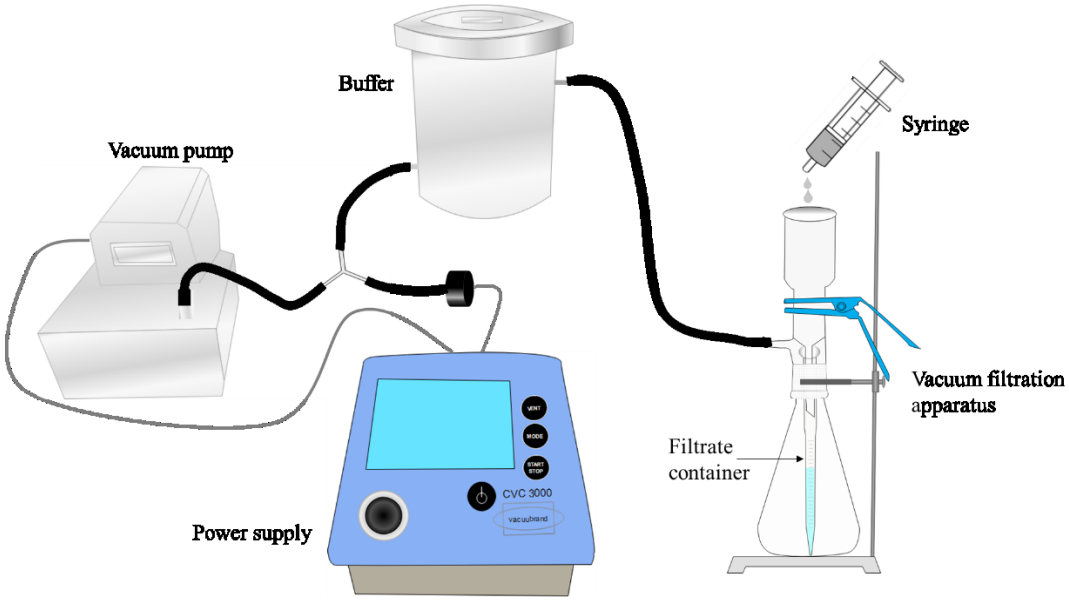


Figure 3-1 Schematic of the vacuum filtration setup

In a typical vacuum filtration test, 40 mL slurry of a mineral sample was prepared by mixing a weighed amount of solids with DI water in a 200 mL beaker. The slurry was stirred by a magnetic stir bar at 800 rpm for 2 mins, then treated in an ultrasonic bath for 3 mins before being stirred for another 5 mins. Afterwards, 20 mL of the prepared slurry was transferred to the filter funnel using a 20 mL syringe, and the filtrate volume was recorded as a function of time at an interval of 1 minute.

The initial filtration rate (IFR), mL/min/$cm^2$, was used as an indicator of the filtration performance. It was calculated by the slope of the filtrate volume versus time plot for the first 5 data points. For the mineral slurry with little collected filtrates, the filtration rate was

calculated by the final filtrate volume divided by the total filtration time (30 min). Therefore, in this case it was an average filtration rate. But for simplicity and consistency the abbreviation IFR was still used for these cases.

### 3.2.3 Capillary suction time (CST) measurements

The capillary suction time (CST) was used to assess the easiness of water flow through the slurries and was measured using a Type 319 Multi-Purpose Capillary Suction Timer (Triton Electronics Ltd., U.K.). The CST was the time for the seepage water to spread from the first electrical contact to the second contact, separated by 6 mm. The sample preparation procedure was the same as that used for the vacuum filtration test. For each test, 5 mL of the prepared mineral slurry was transferred to the sample cell with a syringe, and the CST was recorded. Each test was repeated 4 times and the average was reported.

### 3.2.4. Analytical instrumentation methods

The elemental compositions of the mineral samples were determined by a Bruker CTX800 X-ray fluorescence analyzer. The samples were dried in an oven at 110°C for 24 h. The dried sample in powder form was placed in the sample cups of the CTX800 for analysis. Table 3-1 shows the chemical composition of the samples and their purity, which was calculated based on the theoretical formula composition. Loss on ignition (LOI) was determined by the weight loss of the samples between 110ºC and 1000ºC and each sample was tested 3 times. It can be seen that the samples were of high purity.

Table 3-1 Chemical composition of the tested mineral samples.

| Sample | Chemical Composition (wt%) | | | | | | | | |
|---|---|---|---|---|---|---|---|---|---|
| | MgO | $Al_2O_3$ | $SiO_2$ | $K_2O$ | Ca | Ti | Fe | LOI | Purity (%) |
| Rutile | 1.77±0.83 | 0.91±0.22 | 0.09±0.07 | 0.05±0.00 | 0.06±0.01 | 52.46±0.12 | 0.02±0.00 | 0.22±0.03 | 88 |
| Quartz | 0.84±0.53 | - | 93.87±0.59 | - | 0.03±0.01 | - | 0.03±0.00 | 0.14±0.08 | 94 |
| Kaolinite | 1.46±0.67 | 37.63±0.52 | 51.56±0.45 | 0.13±0.45 | 0.04±0.02 | 0.99±0.03 | 0.49±0.01 | 13.72±0.05 | 90 |
| Illite | 2.02±0.76 | 18.66±0.39 | 57.12±0.46 | 3.93±0.03 | 0.39±0.03 | 0.59±0.02 | 2.64±0.02 | 7.09±0.08 | 80 |
| Illite-Smectite | 3.00±0.69 | 15.59±0.35 | 59.42±0.56 | 3.61±0.03 | 0.19±0.02 | 0.06±0.01 | 0.62±0.01 | 4.55±0.07 | 97 |
| Montmorillonite | 3.03±0.73 | 16.16±0.35 | 56.26±0.45 | 0.41±0.01 | 0.97±0.04 | 0.08±0.01 | 3.21±0.02 | 14.19±0.04 | 84 |
| MFT | 1.15±0.70 | 16.80±0.37 | 52.55±0.44 | 1.81±0.02 | 0.64±0.03 | 0.80±0.02 | 3.41±0.02 | - | - |

The X-ray diffraction (XRD) patterns of the samples were recorded on a Rigaku Ultima IV diffractometer using Cu Kα radiation (40kV, 44mA, FT mode), in the 2θ range of 1–30° with a step size of 0.02° 2θ and a counting time of 1 s. Samples were prepared by the preferred orientation preparation method, and the procedures were as follows: about 150 mg oven-dried mineral sample was dispersed in 2 mL distilled water followed by ultrasonic treatment for 5 mins. The mixture was pipetted onto a glass slide and left to dry in a fume hood. Clay samples were also prepared by ethylene glycol (EG) treatment. For this purpose, the previously oven-dried sample was placed in a desiccator over ethylene glycol, and left in an oven at 60°C for 12 h. The EG treated clay samples were analyzed by XRD using the same preferred orientation sampling method. The XRD patterns of the tested mineral samples are shown in Figure 3-2. All the XRD measurements for the clay minerals were repeated twice and similar XRD patterns were observed in both measurements.

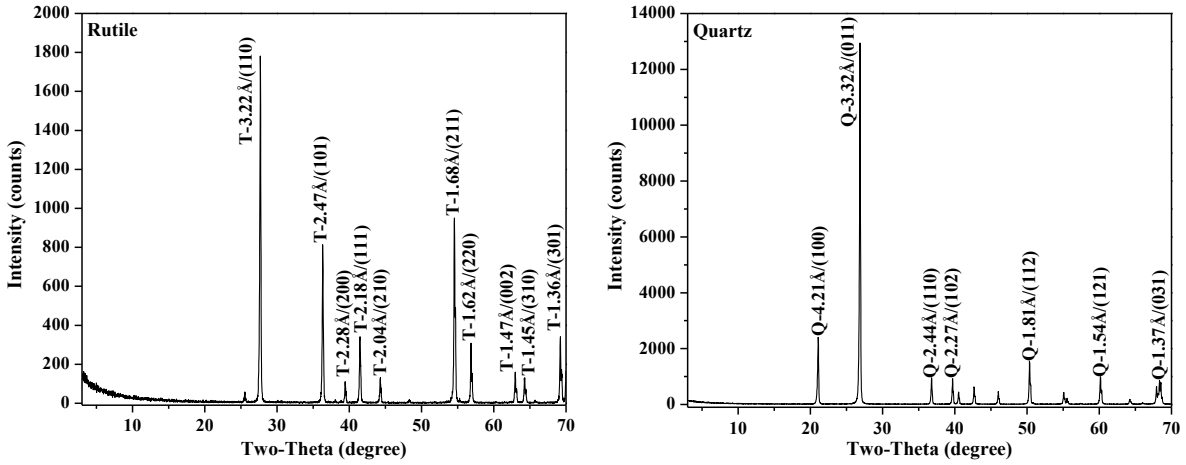

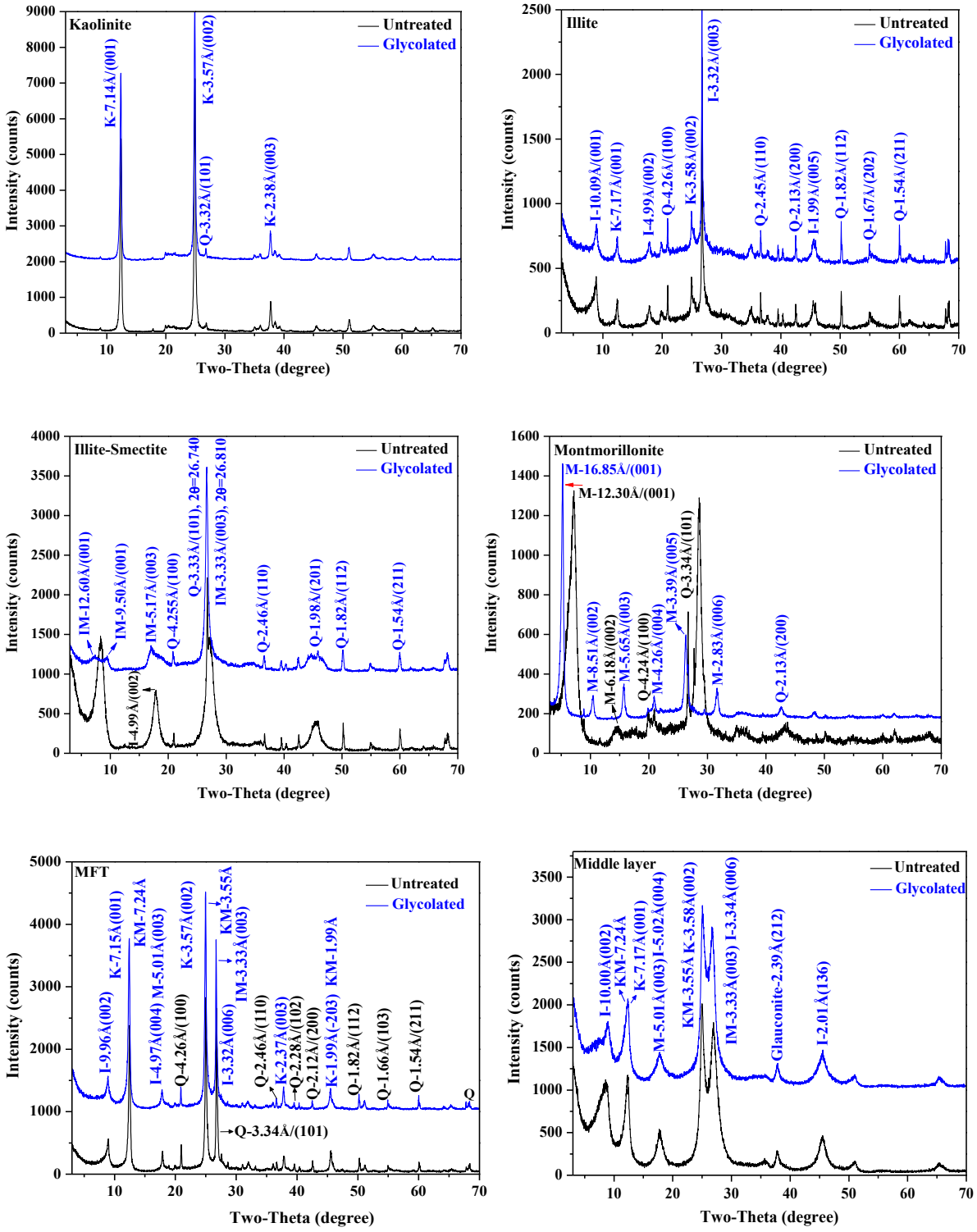


Figure 3-2 The XRD patterns of untreated and glycolated mineral samples, MFT, and a "middle layer" sample that was obtained by centrifuging the MFT at 17300 RCF for one hour.

Figure 3-2 indicates that the relative intensity for clay minerals increased after EG treatment, which may be due to the better orientation of the clay platelets. The EG treated clays had more regular preferred orientation and seemed to also have higher crystallinity than the untreated ones. For montmorillonite, in addition to the intensity change, its 001 reflection shifted to a smaller 2θ angle, indicating an increase in the basal spacing after EG treatment. Comparatively, the expansion of interstratification (smectitic layer) in illite-smectite after EG treatment caused a minor shift of the peaks, while the non-swelling clay samples did not show any peak shift after EG treatment. The percentage of the smectitic layer in the illite-smectite was estimated to be larger than 8% using the Kubler index of the illite 001 XRD reflection [29,30]. XRD analysis showed that the main minerals in the MFT and "middle layer" product of the centrifuged MFT were quartz, kaolinite, illite, kaolinite-montmorillonite (KM), and illite-montmorillonite (IM). The presence of swelling clays (montmorillonite, kaolinite-montmorillonite and illite-montmorillonite) was more readily seen in the XRD patterns of the centrifuge "middle layer" sample, clearly due to the enrichment of these clays in the "middle layer" product after the high-speed centrifugation.

The particle size distribution of the mineral samples was measured using a Malvern Mastersizer 3000 particle size analyzer. For each measurement, the sample was slurried in DI water at 3 wt% solids and agitated with a magnetic stir bar at 800 rpm for 2 mins. This was followed by 5 min ultrasonic treatment and another 3 min of stirring before the measurement.

The specific surface area of the sample was measured by an Autosorb Quantachrome 1 MP gas sorption analyzer using nitrogen gas adsorption, and the specific surface area was calculated by the Brunauer-Emmett-Teller (BET) method in the relative pressure range of $P/P^{\circ}$ = 0.05 to 0.3. For this measurement, a proper amount of sample was weighed accurately and

loaded to the sample cell. The sample was outgassed for 2 hours and weighed again, then loaded to the equipment for nitrogen adsorption measurement.

Methylene blue index (MBI) of the mineral samples was determined by titration. Methylene blue (MB) trihydrate (M.W. 373.9 g/mol) was used as the titrant. A 6 mM MB solution was prepared by dissolving 1.1218 g MB trihydrate in 500 mL deionized water in a 1 L polycarbonate bottle. For the titration test, a weighed quantity of dried fine solids was mixed with 50 mL 0.015 M $NaHCO_3$ in a 250 mL polycarbonate bottle (sodium bicarbonate was used as the dispersing aid). After adjusting the pH to 10-10.5, the sample was stirred with a magnetic stir bar for 10 mins at 800 rpm, and treated in an ultrasonic bath for another 15 mins to fully disperse the sample. The treated sample was placed on a magnetic stirrer plate, set underneath the titrating burette, and stirred at 500 rpm for the entire titration process. A 10 wt% $H_2SO_4$ solution was added to acidify the suspension to pH 2.5-3, and the suspension was titrated with the 6 mM MB solution in 1 mL increment initially, and 0.5 mL increment when it was close to the endpoint. After each addition of the MB solution, one drop of the slurry sample was deposited on a piece of Whatman 41 ashless filter paper to observe the appearance of a light blue halo around the drop. The titration was continued until such a light blue halo was observed (2-3 drops of MB solutions were added to verify this endpoint). The MBI measurement experiment was carried out in triplicates. The MBI was calculated by the following equation:

$$\text{MBI}\left(\frac{meq}{100g}\right) = \frac{Volume\ of\ MB \times Normality\ of\ MB}{Mass\ of\ dry\ sample} \times 100 \qquad 3.1$$

The normality of MB is 6 meq/L. As can be seen, the MBI is a measure of the cationic exchange capacity (CEC) of the tested samples. The specific surface area was calculated as [31],

$$\text{Specific Surface Area (SSA)}\left(\frac{m^2}{g}\right) = \text{MBI} \times 130 \times 0.06022 \qquad 3.2$$

### 3.3. Results and Discussion

#### 3.3.1. Properties of the tested minerals

##### 3.3.1.1. Particle size distribution and specific surface area

Figure 3-3 and Table 3-2 shows the particle size distribution of the six mineral samples. All the particle size distribution measurements were carried out in triplicates and the standard deviation was reported in Table 3-2. As can be seen, the rutile sample had a medium size $d_{50}$ of 0.7 μm while the other five mineral samples were coarser with $d_{50}$ between 2.7 and 4.1 μm. The particle sizes of these five mineral samples were on par with the previous centrifuged "middle layer" sample from MFT, and was about half of the medium size of typical MFT samples. Therefore, the particle sizes of the mineral samples were appropriate to study their filtration behaviors related to oil sands tailings.

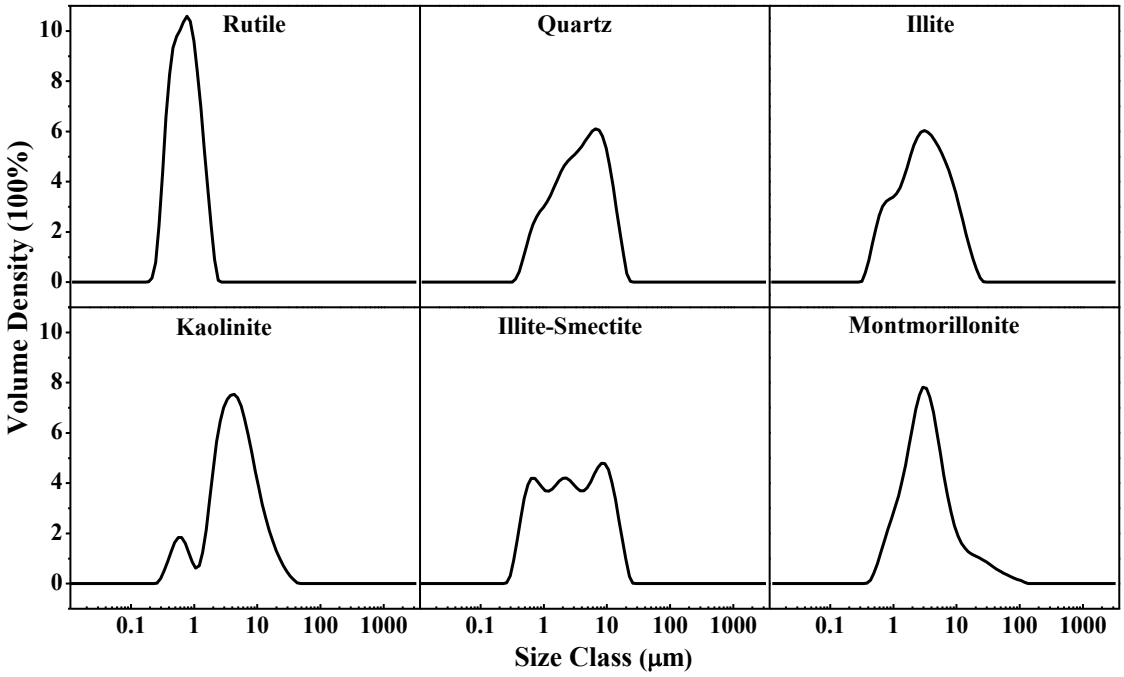


Figure 3-3 The particle size distribution of rutile, quartz, kaolinite, illite, illite-smectite, and montmorillonite.

Table 3-2 The particle size distribution and specific surface area (SSA) of tested mineral samples.

| Sample | Representative particle size, μm | | | BET SSA | MBI SSA | Calculated SSA* |
|---|---|---|---|---|---|---|
| | $d_{10}$ | $d_{50}$ | $d_{90}$ | $m^2/g$ | $m^2/g$ | $m^2/g$ |
| Rutile | 0.34±0.03 | 0.66±0.03 | 1.28±0.21 | 5.63 | 0.37±0.23 | 2.03 |
| Quartz | 0.86±0.02 | 3.64±0.04 | 10.60±0.05 | 2.98 | 1.88±0.47 | 0.63 |
| Kaolinite | 1.01±0.04 | 4.14±0.05 | 11.90±0.12 | 15.56 | 37.19±1.00 | 0.55 |
| Illite | 0.72±0.03 | 2.83±0.21 | 9.29±0.80 | 40.51 | 117.70+8.34 | 0.81 |
| Illite-Smectite | 0.58±0.02 | 2.67±0.06 | 11.50±0.41 | 51.66 | 194.74±0.97 | 0.84 |
| Montmorillonite | 0.99±0.20 | 2.83±0.10 | 11.10±0.23 | 16.95 | 642.19±9.39 | 0.81 |
| MFT | 1.29±0.01 | 8.35±0.07 | 32.8±0.49 | 14.19 | 76.94±1.88 | 0.30 |

* Calculated specific surface area of spheres with diameters equal to the $d_{50}$. $SSA=6/(\rho \cdot d_{50})$. $\rho$ is the density of the mineral, $g/m^3$, and $d_{50}$ is medium size in unit of μm.

The specific surface areas (SSA) of the mineral samples were measured by the BET method and are shown in Table 3-2 as BET SSA. As can be seen, kaolinite (15.56 $m^2/g$) had similar BET SSA as montmorillonite (16.95 $m^2/g$), and both minerals had lower BET SSA than illite (40.51 $m^2/g$) and illite-smectite (51.66 $m^2/g$). The last column in Table 3-2 shows the calculated SSA assuming the particles were uniform-sized spheres with diameters equal to the $d_{50}$. It only accounts for the outer surface of the spheres. As can be seen, the measured BET SSA and the calculated SSA for rutile or quartz were on the same order of magnitude and close to each other, likely indicating the absence of fine pores in these minerals, and the discrepancies may be due to the irregular shapes of the samples and the omission of fine particles. However, for the clay minerals, the measured BET SSA was significantly higher than the calculated SSA, indicating that the contribution to the SSA was primarily from the fine

pores in the clay samples. These fine pores would likely contribute to their water-holding capacities during filtration.

Table 3-2 also shows the MBI which was the specific surface area calculated from equation 3.2. Interestingly, the MBI SSA was lower than the BET SSA for the two non-clay minerals (rutile and quartz), but much higher than the BET SSA of clay minerals, particularly the swelling clays. It was clear that during MB titration of the mineral slurries, MB molecules could not only adsorb on external surfaces but also access the interlayer surfaces of the clay minerals. In contrast, in the BET SSA measurements the nitrogen gas molecules may be unable to access the interlayer surfaces of clays when they were dry and outgassed [32]. Therefore, swelling clays such as montmorillonite and smectite showed much higher MBI SSA than BET SSA. Overall, when considering the SSA of clays, the method of MBI would be more reliable than the BET method to reflect the specific surface area of the minerals.

#### 3.3.1.2. Methylene blue index (MBI)

Figure 3-4 shows the MBI of the tested mineral samples. The MB molecules could adsorb on clay minerals by cation exchange so the MBI can be used to indicate the cation exchange capacity (CEC) of the clays [33]. The results show that the MBI (or CEC) of rutile, quartz, and kaolinite were very low, at 0-5 meq/100g. The non-clay minerals (rutile, quartz) have little exchangeable cations on the surface, and kaolinite has low isomorphic substitution [34], thus low MBI. Unlike kaolinite, illite is a 2:1 type clay mineral in which the interlayer was bound together with cations, mainly potassium. The strong interlocking bonds hold the layers together, which prevents water molecules from entering the interlayers. Illite had a higher isomorphic substitution and MBI (15.03 meq/100g) than kaolinite. The swelling clays (illite-smectite, montmorillonite) had a much higher MBI (CEC) than other tested minerals. One reason that

could account for the high MBI (CEC) was the high degrees of isomorphic substitutions in both the tetrahedral and octahedral sheets of the swelling clays. Another main reason is that the delocalized permanent charges in the octahedral sheet allow the compensating ions to drift away from the octahedral sheet, weakening the interlayer binding and making the interlayer cations accessible for cation exchange [35–37].

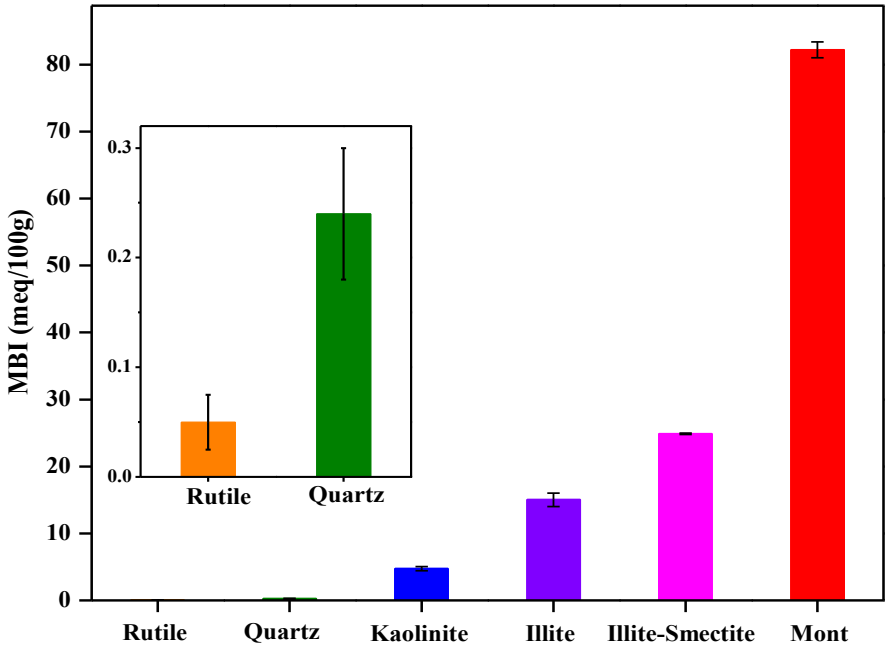


Figure 3-4 The methylene blue index (MBI) of the tested mineral samples.

### 3.3.2. The capillary suction time (CST)

#### 3.3.2.1. The CST of the tested single mineral samples

The CST of tested mineral samples are reported in Figure 3-5 as a function of solids content in the slurries. CST increased with increasing solid content in the mineral slurries, indicating the water-holding capacity of the water/mineral interfaces for all tested minerals. Comparatively, rutile seemed to have the lowest water-holding capacity despite its finest particle size of the six tested mineral samples. Not only was the CST of the rutile sample slurry very low (so the

water flowed out of the slurry fast), but the CST also only increased slightly from 24 s to 35 s when its solids content was increased from 10 wt% to 20 wt%.

Similarly, neither quartz nor kaolinite showed a strong water-holding capacity. When the solids content increased from 10 wt% to 37 wt% (typical solid content found in MFT), the CST of quartz slurry increased from 32 s to 118 s, and that of the kaolinite slurry increased from 37 s to 183 s.

Illite showed moderate water-holding capacity. It registered a CST of 22 s at 5 wt% solids, similar to rutile, quartz and kaolinite. However, when the solids content was increased to 15 wt%, the CST of the illite slurry reached 263 s, higher than the three mineral samples (quartz, rutile and kaolinite).

The swelling clays and the MFT samples showed the highest water-holding capacity as can be seen from the high CST of their slurries. In fact, the CST of these samples were so high that their slurries needed to be prepared at a lower wt% solids in order to register a comparable CST. Thus, both the illite-smectite and montmorillonite samples had CSTs in the 20-30 s range when their slurries contained only 1 wt% solids, and while the CST of illite-smectite remained low at 37 s at 5 wt% solids, the CST of montmorillonite increased sharply to 890 s at a slurry concentration of 5 wt% solids. Interestingly, the CST of the MFT sample was between illite-smectite and montmorillonite, showing a value of 450 s at 5 wt% solids, and 1530 s at 32 wt% solids (Figure 3-5).

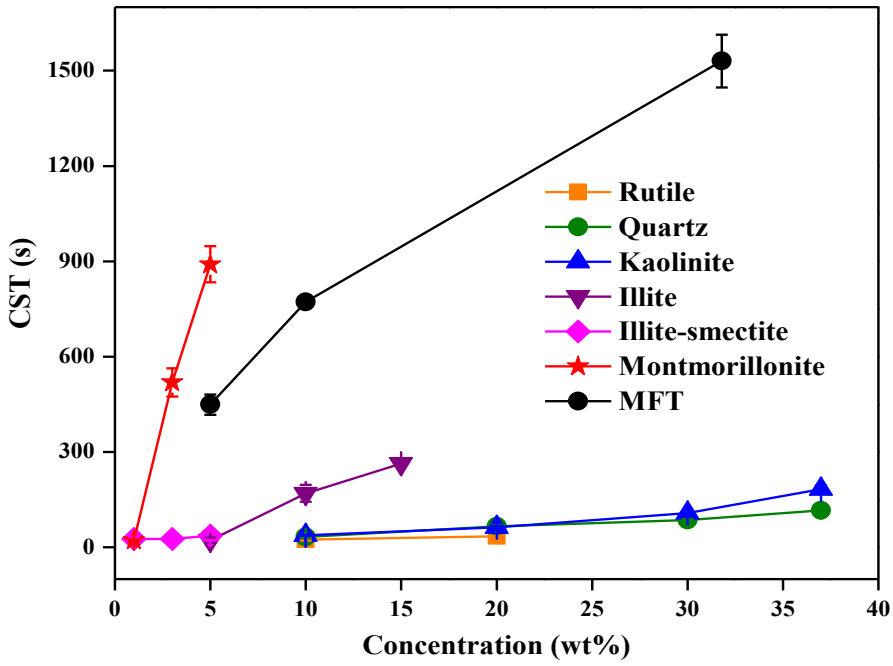


Figure 3-5 Capillary suction time (CST) of the tested mineral samples and MFT at different solids concentrations (wt%).

The CST measurement results indicated that montmorillonite had the highest water-holding capacity than the rest of the mineral samples tested. The observations that the MFT sample was known to contain quartz, kaolinite, illite and swelling clays such as illite-montmorillonite and kaolinite-montmorillonite, and that its CST was found to be situated between that of montmorillonite and quartz/kaolinite, seem to reveal that the high water-holding tendency of the oil sands tailings may be mainly contributed by montmorillonite, the effects of the residual bitumen in the MFT notwithstanding. The montmorillonite was then mixed with other mineral samples to examine how the CST was affected.

### 3.3.2.2. The CST of mixtures of mineral samples with montmorillonite

Montmorillonite was mixed with rutile, quartz, kaolinite, and illite at a mass ratio of 3:7, to test the effect of montmorillonite on the water-holding capacity of the mineral samples. The

mixed minerals were prepared into slurries at 10 wt% solids (i.e., 3 wt% montmorillonite and 7 wt% other mineral sample in the prepared slurries). The results of the measured CST of the mixtures are shown in Figure 3-6, together with "calculated" CST of the mixture assuming the CST values were simple additive of the 3 wt% montmorillonite and 7 wt% other minerals. As can be seen, after mixing with montmorillonite, the water-holding capacity of the mixtures increased significantly. The rutile-montmorillonite sample had a lower CST 345.7 s than the kaolinite-montmorillonite (640.6 s) and illite-montmorillonite (653.1 s) samples. Unexpectedly, while pure quartz had lower CST than kaolinite and illite, the quartz-montmorillonite mixture sample registered the highest CST (834.0 s) among the tested mineral mixtures. It can be seen that not only did montmorillonite have a high water-holding capacity, it also helped to increase the water-holding capacity of other minerals, particularly quartz.

The calculated CST for the mineral mixtures was based on the assumption that the final CST was the simple sum of the CST of 3 wt% montmorillonite and 7 wt% of other minerals. Interestingly, except for the rutile-montmorillonite mixture whose measured CST was actually lower than the calculated CST, the other three mineral mixture samples had lower calculated CST values than the measured CST, indicating that there was a "synergistic effect" for the montmorillonite to enhance the water-holding capacity of minerals (quartz, kaolinite, and illite).

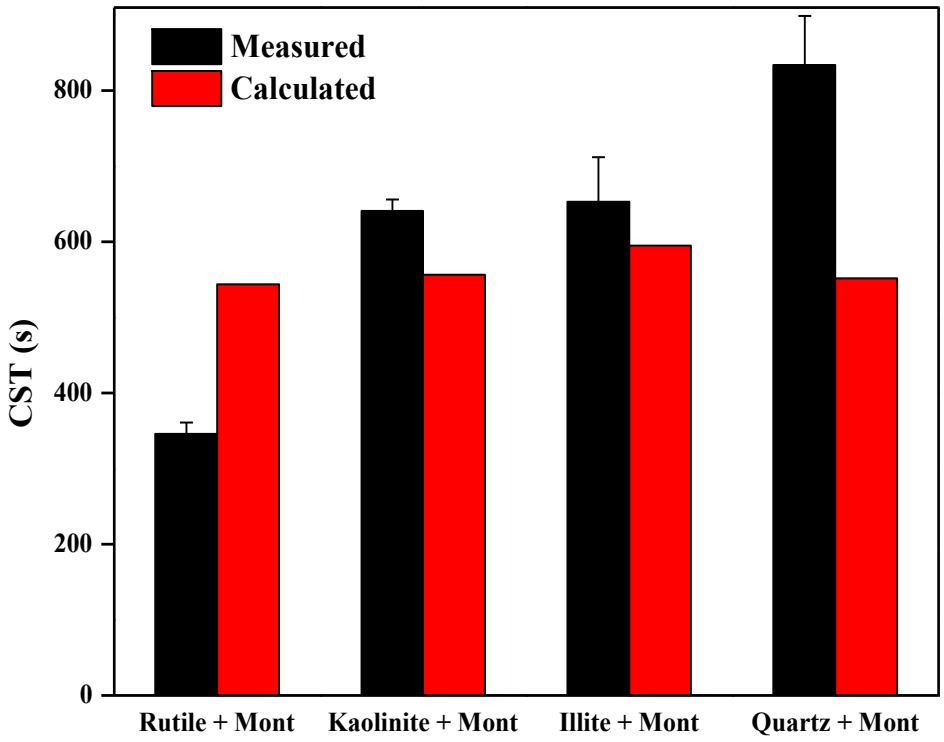


Figure 3-6 Measured and calculated CST of montmorillonite mixed with other mineral samples (at 3:7 weight ratio), and tested at 10 wt% solids content. The calculated CST of the mixed minerals was the simple sum of the 3 wt% montmorillonite and 7 wt% other mineral, which was read off Figure 3-4 by extrapolation.

### 3.3.3. Filtration of mineral samples

Figure 3-7 shows the vacuum filtration performance of the six tested mineral samples. As can be seen, the overall trend was similar to the CST results, i.e., samples with lower CST showed higher filtration rate. Rutile had the highest filterability among the tested minerals at the same solids content despite having the smallest particle size. Quartz and kaolinite had similar filterability and both remained filterable even at 37 wt% solids. Illite had lower filterability than kaolinite, and a direct comparison can be seen at 10 wt% solids. The two swelling clays, illite-smectite and montmorillonite, showed the lowest filterability, particularly

montmorillonite. Even at a very dilute 1 wt% solids, the montmorillonite slurry was not as filterable as the kaolinite slurry at 37 wt% solids. The montmorillonite was completely unfilterable under the vacuum filtration conditions when the concentration was increased to greater than 3 wt% compared with other minerals under the same applied pressure.

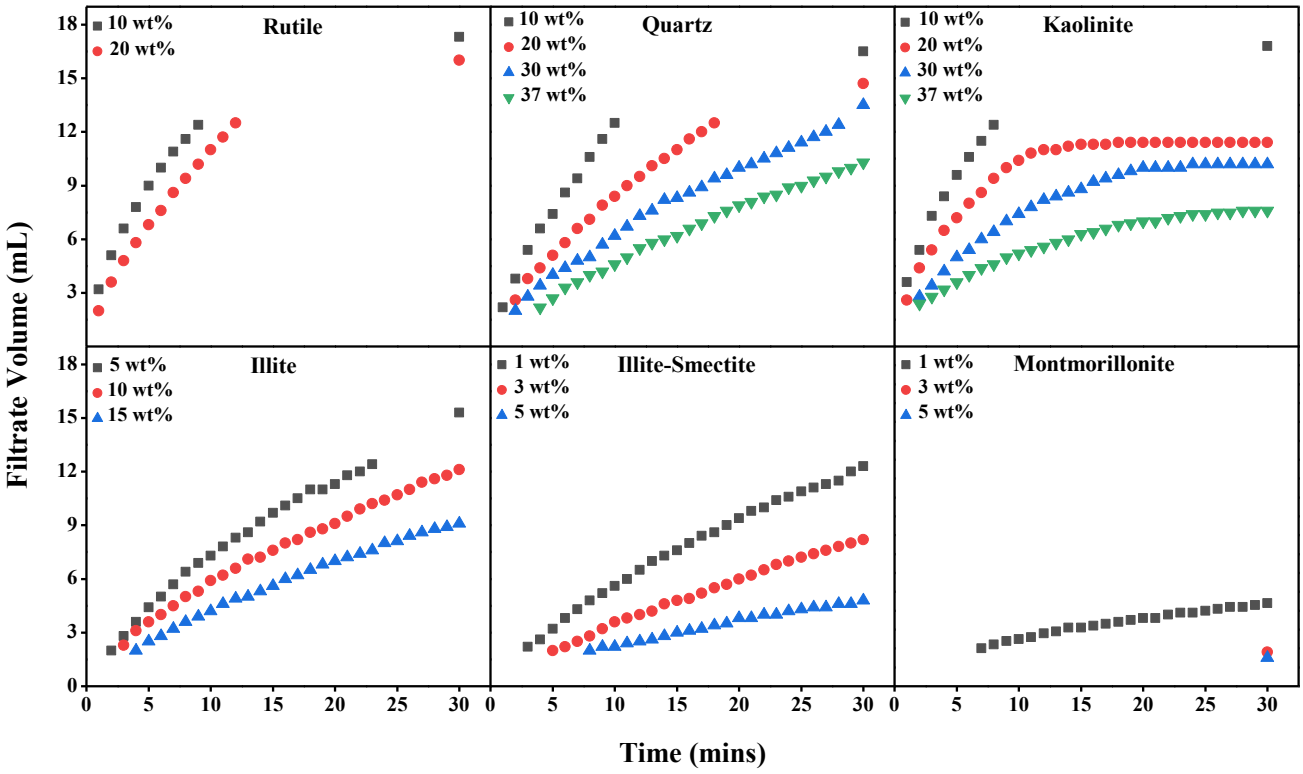


Figure 3-7 Vacuum filtration curves of the tested mineral samples at different solids concentrations. The effective operating pressure was 30-50 mbar and the filter area was 9.6 $cm^2$. The total slurry volume was 20 mL.

It can be seen from Figure 3-7 that the cumulative filtrate volume mostly followed a near linear relationship with filtration time. Therefore, the slope of the initial linear segment of the filtration curves was taken as the initial filtration rate, IFR, with unit of $mL/min/cm^2$, and the results are re-plotted in Figure 3-8 showing IFR as a function of wt% solids for the tested

minerals. Figure 3-8 also included filtration results of MFT as well as mixtures of montmorillonite and other mineral samples at a weight ratio of 3:7.

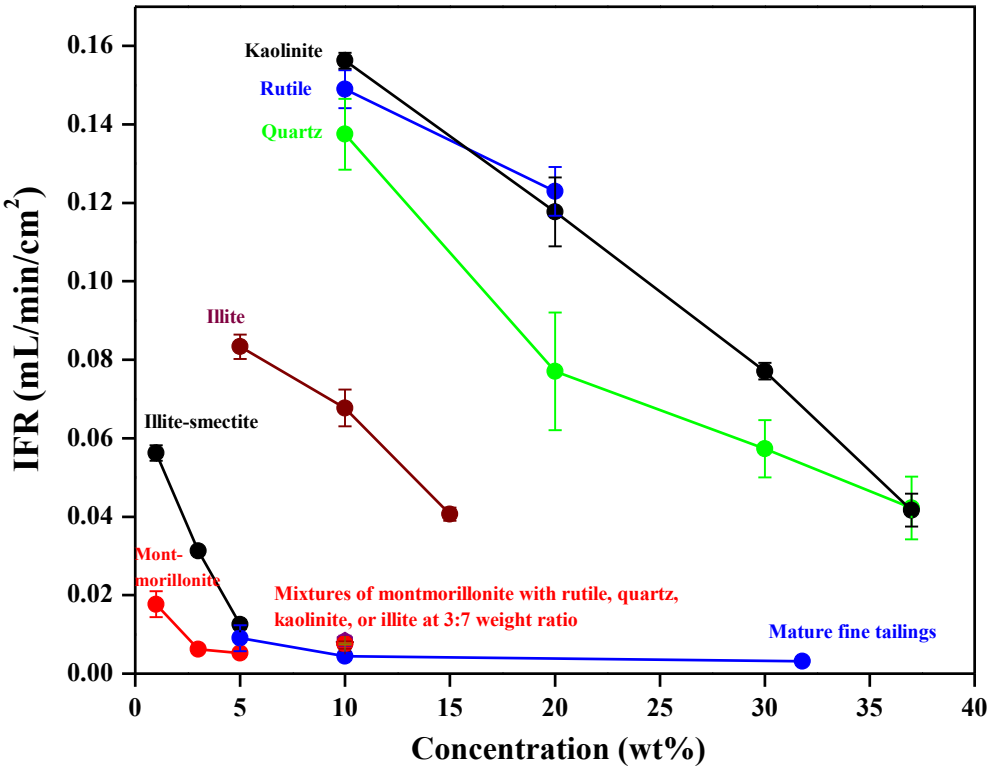


Figure 3-8 Initial filtration rate (IFR) as a function of solids concentration of the tested mineral slurries.

Figure 3-8 clearly shows that the tested minerals and mineral mixtures were divided into three groups. Group 1 included rutile, quartz and kaolinite, i.e., non-clay minerals and non-swelling clays. These minerals were easy to filter and had high filtration rate even at high solids content in the slurry. Group 2 included a single non-swelling clay mineral illite, that had a moderate filterability. Group 3 included the swelling clays either alone or mixed with other minerals (at 3:7 weight ratio), as well as MFT. These samples were extremely difficult to filter even when the slurry was diluted to less than 5 wt% solids.

The IFR of the mixtures of montmorillonite with other mineral sample (at 3:7 weight ratio) at 10 wt% solids was all very low and close to that of montmorillonite at 3 wt% solids. The results indicate that even the addition of small amount of montmorillonite could dominate the filterability of the mineral mixtures. It was also noted that the IFR of MFT was similar to that of swelling clays and to mineral samples mixed with montmorillonite. Specifically, the IFR of illite-smectite and montmorillonite was the same as MFT at 5 wt% solids, and the IFR of the 10 wt% solids slurry of mixtures of the tested mineral samples (rutile, quartz, kaolinite, and illite) with montmorillonite was the same as the 10 wt% MFT. If the kaolinite sample contained 30 wt% montmorillonite, the filtration rate of a 30 wt% kaolinite slurry would be reduced from 0.08 mL/min/cm$^2$ to less than 0.02 mL/min/cm$^2$, corresponding to a 1 wt% montmorillonite slurry.

From the CST and filtration results, it can be concluded that the swelling clays were the most difficult to filter, and the challenge of dewatering oil sands tailings originated from the swelling clays present in the oil sands tailings, residual bitumen notwithstanding.

How did the observed filtration behaviors of the mineral samples relate to their properties reported in Section 3.3.1? Interestingly, rutile had the smallest particle size (predominantly less than 1.3 μm with a median size of 0.7 μm) but it showed the highest filterability among all the mineral samples tested. In contrast, the coarser montmorillonite (with $d_{90}$ of 11 μm and median size of 2.8 μm) filtered extremely slowly. Quartz, kaolinite, illite, illite-smectite, and montmorillonite all had similar particle size distribution, yet they showed drastically different filterability from moderately filterable (quartz and kaolinite) to completely unfilterable (montmorillonite). Indeed for the same minerals, the free volume (or pore volume) would be much smaller when the particle size is small, so the slurry would be more difficult to filter. But

when different minerals are mixed, the results in this work showed that particle size was not the primary factor that determined the filterability of the tested mineral samples. The type of minerals played a more critical role. Non-clay minerals (rutile, quartz) were the easiest to filter, non-swelling clays (kaolinite, illite) were moderately filterable, and swelling clays (illite-smectite, montmorillonite) were unfilterable under the vacuum filtration test conditions used in this work.

As is well known, when minerals are immersed in water, hydration layers are formed on the mineral surface (most of the minerals are naturally hydrophilic, as are the six minerals tested in this work), with typical length scale in the nanometer range [38]. With such a small length scale the hydration layer did not usually manifest itself, unless the sample had a very large specific surface area. In practice, the "effective volume fraction" of the solids could be used to quantify the volume fraction taken by the solids and their hydration layers, i.e., taking the solid particles and their surface hydration layers as solid phases in calculating the volume fraction of the solids. This effective volume fraction can be calculated from the following equation [39–41],

$$\emptyset_{eff} = \emptyset \times \left(1 + \frac{t_{DL}}{R_p}\right)^3 \qquad 3.3$$

Where $\emptyset$ is the volume fraction of mineral solids, $t_{DL}$ is the hydration layer thickness which is approximated as the thickness of the electrical double layer, $R_p$ is the radius of the particle which can be approximated from the density ($\rho$) and the specific surface area (SSA) as $Rp$=3/($SSA\times\rho$). For an aqueous solution of a symmetrical electrolyte, the electrical double layer thickness is governed by the valency (z) and the concentration, expressed as molarity (c) of the electrolyte [42]:

$$t_{DL} = \frac{3\times10^{-8}}{ZC^{\frac{1}{2}}}\ cm \qquad 3.4$$

With DI water, the concentration of dissolved salt originating from mineral surface were typically less than 100 mg/L. Therefore, the thickness of the electrical double layer was estimated to be in the 4-5 nm range, and 4.5 nm thick bound water layer was used to calculate the effective volume fraction. The high dissolved salt concentrations in oil sands tailings water could compress the electrical double layer to 1-2 nm [43]. The SSA calculated from the MBI was used for the effective volume fraction calculation for the minerals.

The relationship between the IFR of the tested mineral samples and mineral mixtures as a function of the effective volume fraction is shown in Figure 3-9. The SSAs of mineral mixtures in this figure were calculated as a weighted average from the MBI SSA. As can be seen, the IFR was negatively correlated to the effective volume fraction for the pure minerals, i.e., as the effective volume fraction values increased, the IFR decreased.

Figure 3-9 shows that the IFR of non-clay minerals and non-swelling clays dropped rapidly as the effective volume fraction increased within a narrow range (from 2 vol% to about 30 vol%, i.e., the volume fraction is expressed as a percentage). The reason for the rapid drop was because of the high filtration rate at low effective volume fraction. The IFR of montmorillonite was low, and it dropped more slowly with the increase in effective volume fraction (from about 15 vol% to 76 vol%). Mixtures of montmorillonite with other minerals (rutile, quartz, kaolinite, illite) became unfilterable, and their IFR was low and similar under the test conditions even when their effective volume fraction spaned from about 20 vol% to 40 vol%. MFT became unfilterable at much lower effective volume fraction (of less than 10 vol%), possibly due to the effects of the residue bitumen in the MFT.

Therefore, Figure 3-9 shows a general inverse relationship between filtration rate and effective volume fraction of solids in the slurry, and that the minerals followed two "bands" on this plot. The non-clay minerals and non-swelling clays followed the band with a steep negative slope, and the reason for the steep decline in filtration rate was because of the high filtration rate at low effective volume fraction. The swelling clays and MFT, on the other hand, followed the band with a much smaller negative slope, and the reason for the smaller slope was because of the very low filtration rate even at low effective volume fraction of the solid. In other words, the swelling clays followed a different patterm from the non-clay minerals and non-swelling clays with regards to their filtration behavior.

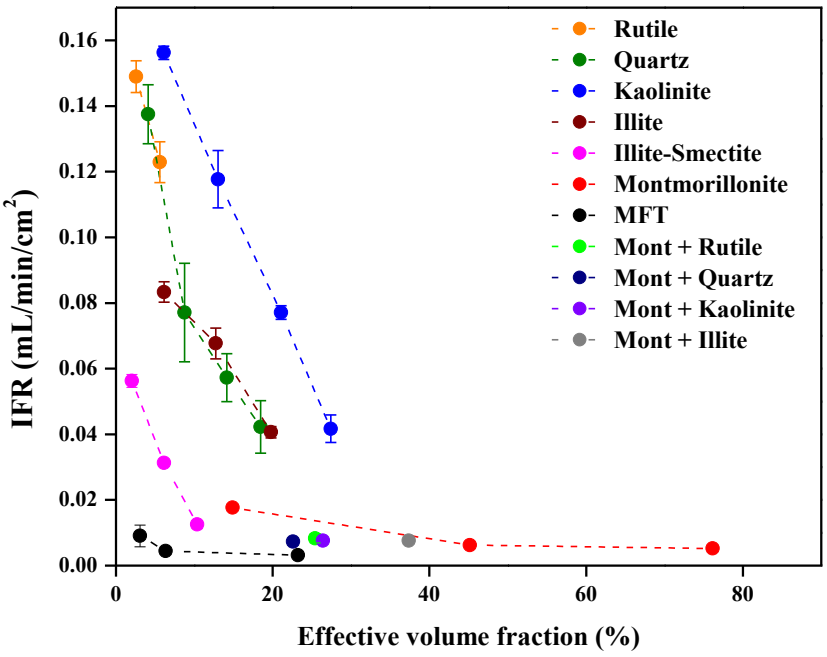


Figure 3-9 The relationship between IFR and effective volume fraction of tested single minerals and mixtures of montmorillonite with other minerals (at a weight ratio of 3:7).

### 3.3.4 Filtration of montmorillonite after acid treatment and heating

The foregoing description shows that, of the six tested mineral samples, swelling clays were the most difficult to filter. It was reported that acid treatment could lead to the leaching of metal ions and thus a change in montmorillonite structures [44]. Suspecting that the acid treatment may change the property of the swelling clays, montmorillonite was treated with 0.5 mol/L HCl for 12 hours in this work. After the treatment, the sample slurry was centrifuged at 20,000 RCF for 30 mins. The resulting acid-treated montmorillonite was dried in an oven at 110℃ overnight. The dried acid-treated montmorillonite was then prepared into a 3 wt% slurry and filtered using the vacuum filtration set up. The filtration result of the treated montmorillonite are shown in Figure 3-10, together with control blank tests. As can be seen, the filterability of the montmorillonite increased dramatically after the acid treatment and 110°C drying (pink triangle in Figure 3-10) compared with samples that were acid-treated but dried at 25°C (blue triangle in Figure 3-10), or samples that were wetted by water and dried at 110°C without acid-treatment (red circle in Figure 3-10). The IFR increased more than 10 times from 0.0063 mL/min/cm$^2$ for the original montmorillonite to 0.065 mL/min/cm$^2$ of the acid-treated and 110°C dried montmorillonite, both at 3 wt% solids (Figure 3-10). After the acid-treatment and 110°C drying, the 3 wt% montmorillonite had similar filterability as the 30 wt% quartz slurry. Interestingly, despite the significant improvement in filtration rate after the acid treatment and drying at 110°C, the MBI of this acid-treated montmorillonite remained high at 72-74 meq/100g (the original untreated montmorillonite had a MBI of 80 meq/100g, Figure 3-4). This is understandable since acid treatment only replaced the exchangeable metal ions with $H^+$ but did not remove the ion exchange sites.

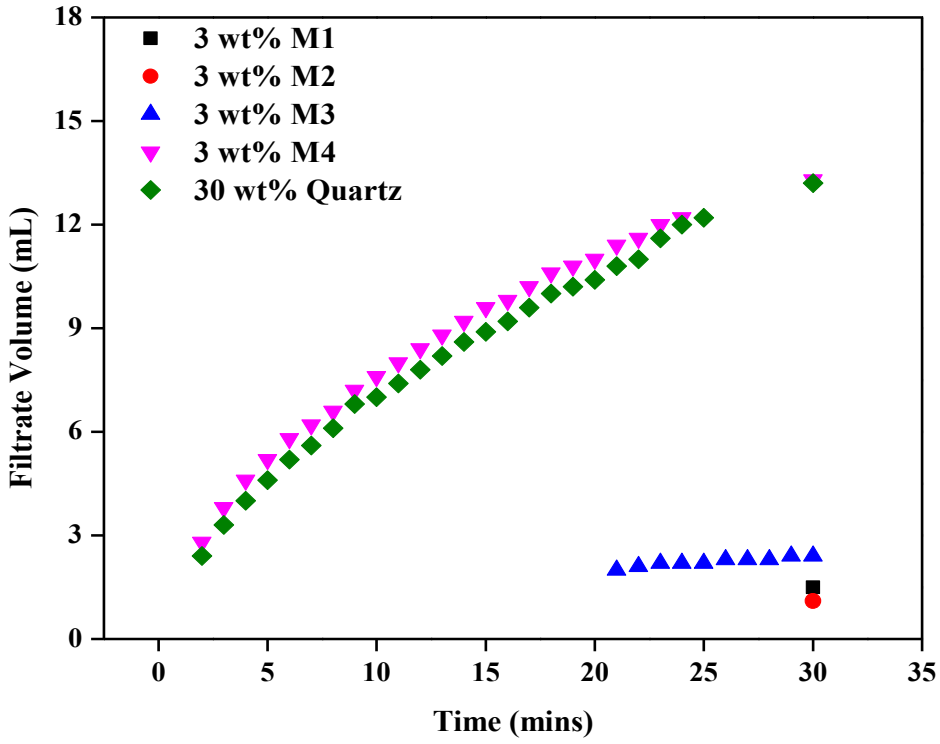


Figure 3-10 Vacuum filtration curves of montmorillonite samples after different treatments. The black square shows the untreated montmorillonite (M1). The red circle shows montmorillonite that was submerged in water then dried at 110°C overnight (M2). The blue triangle shows montmorillonite that was treated with 0.5 M HCl and dried at 25°C overnight (M3). The pink triangle shows montmorillonite that was treated with 0.5 M HCl and dried at 110°C overnight (M4).

The elemental composition of montmorillonite before and after acid treatment and drying was determined with a Thermo iCAP6300 Duo ICP-OES, and the results are shown in Table 3-3. The result of M1 was repeated two times, and it showed good reproducibility. As can be seen, the concentrations of metal cations such as $Na^{+}$, $Ca^{2+}$, $Fe^{2+}$, $Mg^{2+}$, $K^{+}$, $Mn^{2+}$ were reduced significantly after the acid treatment. However, the increased filterability seems to be unrelated

to the reduced metal cation concentrations: Samples M3 and M4 showed similar metal cation concentration after the acid treatment, but M4 (dried at 110°C) filtered much faster than M3 which was dried at 25°C.

Table 3-3 Elemental composition (in mg/kg) of montmorillonite determined by ICP-OES

| Sample | Al | Si | Na | Ca | Fe | Mg | S | K | P | Mn | Pb | Sr | Zn |
|---|---|---|---|---|---|---|---|---|---|---|---|---|---|
| M1 | 5334.0 | 1497.9 | 11246.8 | 8289.9 | 8691.6 | 2483.6 | 2098.3 | 938.7 | 181.6 | 304.5 | 38.5 | 212.6 | 58.9 |
| | ±14.9 | ±22.0 | ±28.2 | ±41.2 | ±93.1 | ±6.6 | ±4.4 | ±8.3 | ±1.8 | ±6.8 | ±5.6 | ±1.2 | ±1.0 |
| M2 | 6515.7 | 1586.5 | 9939.7 | 8427.8 | 8365.8 | 2554.5 | 1601.5 | 972.1 | 192.1 | 285.8 | 34.1 | 224.8 | 62.0 |
| M3 | 5727.1 | 1357.1 | 1465.7 | 3004.5 | 4688.6 | 1224.3 | 1383.8 | 499.3 | 47.9 | 118.9 | 17.0 | 83.2 | 68.7 |
| M4 | 6297.2 | 1606.9 | 1441.8 | 3073.5 | 5016.0 | 1309.3 | 1341.6 | 490.1 | 47.2 | 116.5 | 17.4 | 83.5 | 60.4 |

M1 - Untreated montmorillonite.

M2 - Montmorillonite treated with DI water and dried at 110°C overnight.

M3 - Montmorillonite treated with 0.5 M HCl for 12 hours and dried at 25°C overnight.

M4 - Montmorillonite treated with 0.5 M HCl for 12 hours and dried at 110°C overnight.

The XRD patterns of the untreated and acid-treated and dried montmorillonite samples are shown in Figure 3-11. The samples for XRD measurement were prepared by the same preferred orientation method described in section 3.2.4. As can be seen, the water wetted and 110°C dried montmorillonite (M2) had essentially the same XRD pattern as the untreated montmorillonite (M1), differing only in the relative diffraction intensity from the major peak d(001) and d(310) (green dot line 1 and 2). Both the M3 and M4 samples showed apparent reductions in intensity and shift in the characteristic reflections d(001) peak, indicating that the basal interlayer spacing of montmorillonite increased and the crystallite size decreased after the acid treatment [44]. Furthermore, the existence of (001) peaks also demonstrated that the montmorillonite layer structure was not changed after the treatment. This was also confirmed

by the ICP results (Table 3-3) which show that the concentrations of octahedral Al and tetrahedral Si were at the same level before and after the acid treatment. Another notable observation was that the sharp peak at 2θ angle of about 29° (in green dot line 2) broadened with much reduced intensity, signifying the conversion to an amorphous phase with increased crystal defects and decreased crystallite size. Therefore, it was deduced that after the acid treatment, the interlayer exchangeable cations, such as $Ca^{2+}$, $Mg^{2+}$, $Fe^{2+}$, $Na^{+}$ were leached off.

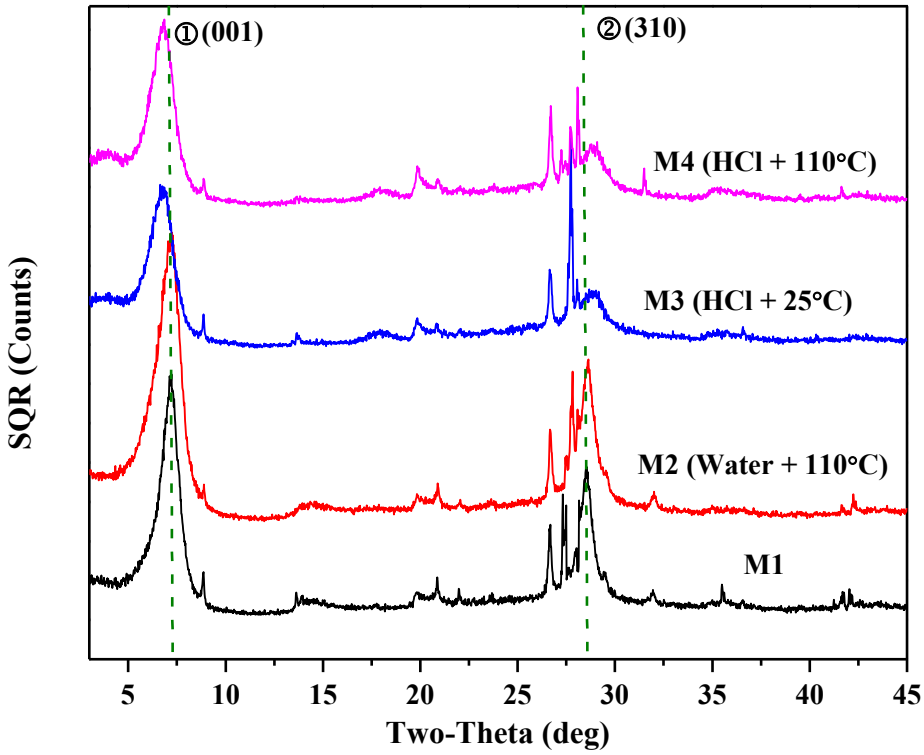


Figure 3-11 XRD patterns of untreated montmorillonite (M1), montmorillonite treated with DI water and dried at 110°C overnight (M2), montmorillonite treated with 0.5 M HCl for 12 hours and dried at 25°C overnight (M3), and montmorillonite treated with 0.5 M HCl for 12 hours and dried at 110°C overnight (M4).

The acid treatment also caused an increase in the peak intensity ratio of 002/003 planes as shown in Table 3-4. The acid treatment therefore removed the interlayer exchangeable cations and also changed part of the montmorillonite crystalline structure.

Table 3-4 Peak intensity ratio of 002/003 of montmorillonite sample before (M1, M2) and after (M3, M4) acid treatment.

| Sample | M1 | M2 | M3 | M4 |
|---|---|---|---|---|
| 002/003 | 1.7 | 1.8 | 2.6 | 2.3 |

In summary, the hydrochloric acid could help leach off interlayer exchangeable cations such as $Ca^{2+}$, $Mg^{2+}$, $Fe^{2+}$, $Na^{+}$. The ICP-OES results showed that water alone could not remove these interlayer cations (sample M2). For the acid-treated montmorillonite (samples M3 and M4), the interlayer exchange cations were leached off. The cations could re-dissolve when the dried samples M3 and M4 were suspended in DI water. The dissolved cations could then compress the electrical double layer to lower its thickness, so that samples M3 and M4 would have a smaller effective volume fraction and thus higher filtration rate than samples M1 and M2. This was indeed observed in our experiments. The higher filterability of sample M4 than sample M3 could also be caused by the higher available cation concentration in sample M4 than sample M3. As M4 was dried at 110ºC, it could facilitate the leaching of exchangeable cations. Indeed, when sample M4 was repeatedly washed with DI water followed by centrifugation to remove the wash water, the IFR decreased from 0.08 mL/min/cm$^2$ to 0.01 mL/min/cm$^2$, which was similar to M3. Clearly, the repeated wash progressively removed more cations, resulting in lower cation concentration and higher double layer thickness, and thus higher effective volume fraction than the acid-treated montmorillonite (sample M3) that was washed only once.

Since the MBI of the acid-treated montmorillonite was essentially the same as the untreated montmorillonite, it can be concluded that the filterability difference of acid-treated montmorillonite was caused by the different amount of the acid-leached and then water-mobilized cations in the slurry.

Previous research reported in the literature [45,46] indicated that the presence of montmorillonite in phosphatic clay slurry and kimberlite clay slimes rendered the slurries completely impermeable to water. We observed in this work that the swelling clays in the oil sands were likely responsible to the slow filtration of the oil sands mature fine tailings. To solve the oil sands tailings dewatering problem, mitigation measures need to be developed to deal with swelling clays. Clearly, the acid treatment is impractical and the heat treatment is out of the question. Other techniques to lower the thickness of the hydration layer of swelling clays in the tailings should be studied with an objective to exploit them in commercial applications.

### 3.4. Conclusions

The filtration behaviors of six different mineral samples, rutile ($d_{50}$ = 0.7 μm), quartz ($d_{50}$ = 3.6 μm), kaolinite ($d_{50}$ = 4.1 μm), illite ($d_{50}$ = 2.8 μm), illite-smectite ($d_{50}$ = 2.7 μm), and montmorillonite ($d_{50}$ = 2.8 μm), were investigated in this study by vacuum filtration and capillary suction time (CST) measurements. The filtration performance was correlated to the properties of the mineral samples. It was observed that:

(1) Particle size was not the primary factor that affected the filtration behavior of the six tested minerals. The rutile sample had the smallest particle size of all six tested mineral samples, with a submicron medium size of 0.7 μm, yet it had the best filterability. The other five mineral samples had similar medium particle sizes but showed very different filterability.

(2) The filterability was significantly affected by the type of minerals. The swelling clays (montmorillonite, illite-smectite) were much more difficult to filter than the non-swelling clays (kaolinite, illite), which in turn was more difficult to filter than the non-clay minerals (quartz, rutile). Since the particle sizes were mostly similar, this conclusion was not masked by particle size effect. Also, the presence of a small amount of swelling clays in a mineral mixture was found to significantly affect the filtration behavior.

(3) The filtration rate decreased with an increase in the effective volume fraction of the minerals. When the effective volume fraction was above 20% for the tested minerals mixed with montmorillonite, the slurry became unfilterable under the test conditions. Swelling clays followed a different band on the filtration rate – effective volume fraction of solid plot from the non-clay minerals and non-swelling clays, indicating that swelling clays had distinctly different filtration behavior.

(4) Acid treatment followed by heating at 110°C, led to a dramatic improvement in the filterability of montmorillonite, while the MBI (CEC) remained essentially the same. The filterability difference of acid-treated and 110°C heated montmorillonite was likely caused by the exchange of $H^+$ with the exchangeable metal cations from the interlayer space of montmorillonite. These "leached-off" metal cations then became available to compress the electrical double layer when the dried montmorillonite was re-slurried, leading to a thinner hydration layer and lower effective volume fraction. Indeed, repeated wash of the acid-treated montmorillonite, which completely removed these leached-off metal cations, was observed to restore the difficult filtration behavior of the montmorillonite despite the acid treatment. Clearly the repeated wash removed the metal cationic species permanently so that when the dried sample was re-slurried, there were no more metal ions to compress the double layer.

This study revealed swelling clays as the most difficult to filter of all the mineral samples tested. Since swelling clays are known to present in oil sands tailings in various quantity, it is likely that the difficulty associated with oil sands tailings filtration was caused by these swelling clays. Further study needs to be carried out to quantify the concentration of swelling clays in oil sands tailings and the corresponding filtration behavior, and to find effective methods to mitigate the detrimental effects of the swelling clays on oil sands tailings filtration.

**References**


[1] Alberta Energy Regulator. Alberta Energy Regulator 2016/17 Annual Report. 2017. https://doi.org/https://static.aer.ca/prd/documents/reports/AER2016-17AnnualReport.pdf.

[2] Clarke TP. Oil sands hot water extraction process. US 4240897, 1980. https://doi.org/https://www.osti.gov/biblio/6555796.

[3] Alberta Environment and Parks. OSIP - Data Library 2015. http://osip.alberta.ca/library/Dataset/Details/542 (accessed April 4, 2015).

[4] Avagyan AB. Environmental building policy by the use of microalgae and decreasing of risks for Canadian oil sand sector development. Environ Sci Pollut Res 2017;24:20241–53. https://doi.org/10.1007/s11356-017-9864-x.

[5] Farrow JB, Johnston RRM, Simic K, Swift JD. Consolidation and aggregate densification during gravity thickening. Chem Eng J 2000;80:141–8. https://doi.org/10.1016/S1383-5866(00)00083-6.

[6] Rao SR. Flocculation and dewatering of Alberta oil sands tailings. Int J Miner Process 1980;7:245–53. https://doi.org/10.1016/0301-7516(80)90020-4.

[7] Liu D, Edraki M, Berry L. Investigating the settling behaviour of saline tailing suspensions using kaolinite, bentonite, and illite clay minerals. Powder Technol 2018;326:228–36. https://doi.org/10.1016/J.POWTEC.2017.11.070.

[8] Zhu Y, Tan X, Liu Q. Dual polymer flocculants for mature fine tailings dewatering. Can J Chem Eng 2017;95:3–10. https://doi.org/10.1002/cjce.22628.

[9] Mikula RJ, Kasperski KL, Burns RD, MacKinnon MD. Nature and fate of oil sands fine tailings. Suspens Fundam Appl Pet Ind 1996;251:677–723.

[10] Li Y, Chen Y, Xia W, Xie G. Filtration of kaolinite and coal mixture suspension: Settling behavior and filter cake structure analysis. Powder Technol 2021;381:122–8. https://doi.org/10.1016/J.POWTEC.2020.12.050.

[11] Ottley DJ. Gravity Concentration In Modern Mineral Processing. 1986. https://doi.org/10.1007/978-94-009-4476-3_11.

[12] Liu D, Edraki M, Fawell P, Berry L. Improved water recovery: A review of clay-rich tailings and saline water interactions. Powder Technol 2020;364:604–21. https://doi.org/10.1016/J.POWTEC.2020.01.039.

[13] Wright HJL, Kitchener JA. The problem of dewatering clay slurries: Factors controlling filtrability. J Colloid Interface Sci 1976;56:57–63. https://doi.org/10.1016/0021-9797(76)90146-6.

[14] Sabah E, Yüzer H, Çelik MS. Characterization and dewatering of fine coal tailings by dual-flocculant systems. Int J Miner Process 2004;74:303–15. https://doi.org/10.1016/J.MINPRO.2004.03.001.

[15] Onuaguluchi O, Eren Ö. Recycling of copper tailings as an additive in cement mortars. Constr Build Mater 2012;37:723–7. https://doi.org/10.1016/J.CONBUILDMAT.2012.08.009.

[16] Adeyinka OB, Samiei S, Xu Z, Masliyah JH. Effect of particle size on the rheology of athabasca clay suspensions. Can J Chem Eng 2009;87:422–34. https://doi.org/10.1002/cjce.20168.

[17] Chen Q, Liu Q. Bitumen Coating on Oil Sands Clay Minerals: A Review. Energy and Fuels 2019;33:5933–43. https://doi.org/10.1021/acs.energyfuels.9b00852.

[18] Majid A, Ripmeester JA. Characterization of unextractable organic matter associated with heavy minerals from oil sand. Fuel 1986;65:1714–27. https://doi.org/10.1016/0016-2361(86)90275-9.

[19] Omotoso OE, Mikula RJ. High surface areas caused by smectitic interstratification of kaolinite and illite in Athabasca oil sands. Appl Clay Sci 2004;25:37–47. https://doi.org/10.1016/j.clay.2003.08.002.

[20] Omotosoa O, Mikulaa R, Urquhartb S, Sulimmab H, Stephensc P. Characterization of Clays from Poorly Processing Oil Sands using Synchrotron Techniques. Clay Sci 2006;12:88–93.

[21] Kessick MA. Structure and properties of oil sands clay tailings. J Can Pet Technol 1979:49–52. https://doi.org/10.2118/79-01-01.

[22] Loerke R, Tan X, Liu Q. Dewatering of Oil Sands Mature Fine Tailings by Dual Polymer Flocculation and Pressure Plate Filtration. Energy and Fuels 2017;31:6986–95.

https://doi.org/10.1021/acs.energyfuels.7b00938.

[23] Besra L, Sengupta DK, Roy SK. Particle characteristics and their influence on dewatering of kaolin, calcite and quartz suspensions. Int J Miner Process 2000;59:89–112. https://doi.org/10.1016/S0301-7516(99)00065-4.

[24] Forbes E, Chryss A. Fundamentals of clays: Surface and colloid science, and rheology. Clays Miner. Process. Value Chain, 2017, p. 81–110. https://doi.org/10.1017/9781316661888.004.

[25] Bleam WF. Clay Mineralogy and Clay Chemistry. Soil Environ. Chem., 2012, p. 85–116. https://doi.org/10.1016/b978-0-12-415797-2.00003-0.

[26] Madsen FT, Muller-vonmoos MAX. The Swelling Behaviour of Clays. Appl Clay Sci 1989;4:143–56. https://doi.org/https://doi.org/10.1016/0169-1317(89)90005-7.

[27] Geramian M, Osacky M, Ivey DG, Liu Q, Etsell TH. Effect of Swelling Clay Minerals (Montmorillonite and Illite-Smectite) on Nonaqueous Bitumen Extraction from Alberta Oil Sands. Energy and Fuels 2016;30:8083–90. https://doi.org/10.1021/acs.energyfuels.6b01026.

[28] Osacky M, Geramian M, Ivey DG, Liu Q, Etsell TH. Influence of nonswelling clay minerals (illite, kaolinite, and chlorite) on nonaqueous solvent extraction of bitumen. Energy and Fuels 2015;29:4150–9. https://doi.org/10.1021/acs.energyfuels.5b00269.

[29] Gupta SK, Gartley MG. XRD analysis of illite-smectite interstratification in clays from oil sands ores. Adv. X-ray Anal., vol. 62, 1999, p. 22–31.

[30] Eberl DD, Velde B. Beyond the Kubler Index. Clay Miner 1989;24:571–7.

https://doi.org/10.1180/claymin.1989.024.4.01.

[31] Pham Thi，Hang, G. W. Brindley. Methylene Blue Absorption by Montmorillonites. Determinations of Surface Areas and Exchange Capacities with Different Initial Cation Saturations (Clay-Organic Studies XIX). Isr J Chem 1970;8:409–15. https://doi.org/10.1002/ijch.197000047.

[32] Osacky M, Geramian M, Liu Q, Ivey DG, Etsell TH. Surface properties of petrologic end-members from alberta oil sands and their relationship with mineralogical and chemical composition. Energy and Fuels 2014;28:934–44. https://doi.org/10.1021/ef402150z.

[33] Kahr G, Madsen FT. Determination of the cation exchange capacity and the surface area of bentonite, illite and kaolinite by methylene blue adsorption. Appl Clay Sci 1995;9:327–36. https://doi.org/10.1016/0169-1317(94)00028-O.

[34] Chen Q, Stricek I, Gray MR, Liu Q. Interface Science Influence of hydrophobicity distribution of particle mixtures on emulsion stabilization. J Colloid Interface Sci 2017;491:179–89. https://doi.org/10.1016/j.jcis.2016.12.045.

[35] Bergaya F, Lagaly G, Vayer M. CATION AND ANION EXCHANGE. Handb. Clay Sci., vol. 1, 2006, p. 979–1001. https://doi.org/10.1016/S1572-4352(05)01036-6.

[36] Masliyah JH, Czarnecki J, Xu Z. Handbook on Theory and Practiceon Bitumen Recovery from Athabasca Oil Sands. 2011. https://doi.org/https://doi.org/10.7939/r3-nr43-8t34.

[37] Foster MD. The relation between composition and swelling in clays. Clays Clay Miner

1954;3:205–20. https://doi.org/10.1346/ccmn.1954.0030117.

[38] Dolinar B, Macuh B. Determining the thickness of adsorbed water layers on the external surfaces of clay minerals based on the engineering properties of soils. Appl Clay Sci 2016;123:279–84. https://doi.org/10.1016/J.CLAY.2015.12.029.

[39] Lim HM, Misni M. Colloidal and rheological properties of natural rubber latex concentrate. Appl Rheol 2016;26:1–10. https://doi.org/10.3933/ApplRheol-26-15659.

[40] Liang H, Guan D, Yang L, Zhang L, Song Y, Zhao J. Multi-scale characterization of shell thickness and effective volume fraction during gas hydrates formation: A kinetic study. Chem Eng J 2021;424:130360. https://doi.org/10.1016/J.CEJ.2021.130360.

[41] Prestidge C, Tadros TF. Viscoelastic properties of aqueous concentrated polystyrene latex dispersions containing grafted poly(ethylene oxide) chains. J Colloid Interface Sci 1988;124:660–5. https://doi.org/10.1016/0021-9797(88)90204-4.

[42] Doroszkowski A. The physical chemistry of dispersion. Second Edi. Woodhead Publishing Ltd; 1999. https://doi.org/10.1533/9781855737006.198.

[43] Siddique T, Kuznetsov P, Kuznetsova A, Arkell N, Young R, Li C, et al. Microbially-accelerated consolidation of oil sands tailings. Pathway I: Changes in porewater chemistry. Front Microbiol 2014;5:1–11. https://doi.org/10.3389/fmicb.2014.00106.

[44] Bendou S, Amrani M. Effect of hydrochloric acid on the structural of sodic-bentonite clay. J Miner Mater Charact Eng 2014;02:404–13. https://doi.org/10.4236/jmmce.2014.25045.

[45] D.R., Nagaraj, P., Somasundaran, L., McAllister. Subsidence of suspensions of

phosphatic slime and its major constituents. Int J Miner Process 1977;4:111–29. https://doi.org/https://doi.org/10.1016/0301-7516(77)90020-5.

[46] J.V.， O’Gorman, J.A.， Kitchener. The flocculation and de-watering of kimberlite clay slimes. Int J Miner Process 1974;1:33–49. https://doi.org/https://doi.org/10.1016/0301-7516(74)90025-8.

# CHAPTER 4 The Role of Bitumen in the Filtration of Oil Sands Tailings

## 4.1. Introduction

The oil sands deposit in Alberta, Canada is an important unconventional oil resource and constitutes almost 96% of the known oil reserves in Canada. The extraction of the heavy oil (bitumen) from the oil sands involves the use of warm water (~50ºC) and caustic soda, followed by bitumen flotation. In this process, a large volume of slow-settling tailings is produced and discharged to the tailings ponds. The coarse sands in the tailings settle quickly to the bottom, the water released to the top, while the middle layer of tailings forms a stable viscous suspension commonly known as mature fine tailings (MFT), which remain stable for many decades. Since the start of oil sands operation in the 1960s, the accumulated MFT had reached about 800 million cubic meters by 2016 [1], posing severe environmental risks. The oil sands industry has so far invested more than $10 billion in R&D to speed up the water release and reclamation of the oil sands tailings [2]. However, an effective oil sands tailings treatment process is still elusive.

The dewatering of oil sands fluid fine tailings is more difficult than dewatering other mine tailings, such as the coal tailings with similar solids content and particle size distribution [3]. One of the main differences of oil sands tailings from other mine tailings is the presence of bitumen. During the bitumen extraction process from oil sands, a few percent of bitumen is lost to the tailings. However, the role of the residual bitumen in the oil sands tailings dewatering, more specifically in filtration, has not been studied vigorously as most studies targeted the fine clays as the reason for the difficult dewatering of oil sands tailings [4–7].

Bitumen shows colloid and gelling behaviors because of its high asphaltene/resin concentrations [8]. Scott et al. [9] proposed that the high gel strength of MFT could be

attributed to the existence of residual bitumen. The highly viscous bitumen droplets could adhere to the edges of the clay surface, aggregate the clay, and eventually block the flowing channels of water [10,11]. Therefore, it was assumed that the viscous bitumen made the conventional dewatering processes such as thickening and filtration more difficult [12]. Researchers also suggested that bitumen exists as small globules traveling inside the tailings mineral matrix during the hydraulic conductivity measurement until they run into pore throats. The high viscosity of bitumen makes it difficult to flow through the pore throats and hence plugging the pore channels [13,14]. After removing the residual bitumen and organic matter-coated fine mineral solids from the oil sand tailings, the settling time of the remaining tailings was shortened substantially [15,16]. The settling tests of oil sands tailings conducted by Klein et al. [17] also seemed to support the retardation effects of bitumen in solids-liquid separation in the diluted MFT. In their tests, the bitumen was removed from the MFT by froth flotation, and the initial settling rate of the resulting MFT was found to increase from 2.5 m/h to more than 9 m/h. Furthermore, it was suggested that bitumen could attach to the filter media, impeding filtration, and most of the introduced polymer flocculants were in fact consumed by the residual bitumen during the flocculation and pressure filtration of MFT [18].

The bitumen lost to the oil sands tailings could be in the form of dispersed free bitumen or otherwise trapped in the process water as emulsified bitumen or adsorbed on mineral surfaces [12,19–22]. The objective of this work was to study the effects of these different forms of residual bitumen in the oil sands tailings on their pressure filtration in order to better understand the solid-liquid separation of the oil sands tailings in the presence of bitumen.

## 4.2. Materials and Methods

### 4.2.1. Materials

A mature fine tailings (MFT) sample was collected from one of the oil sands operators in northern Alberta, Canada in 2017 and stored in a freezer before use. A bitumen froth (BF) sample, containing 58.1 wt% bitumen, 4.0 wt% solids and 37.9 wt% water, was also obtained from an oil sands operator in northern Alberta and used as bulk bitumen. A high purity vacuum residue bitumen (99.5 wt% bitumen), provided by the Institute for Oil Sands Innovation (IOSI), University of Alberta, was diluted to 60 wt% with toluene to use as a stock solution to create bitumen coating on model mineral surface. Kaolinite (ASP 600, BASF) was used as a model clay sample in pressure and vacuum filtration, and it had characteristic particle sizes of $d_{10}$ = 1.0 μm, $d_{50}$ = 4.1 μm, and $d_{90}$ = 11.9 μm. An anionic polyacrylamide polymer flocculant, with a trade name A3335 from SNF, and a cationic polyDADMAC polymer coagulant, with a trade name Alcomer 7115 from BASF, were used to treat the kaolinite and MFT samples. According to the vendors, A3335 had a molecular weight of $17\times10^6$ g/mol and an anionic charge density of 30%, and the Alcomer 7115 had a molecular weight between $2\times10^5$ and $4\times10^5$ g/mol and a high cationic charge density. Aqueous solutions of 0.4 wt% A3335 and 0.2 wt% of Alcomer 7115 were prepared with deionized (DI) water and used within one day of preparation. The polymer dosages (g/t) were reported as grams of dry polymer per tonne of MFT dry solids or kaolinite. In addition to BASF ASP 600 kaolinite, quartz (US Silica), rutile ($TiO_2$, US Research Nanomaterials), and montmorillonite (Ward's Sciences, USA) were also used as model minerals in selected experimental work to represent non-clay minerals and swelling clay.

### 4.2.2. Separation of MFT components by centrifugation

The MFT sample was separated into different components by high-speed centrifugation using a Beckman Coulter Avanti J-30I Centrifuge. After centrifuging the MFT sample at 9900 rpm (17340 RCF) for 3 hours, three distinct layers were formed, as shown in Figure 4-1A: the supernatant, middle layer (ML), and bottom layer (BL). Judging by the color difference, the ML seemed to have collected most of the residual bitumen together with ultrafine mineral particles. The ML was removed, dispersed in DI water, and centrifuged again at 14,000 rpm (27,000 RCF) for 2 h. After centrifugation, a blackish "ML_top" and greyish "ML_bottom" fraction were obtained, as shown in Figure 4-1B. In this process, it was observed that the middle layer was easily dispersed in water, showing that the middle layer contained a bitumen-in-water emulsion as one of its components. The ML could not be dispersed in toluene. To prepare bitumen-free ML, ML_top and ML_bottom samples, the ML was dispersed in water and repeatedly washed with toluene until the toluene phase was colorless. The toluene-washed ML was then re-suspended with water followed by centrifugation at 14,000 rpm (27,000 RCF) for 2 h, and the sediment image was taken, as shown in Figure 4-1C. This yielded bitumen-free ML_top (T) and bitumen-free ML_bottom (T) samples with solids contents of 43.9 wt% and 63.6 wt%, respectively.

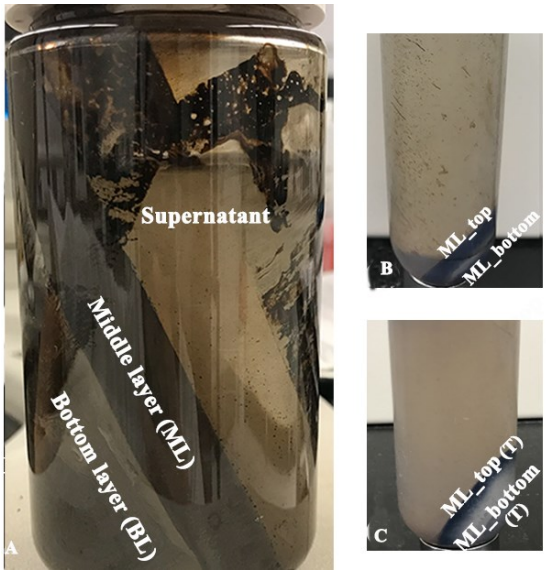


Figure 4-1 (A) The MFT sample after centrifugation at 17340 RCF for 3 h; (B) The middle layer that was dispersed in DI water and centrifuged at 27000 RCF for 2 h; (C) The middle layer that was washed with toluene and centrifuged at 27000 RCF for 2 h.

The composition of each fraction was measured by the Dean-Stark method, and each sample was repeated four times. The composition together with a mass balance is shown in Table 4-1. As can be seen, the ML contained 12 wt% bitumen, 42.6 wt% solids and 45.4 wt% water, and collected 13.5% of the mass, 52.2% of the bitumen, and 18.2% of the mineral solids from the original MFT sample. Surprisingly, the bottom layer sample (BL) still contained 3.46 wt% bitumen despite the greyish color, and therefore it collected almost half of the bitumen in the original MFT. As expected, the ML had a much higher bitumen to solid mass ratio, at 0.28, than the BL, at 0.049. The ML was found to have a medium size of about 2.5 μm, significantly larger than the clay particle size under the centrifugal force used. It was therefore assumed that the 12 wt% bitumen in ML was mostly a bitumen-in-water emulsion, or bitumen that were coated on the ultrafine clay surfaces.

Table 4-1 Composition and mass balance of the MFT sample.

| Sample | Wt% | Content (%) | | | Distribution (%) | |
|---|---|---|---|---|---|---|
| | | Bitumen | Solids | Water | Bitumen | Solids |
| MFT | 100.0 | 3.10±0.02 | 31.80±0.23 | 65.1 | 100.0 | 100.0 |
| Water | 50.0 | 0 | 0 | 100.0 | 0 | 0 |
| Bottom layer, BL | 36.5 | 3.46±0.23 | 70.90±0.20 | 25.6 | 40.8 | 81.8 |
| Middle layer, ML | 13.5 | 11.98±0.52 | 42.61±0.24 | 45.4 | 52.2 | 18.2 |
| ML_top | 9.69 | 13.30±0.37 | 45.33±1.99 | 41.4 | | |

### 4.2.3. Preparation of bitumen-coated minerals

After drying the minerals at 110℃ for 24 h, 20 g dried minerals were treated in 200 mL 10 wt%, 30 wt%, or 50 wt% bitumen-in-toluene solutions for one day or one week, with 12-hours of magnetic stirring every other day. The treated mineral samples were centrifuged at 12860 rpm (20,000 RCF) for 30 min to separate solids and liquid. The centrifuge cake was mixed with toluene and centrifuged again. The toluene washing and centrifugation were repeated 4 - 5 times until the toluene phase was colorless. The bitumen-coated minerals were dried in a fume hood at 25℃ overnight. As control, toluene-treated kaolinite and montmorillonite were obtained in the same manner but without the addition of bitumen.

### 4.2.4. Filter press filtration and vacuum filtration tests

The detailed procedures of the dual-polymer treatment and filter press operation were reported in our work published earlier [18,23] and closely followed in this work. Briefly, the MFT or model minerals were prepared in batches of 500 g slurry and homogenized at 300 rpm for 10 min with a PBT axial-flow impeller. To study the effect of bulk bitumen on filtration, the samples were mixed with the bitumen froth (BF) sample at different bitumen concentrations. The samples were then treated with A3335 and Alcomer 7115 at specified dosages as required. The first polymer A3335 was introduced to the impeller tips by a syringe after stirring the slurry for 10 mins, and the second polymer Alcomer 7115 was injected 5 seconds after the

torque of the slurry reached a peak following the first polymer addition. The stirring was stopped 5 seconds after the torque reached a second peak after the addition of the second polymer. The polymer-treated slurry was then preloaded into the filter chamber of a SERFILCO 0.02-7PPHM laboratory filter press and filtered at 6.2 bar for 1 hour. Following the filtration, the solids content of the filter cake was obtained by drying the cake in a vacuum oven at 70°C and 0.8 bar for 24 hours.

The previously established vacuum filtration setup (Figure 3-1) was used to conduct the vacuum filtration tests. In a typical test, 40 mL slurry of the filtration feed sample at a pre-determined solids content was prepared with DI water. The slurry was stirred by a magnetic stirring bar at 800 rpm for 2 mins, treated in an ultrasonic bath for 3 mins, and then stirred for another 5 mins. An aliquot of 20 mL feed slurry was transferred to the filter funnel, with a filter area of 9.6 $cm^2$, by a syringe and run for 30 min at 30 to 50 mbar depending on the sample. The accumulated filtrate volume was recorded at 1 minute interval, and the filtration performance was determined by the initial filtration rate (IFR), mL/min/$cm^2$. The IFR was calculated by the linear fitting of the first five data points based on the filtration volume versus time. For the very slow filtering samples without enough filtrate data, the IFR was obtained by the final filtrate volume divided by the total filtration time (30 mins).

### 4.2.5. Scanning electron microscopy (SEM) imaging of the ML components

The morphology of MFT components after dispersing in water followed by drying in air was visualized by a Zeiss EVO MA 10 scanning electron microscope (SEM). The ML_top and ML_bottom were prepared at 3 wt% solids. The slurry was stirred by a magnetic stirring bar at 800 rpm for 2 mins, then treated in an ultrasonic bath for 3 mins before stirring for another 5 mins. A small sample of the suspension was drop-casted by a pipet on the SEM stubs coated

with carbon tape. After drying the sample in a fume hood overnight, the solid samples on the stub were coated with gold by sputtering in a Denton gold sputter unit for 90 s, and placed in the SEM sample chamber for imaging. The observation condition was set as follows: the work distance was adjusted in the range of 6.5-10 mm; beam current was set at 50 μA; voltage was fixed at 10 kV.

## 4.3. Results and Discussion

### 4.3.1. Filter press filtration of MFT and model kaolinite slurry

As the residual bitumen in the MFT was segregated in the ML and BL after high-speed centrifugation, to explore the effect of residual bitumen on the filterability of MFT and the model clay mineral kaolinite, filter press tests were conducted after removing ML from MFT or adding ML to kaolinite, and the results are shown in Figure 4-2. As can be seen from Figure 4-2, the MFT could be filtered by a one-hour filter press operation at 6 bar pressure to 67.1 wt% solids after treatment with 1000 g/t A3335 and 3000 g/t Alcomer 7115. When the ML was removed from the MFT, and the remaining MFT (i.e., BL), was re-slurried to 37 wt% solids with the centrifuge supernatant, the solid content of the filter cake (from the BL) increased to 71.0 wt% at half of the polymer dosages (500 g/t A3335 and 1500 g/t Alcomer 7115) (the red bar in Figure 4-2). The 4 percentage points increase in the filter cake solids content obtained at half of the polymer dosages after removing the ML indicated the significant detrimental effect of the ML on the pressure filtration of the MFT. Once the ML was removed, the filtration of the BL was markedly improved.

Similarly, for the model kaolinite slurry at 37 wt% solids, the filter press cake obtained without the use of any polymer flocculant reached 68.5 wt%. However, after adding the ML to the kaolinite to reach 3 wt% of bitumen content, the obtained filter press cake had only 58.2 wt%

solids after flocculation using 1000 g/t A3335 and 3000 g/t Alcomer 7115. In other words, the kaolinite "doped" with ML was more difficult to filter than the original MFT. Interestingly, the addition of the BL to kaolinite at the same amount as ML also affected the filterability of the kaolinite slurry, and the filter press cake contained 67.4 wt% solids, almost the same as the original kaolinite slurry. Since the original kaolinite slurry generated a filter press cake containing 68.5 wt% solids, it would appear that the addition of BL had almost no effect. The difference was that the original kaolinite slurry was not flocculated with any polymer, but the BL-doped kaolinite was flocculated with 1000 g/t A3335 and 3000 g/t Alcomer 7115. Clearly, the BL also had a detrimental effect on the filtration of the kaolinite slurry although it was unlikely to contain any free bitumen or bitumen-in-water emulsion, but the detrimental effect was less severe than the ML.

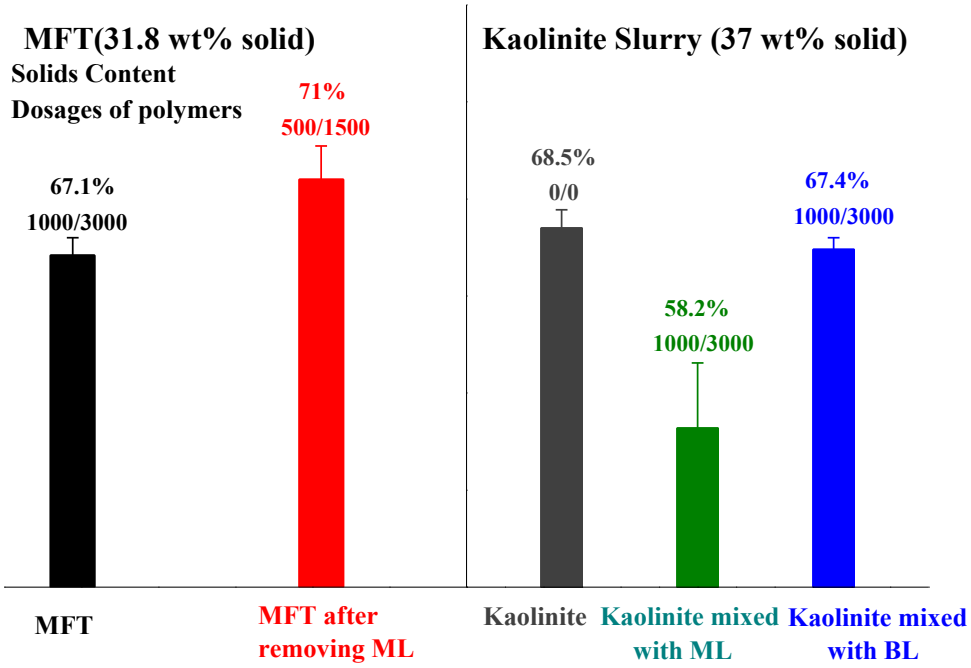


Figure 4-2 Comparison of the solids content of the filter cakes of MFT and model kaolinite from the filter press experiments.

The significantly improved filterability of MFT after removing the ML, and the significantly decreased filterability of kaolinite slurry after adding the ML, indicated that the ML played a critical role in deteriorating the filterability of both MFT and kaolinite slurry.

The ML contained about 40 wt% mineral solids. Particle size and mineralogical analyses showed that the solid phase contained ultrafine <0.45 μm clays and swelling clays. Based on the mineralogical analysis results, a separate study was carried out to study the filtration behaviors of individual types of minerals (non-clay, clay, and swelling clays), and the results were presented in Chapter 3, which identified swelling clays as the most difficult fine minerals to filter.

Both the ML and BL contained bitumen, and the bitumen content in ML was much higher than in BL. It was reasonable to assume that the bitumen in the BL was mostly adsorbed on the mineral surface, while the bitumen in the ML may be either "free" bitumen or bitumen adsorbed on the surface of the ultrafine solids. In view of the detrimental effects of the ML and BL on kaolinite slurry filtration, the roles of both free bitumen and adsorbed bitumen on pressure filtration of mineral solids were investigated.

### 4.3.2. The effect of bitumen froth on filter press filtration of MFT and model kaolinite slurry

The question to be addressed was if bulk bitumen, when added externally to a mineral slurry or MFT, would affect the filtration behavior? To find the answers to this question, MFT or kaolinite slurry was mixed with the bitumen froth (BF) sample to reach different bitumen contents, and the mixture was filtered with the laboratory filter press. As can be seen from Figure 4-3, when bitumen was added to MFT through the addition of BF to get 5 wt% bitumen

content, the solids content of the filter press cake was lowered from 67.1 wt% to 64 wt% while other conditions were kept the same.

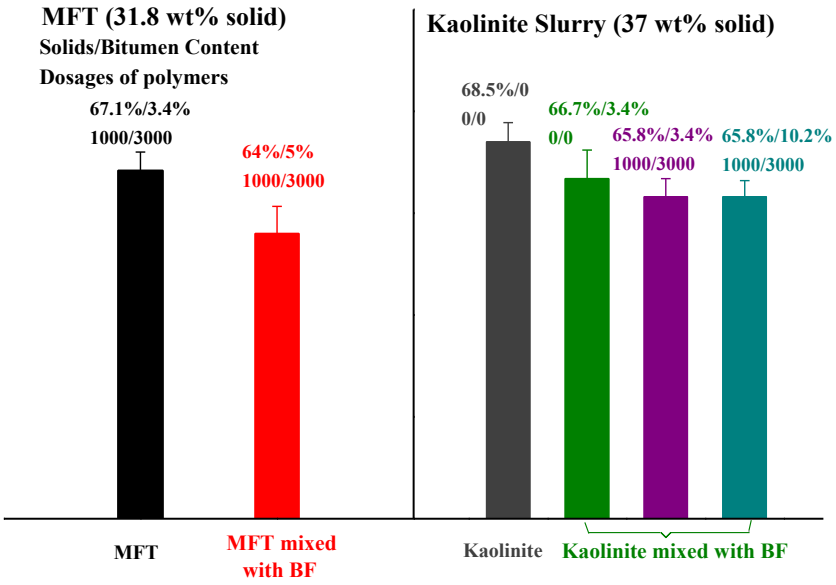


Figure 4-3 Comparison of the solid content of the filter cakes of MFT and model kaolinite slurries after blending in bitumen froth (BF) sample.

For the kaolinite slurry, the addition of the bitumen froth sample to reach a bitumen content of 3.4 wt% lowered the solid content in the filter cake from 68.5 wt% to 66.7 wt%, when no polymer was used. Therefore, the bulk bitumen did not seem to have a significant detrimental effect on the filtration of the kaolinite slurry. Interestingly, in this case, the addition of polymer flocculants (1000 g/t A3335 and 3000 g/t Alcomer 7115) did not increase the solid content of the filter cake but decreased it by about one percentage point, to 65.8 wt% (Figure 4-3). Compared with the results in Figure 4-2, which showed that the two polymer dosages were required to keep the kaolinite filterable when the ML or BL were introduced to kaolinite, it can be seen that the added polymer flocculants were not interacting with the added bulk bitumen.

In fact, even when the bulk bitumen content was increased to 10.2 wt%, the filter cake contained the same 65.8 wt% solids (Figure 4-3).

Loerke et al. [18] observed that the addition of the ML from centrifuged MFT to a kaolinite slurry required a 10-fold increase of polymer dosages to keep the kaolinite filterable. It was considered that the extra polymers were required to overcome the detrimental effect of the bitumen so they were probably interacting with the fine bitumen brought in by the ML. Indeed, Loerke et al. [18] showed that the filter cloths were clean after the addition of the high dosages of polymers, otherwise they were dirty with bitumen smears at low polymer dosages (see Figure 2-9 on page 31). The results obtained with the externally added bitumen froth (BF) in the present work showed that bulk bitumen did not have a drastic detrimental effect on the pressure filtration of either MFT or model kaolinite slurry. Therefore a high polymer dosage was not required.

To eliminate the possibility of sample variation, a different bitumen froth sample was also tested, which contained 65.2 wt% bitumen, 12.6 wt% solids, and 22.2 wt% water. When dosed to the kaolinite slurry to 3.4 wt% bitumen, the pressure filter cake was found to contain 66.9 wt% solids without polymer treatment, and 66.3 wt% solids with 1000 g/t A3335 and 3000 g/t Alcomer 7115. Therefore, the results were very similar to the main bitumen froth (BF) sample used. Overall, the bulk bitumen in the form of bitumen froth seems to have a minor influence on the filtration of MFT and kaolinite slurry. In fact, the bitumen was observed to pass through the filter cake and was visible in the filtrate.

### 4.3.3. The effect of bitumen-in-water emulsion

The ML obtained after high-speed centrifugation (17300 RCF) of the MFT sample was found to have a medium particle size of about 2.5 μm. Furthermore, the ML_top sample, obtained

after centrifugation at 27000 RCF, had an even larger medium size of 5.4 μm. Both were much larger than what may be expected for clay particles at the high centrifugal force. It was therefore assumed that the 12 wt% bitumen in the ML were in the form of bitumen-in-water emulsion or bitumen adsorbed on ultrafine clay surface.

The effect of this bitumen-in-water emulsion was investigated by removing the bitumen from the ML and subject the resulting sample to filtration. For this purpose, the ML_top and ML_bottom samples were washed with toluene repeatedly, and the cleaned samples, designated as ML_top (T) and ML_bottom (T), respectively, were then used in the vacuum filtration tests. The results are shown in Figure 4-4. As can be seen, toluene wash had a negligible effect on the vacuum filtration of ML, ML_top and ML_bottom samples. The results showed that bitumen-in-water emulsion did not affect the filtration behavior. To confirm, vacuum filtration tests were also conducted on a bitumen-in-water emulsion obtained by ultrasonic emulsification of a bitumen-water mixture and it was observed that the emulsion filtered the same as DI water.

The vacuum filtration rates of ML and ML_top were very low even when the samples were diluted 50 times to 1 wt% solids. When it was diluted to 3 wt% solids it was unfilterable and behaved similar to the vacuum filtration of MFT [24].

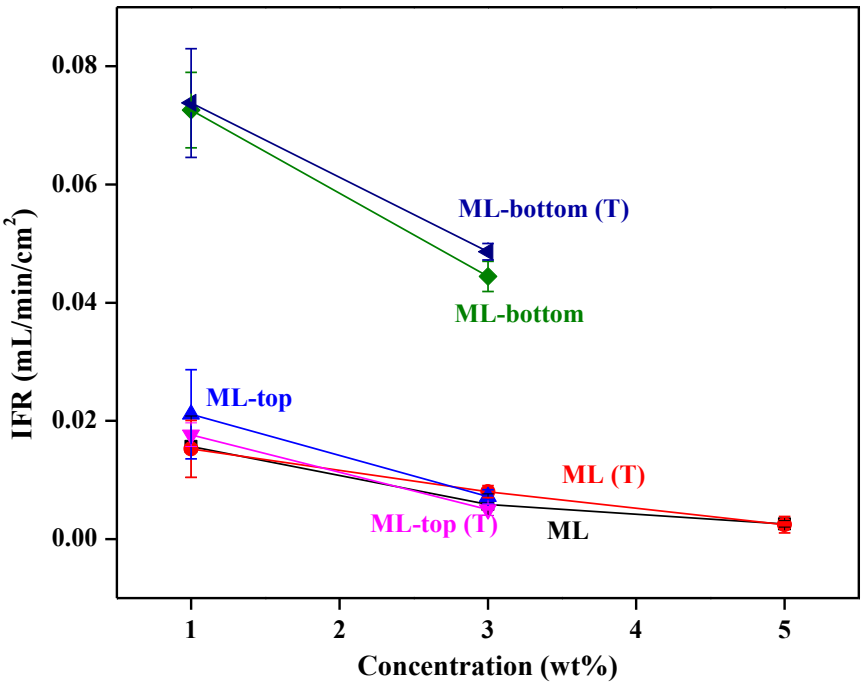


Figure 4-4 Initial filtration rate (IFR) of the ML, ML_top, and ML_bottom before and after washing with toluene. ML_top (T) and ML_bottom (T) represent ML_top and ML_bottom samples washed with toluene.

Figure 4-5 shows the vacuum filtration of kaolinite slurries at 37 wt% solids with or without adding 3 wt% ML_top, ML_bottom, ML_top (T), and ML_bottom (T). As can be seen, removing the bitumen by toluene wash did not change the effects of the ML_top and ML_bottom on the filterability of the kaolinite slurry. The kaolinite slurry alone showed reasonable filterability in vacuum filtration, consistent with its high filterability in the filter press tests. But the filterability of the kaolinite slurry was significantly reduced by introducing the ML_top to a concentration of 3 wt%. On the other hand, the addition of ML_bottom to a 3 wt% concentration had negligible effects on the filtration rate of the kaolinite slurry.

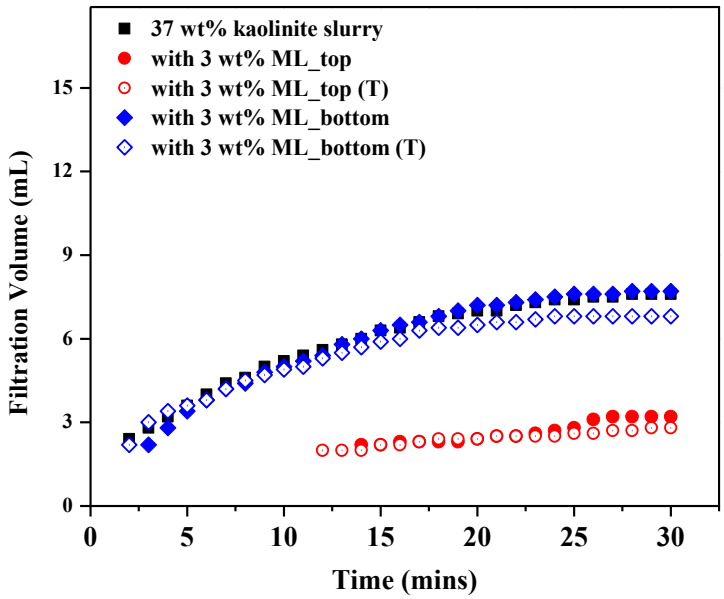


Figure 4-5 The effect of the raw and toluene-washed ML_top and ML_bottom samples on the filtration of kaolinite slurry.

To check if the toluene wash removed the bitumen from the ML_top and ML_bottom samples, and also to find the reasons for the dramatically different effects of the ML_top versus the ML_bottom samples, CHNS elemental analysis, SEM imaging, and X-ray diffraction analysis were performed on the ML_top and ML_bottom samples. Table 4-2 shows the nitrogen, carbon, hydrogen, and sulfur contents of MFT components before and after toluene wash. As can be seen, after toluene wash, the carbon content of ML decreased from 21.5 wt% to 4.1 wt%, indicating that most of the bitumen was removed by toluene. Combined with the filtration results that the toluene wash had little effect on the filterability of ML, it can be concluded that the emulsified bitumen was not responsible for the poor filterability of ML, nor was it responsible for the ML-doped kaolinite slurry. Similar effects about toluene wash was observed for the ML_top and ML_bottom samples.

Table 4-2 CHNS elemental composition of MFT components before and after toluene wash

| Sample | Content (%) | | | |
|---|---|---|---|---|
| | Nitrogen | Carbon | Hydrogen | Sulfur |
| ML | 0.2594±0.0057 | 21.4956±0.6099 | 3.1908±0.0583 | 1.2731±0.0262 |
| ML (T) | 0.1635±0.0138 | 4.0896±0.4779 | 1.4000±0.0543 | 0.2566±0.0293 |
| ML-top | 0.2166±0.0019 | 20.0565±0.0150 | 3.0783±0.0169 | 1.2178±0.0880 |
| ML-top (T) | 0.1565±0.0019 | 8.6158±0.1190 | 1.8833±0.0023 | 0.4159±0.0182 |
| ML-bottom | 0.2314±0.0004 | 15.5492±0.2320 | 2.5385±0.0418 | 0.7874±0.0234 |
| ML-bottom (T) | 0.1727±0.0018 | 4.8836±0.0695 | 1.5436±0.0329 | 0.2468±0.0031 |
| BL | 0.1739±0.0004 | 11.0821±0.0080 | 1.5207±0.0011 | 1.6805±0.0080 |
| BL (T) | 0.0899±0.0015 | 2.3892±0.0877 | 1.5928±0.0152 | 0.1041±0.0051 |

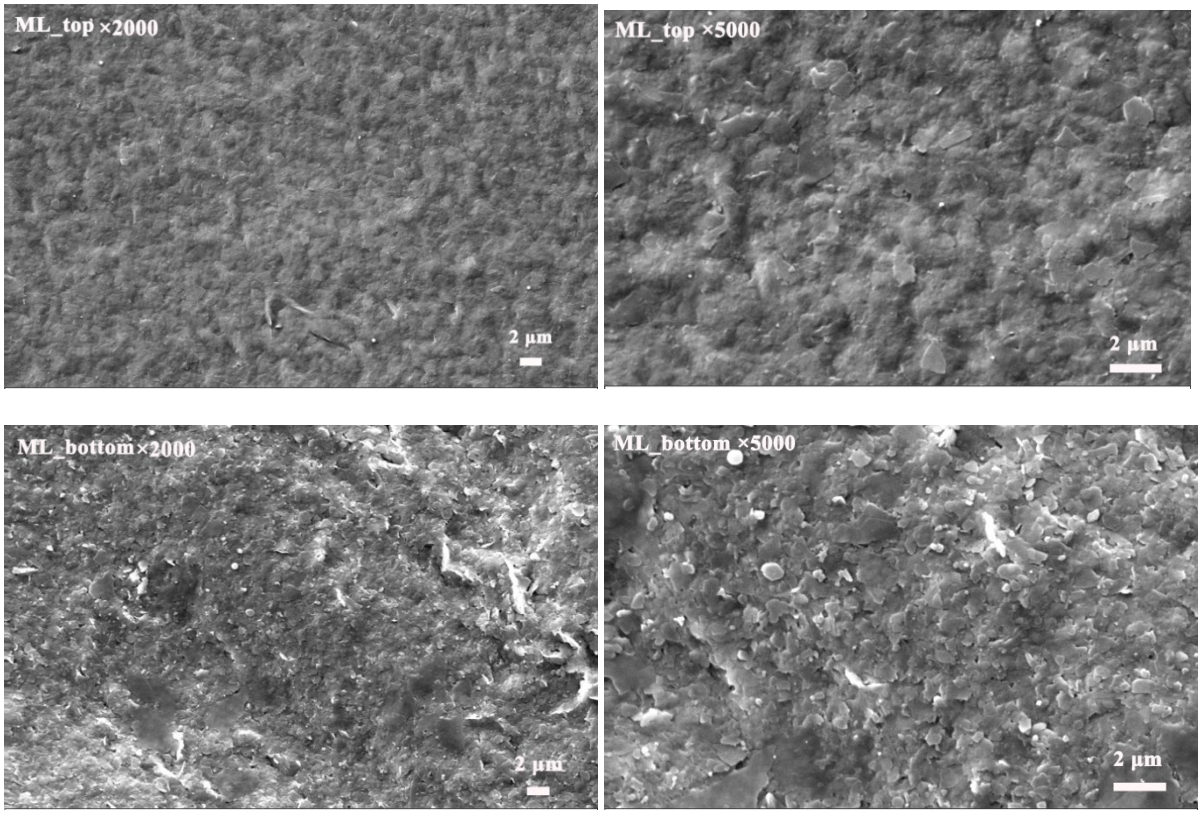


Figure 4-6 SEM images of toluene-washed ML_top and ML_bottom samples at 2000x and 5000x magnifications, respectively.

Figure 4-6 shows the SEM images of the ML_top and ML_bottom samples. As can be seen, the clay platelets in the ML_top sample formed gel-like structure after drying. The different structures of ML_top and ML_bottom may explain the observation that the ML_bottom sample was more filterable than ML_top sample, and also that ML_top sample had a more detrimental effect on kaolinite slurries.

### 4.3.4. The effect of adsorbed bitumen on filtration

The foregoing discussion shows that bulk bitumen and bitumen-in-water emulsion did not seem to affect the filtration of MFT or model mineral slurry. While the bulk bitumen or emulsified bitumen can be removed by the combined toluene wash and centrifugation, the adsorbed bitumen on mineral surface cannot be completely removed by toluene wash or centrifugation [25]. Therefore, the role of adsorbed bitumen in the filtration of model minerals was investigated by vacuum filtration, and the amount of adsorbed bitumen on the mineral surfaces was controlled by changing the treatment conditions of the minerals by bitumen-in-toluene solutions.

#### 4.3.4.1. The effect of treatment time of the model minerals with bitumen-in-toluene solution

Kaolinite and montmorillonite were used as the model clay minerals, and they were treated in 10 wt% bitumen-in-toluene solutions for 1 day or 1 week. Control tests were performed by treating the clays in toluene only, without bitumen. The vacuum filtration results of the treated clay samples are shown in Figure 4-7. As can be seen, the filtration rate of kaolinite after treatment with 10 wt% bitumen-in-toluene increased dramatically. Considering that treatment of the kaolinite by toluene slightly decreased the kaolinite filterability, it can be seen that the increased filtration rate of kaolinite was caused by the adsorbed bitumen on the kaolinite

surface. For montmorillonite, the filtration rate was increased significantly after 1 week of treatment in the 10 wt% bitumen-in-toluene solution, and the increase in filtration rate was only marginal when the treatment time was shorter at 1 day. Similar to kaolinite, treatment by toluene alone deceased the filtration rate of montmorillonite.

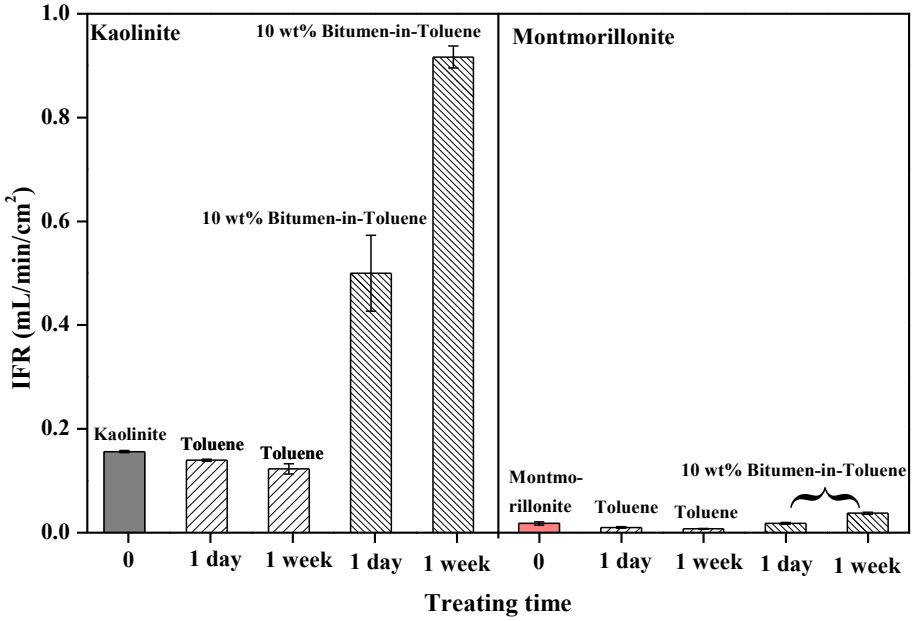


Figure 4-7 The filtration rate of kaolinite and montmorillonite after treatment with 10 wt% bitumen-in-toluene solution for different time periods. Control test results are also shown for untreated minerals and minerals treated with toluene only. In all filtration tests, the solid content of kaolinite slurry was 10 wt% and that of the montmorillonite slurry was 1 wt%.

#### 4.3.4.2. The effect of bitumen-in-toluene concentration

Four minerals with different specific surface areas were selected and treated in bitumen-in-toluene solutions for 1 week at different bitumen concentrations. Figure 4-8 shows the results. The previous section showed that treatment in 10 wt% bitumen-in-toluene solution increased the filtration rates of kaolinite and montmorillonite.

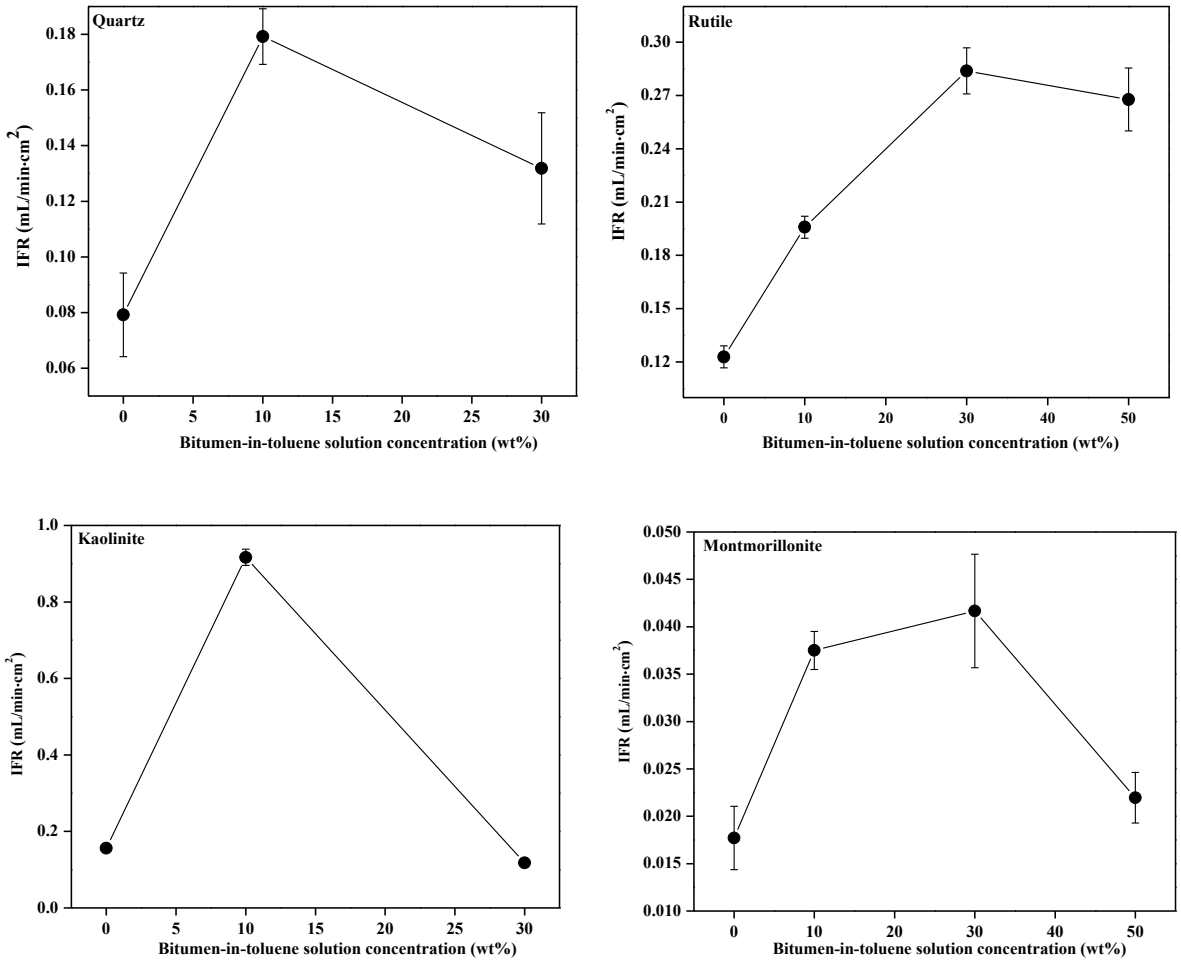


Figure 4-8 The filtration rate of minerals treated at different bitumen concentrations in the bitumen-in-toluene solution for 1 week. In the filtration tests, the quartz and rutile slurries were 20 wt% solids, the kaolinite slurry was 10 wt% solids, and the montmorillonite slurry was 1 wt% solids.

Figure 4-8 shows that quartz and rutile also showed similar increase in filtration rates after treatment in 10 wt% bitumen-in-toluene solution for 1 week. However, when the minerals were treated at higher bitumen concentrations in the bitumen-in-toluene solution, the filtration rate was decreased. For all four minerals, there was an optimum bitumen concentration which resulted in the highest filtration rates. At lower and higher bitumen concentrations, the filtration

rate was lower. Furthermore, it can be seen that for quartz and kaolinite, the optimum concentration was 10 wt% bitumen, but for rutile and montmorillonite, the optimum concentration was 30 wt% bitumen.

From the results obtained, it can be seen that the bulk bitumen and emulsified bitumen had little effect on the filterability of oil sands tailings or model mineral samples, and the adsorbed bitumen on the mineral surface could improve the mineral filtration performance at low bitumen concentration but decrease the filterability at high bitumen concentration. It was shown in Chapter 3 that swelling clays in the oil sands tailings were the main reason for its poor filterability. Combined with the results here, it can be concluded that the poor filterability of MFT may be caused by the relatively high bitumen adsorption density on the mineral surface and the swelling clays in the MFT.

### 4.4. Conclusions

The effect of bitumen on the filtration of oil sands mature fine tailings (MFT) was investigated using MFT and model minerals in pressure filtration and vacuum filtration tests. The possible forms of bitumen were investigated, i.e., bulk bitumen, emulsified bitumen, and adsorbed bitumen on minerals surfaces.

To study the effect of bulk bitumen, a bitumen froth sample was added to MFT or kaolinite slurry up to 10 wt% bitumen. It was found that the bitumen froth only lowered the filter cake solid content slightly.

The effects of emulsified bitumen were investigated by generating a bitumen-in-water emulsion through high-speed centrifugation, dubbed centrifugation middle layer (ML), middle layer top (ML_top), and middle layer bottom (ML_bottom). The ML, ML_top and ML_bottom

samples were filtered directly after dilution, or blended with model kaolinite slurry followed by filtration, with and without repeated wash with toluene beforehand. It was found that the repeated toluene wash did not change the filtration behavior, either of the ML samples, or the ML-doped kaolinite samples. Therefore the bitumen-in-water emulsion was deemed to be benign to the filtration process.

The effects of bitumen adsorbed on mineral surface was studied by coating quartz, rutile, kaolinite and montmorillonite with bitumen by submerging the minerals in bitumen-in-toluene solutions of varying bitumen concentrations and with varying submerging times (1 day or 1 week). It was found that at low bitumen concentration, the filterability of all treated minerals was improved, more so for the non-clay minerals (quartz, rutile) and non-swelling clay (kaolinite), and less so for the swelling clay (montmorillonite). However, at high bitumen concentrations, the filterability was reduced. The optimum bitumen concentration varied with the tested minerals. The results pointed to the possible effect of the thickness of bitumen coating on the filtration of the resulting mineral. The phenomenon was further studied in the next chapter.

**References**

[1] COSIA. Technical Guide for Fluid Fine Tailings Management. 2012. https://doi.org/https://cosia.ca/uploads/documents/id7/TechGuideFluidTailingsMgmt_Aug2012.pdf.

[2] COSI. Innovative Solutions for Sustainable Oil. 2020. https://doi.org/https://cosia.ca/sites/default/files/202106/2020COSIA_AnnualReport.pdf.

[3] Alam N, Ozdemir O, Hampton MA, Nguyen A V. Dewatering of coal plant tailings: Flocculation followed by filtration. Fuel 2011;90:26–35. https://doi.org/10.1016/J.FUEL.2010.08.006.

[4] Adeyinka OB, Samiei S, Xu Z, Masliyah JH. Effect of particle size on the rheology of athabasca clay suspensions. Can J Chem Eng 2009;87:422–34. https://doi.org/10.1002/cjce.20168.

[5] Xu Y, Dabros T, Kan J. Filterability of oil sands tailings. Process Saf Environ Prot 2008;86:268–76. https://doi.org/10.1016/j.psep.2008.04.005.

[6] Mercier PHJ, Ng S, Moran K, Sparks BD, Kingston D, Kotlyar LS, et al. Colloidal Clay Gelation: Relevance to Current Oil Sands Operations. Pet Sci Technol 2012;30:915–23. https://doi.org/10.1080/10916466.2010.495959.

[7] Kotylar LS, Sparks BD, Schutfe R. Effect of Salt on the Floculation Behavior of Nano Particles in Oil Sands Fine Tailings 1996;44:121–31. https://doi.org/10.1346/CCMN.1996.0440111.

[8] Loeber L, Muller G, Morel J, Sutton O. Bitumen in colloid science: a chemical, structural and rheological approach. Fuel 1998;77:1443–50. https://doi.org/10.1016/S0016-2361(98)00054-4.

[9] Scott J., Dusseault MB, Carrier WD. Behaviour of the clay/bitumen/water sludge system from oil sands extraction plants. Appl Clay Sci 1985;1:207–18. https://doi.org/10.1016/0169-1317(85)90574-5.

[10] Chalaturnyk RJ, Scott JD, Özüm B. Management of oil sands tailings. Pet Sci Technol

2002;20:1025–46. https://doi.org/10.1081/LFT-120003695.

[11] Guzma J, Isquierdo F, Carbognani L, Vitale G, Scott CE, Pereira-almao P. X-ray Photoelectron Spectroscopy Analysis of Hydrotreated Athabasca Asphaltenes. Energy & Fuels 2017;31:10706–17.

[12] Baillie RA, Malmberg EW. Removal of clay from the water streams of the hotwater process by flocculation. 3,487,003, 1969.

[13] Suthaker NN, Scott. JD. Measurement of hydraulic conductivity in petroleum sand tailings slurries. Can Geotech J 1996;33:642–53.

[14] Xu K, Zhu P, Huh C, Balhoff MT. Microfluidic Investigation of Nanoparticles Role in Mobilizing Trapped Oil Droplets in Porous Media. Langmuir 2015;31:13673–9. https://doi.org/10.1021/acs.langmuir.5b03733.

[15] Majid A, Sparks BD. Role of hydrophobic solids in the stability of oil sands fine tailings. Fuel 1996;75:879–84. https://doi.org/10.1016/0016-2361(96)00015-4.

[16] Majid A, Ripmeester JA. Characterization of unextractable organic matter associated with heavy minerals from oil sand. Fuel 1986;65:1714–27. https://doi.org/10.1016/0016-2361(86)90275-9.

[17] Klein C, Harbottle D, Alagha L, Xu Z. Impact of fugitive bitumen on polymer-based flocculation of mature fine tailings. Can J Chem Eng 2013;91:1427–32. https://doi.org/10.1002/cjce.21863.

[18] Loerke R, Tan X, Liu Q. Dewatering of Oil Sands Mature Fine Tailings by Dual Polymer Flocculation and Pressure Plate Filtration. Energy and Fuels 2017;31:6986–95.

https://doi.org/10.1021/acs.energyfuels.7b00938.

[19] Pendharker S, Shende S, Jacob Z, Nazemifard N. Three-dimensional optical tomography of bitumen and clay association in oil sands tailings. Fuel 2017;207:262–7. https://doi.org/10.1016/J.FUEL.2017.06.107.

[20] Chen Q, Liu Q. Bitumen Coating on Oil Sands Clay Minerals: A Review. Energy and Fuels 2019;33:5933–43. https://doi.org/10.1021/acs.energyfuels.9b00852.

[21] Liu J, Wang J, Huang J, Cui X, Tan X, Liu Q, et al. Heterogeneous Distribution of Adsorbed Bitumen on Fine Solids from Solvent-Based Extraction of Oil Sands Probed by AFM 2017. https://doi.org/10.1021/acs.energyfuels.7b00396.

[22] Liu J, Zhou Z, Xu Z, Masliyah J. Bitumen-clay interactions in aqueous media studied by zeta potential distribution measurement. J Colloid Interface Sci 2002;252:409–18. https://doi.org/10.1006/jcis.2002.8471.

[23] Zhu Y, Tan X, Liu Q. Dual polymer flocculants for mature fine tailings dewatering. Can J Chem Eng 2017;95:3–10. https://doi.org/10.1002/cjce.22628.

[24] Wang D, Tao H, Wang K, Tan X, Liu Q. The filterability of different types of minerals and the role of swelling clays in the filtration of oil sands tailings. Fuel 2022;316:123395. https://doi.org/10.1016/J.FUEL.2022.123395.

[25] Chen Q, Liu J, Thundat T, Gray MR, Liu Q. Spatially resolved organic coating on clay minerals in bitumen froth revealed by atomic force microscopy adhesion mapping. Fuel 2017;191:283–9. https://doi.org/10.1016/j.fuel.2016.11.091.

# CHAPTER 5 Effects of Mineral Surface Silanization and Bitumen Coating on its Filtration from an Aqueous Slurry

## 5.1. Introduction

Due to the large scale of production, large quantities of tailings are generated in the surface mining and bitumen extraction operation of Alberta oil sands. The accumulation of the fluid fine tailings, which are infinitely stable, has led to large tailings pond areas occupying an estimated 259 $km^2$ of land areas in northern Alberta, Canada as of 2017 [1]. Alberta Energy Regulators mandated Directive 085 in 2017 requiring the oil sands industry to reclaim the tailings within 10 years of the end of mine project life [2]. The industry has yet to develop a viable and economic dewatering technology to meet this regulatory requirement. Meeting this requirement means that the oil sands tailings need to be dewatered to its plastic limit to commence reclamation [3]. In recent years, filter presses have been gaining popularity in sludge dewatering to handle high throughput and generate high solids content filter cakes. For typical mine tailings, such as iron ore and gold ore tailings, commercial filter presses can typically generate filter cakes with >= 85 wt% solids [4–6]. However, when the same technology was used in oil sands tailings, the solids content in the filter cake could only reach around 60 wt% solids even with high dosages of coagulants and/or polymer flocculants [7], far below the plastic limit.

The commercial warm-water bitumen extraction process can only recover slightly more than 90% of the bitumen from high grade oil sands ores, and the rest of the bitumen is lost to the tailings in the form of free bitumen or adsorbed bitumen on sands/clay surfaces. After sedimentation in the tailings ponds, the fluid fine tailings eventually form the so-called mature fine tailings (MFT), containing 30-40 wt% fine solids (mainly clay minerals and fine quartz),

3-5 wt% bitumen, balanced by process water [7–9]. The particle size distribution of the fine solids in the MFT is similar to coal, alumina, phosphate, and copper tailings [10]. The bitumen in the oil sands tailings could coat mineral surfaces and render them hydrophobic, which should lead to improved filtration, yet curiously the oil sands tailings was more difficult to filter than other mine tailings with no adsorbed bitumen.

In Chapter 4, the effects of various forms of bitumen on the filtration of Alberta oil sands tailings were examined. It was observed that the bitumen-in-water emulsion did not have any effect, the free bulk bitumen slightly affected filtration, and the bitumen layer coated on mineral surface showed drastically different effects from promoting filtration to significantly impeding filtration. The results were puzzling because bitumen coating was supposed to render the mineral surface hydrophobic, which should in turn facilitate filtration of an aqueous slurry. The results prompted a systematic investigation into the effects of mineral surface hydrophobicity on the filtration behavior. The hydrophobicity was induced by bitumen coating at different bitumen layer thicknesses. For comparison, the hydrophobicity was also created on selected mineral surfaces by silanization treatment. The amount of bitumen on the treated mineral surfaces was determined by bulk CHNS elemental composition measurements and X-ray photoelectron spectroscopic (XPS) surface analysis. The thickness of bitumen layer was characterized by XPS depth profile analysis. The filter cakes were visualized by X-ray microscope/nanoCT imaging analysis. The results showed that while hydrophobicity of solid surface generally helps filtration from the aqueous slurry, a relatively thick, patchy, and deformable organic layer, such as bitumen, on the mineral surface could severely deteriorate filtration despite the high degree of hydrophobicity it rendered to the mineral surface.

## 5.2. Materials and Methods

### 5.2.1. Materials

Quartz, rutile, kaolinite, and montmorillonite were used as model minerals in this work to represent typical non-clay minerals, non-swelling clay, and swelling clay. Other than rutile, the minerals were typically found in oil sands tailings. The reason the rutile sample was used was because of its submicron size, suitable to examine the particle size effect. The median particle size $d_{50}$ of quartz ($SiO_2$ Min-U-Sil 15 from US silica) was 3.6 μm, determined by a Malvern Mastersizer 3000 particle size analyzer. The kaolinite (BASF ASP 600) had a median size $d_{50}$ of 4.1 μm, and montmorillonite (Ward's Sciences, USA) had a median size $d_{50}$ of 2.8 μm. High purity rutile (US Research Nanomaterial) had a $d_{50}$ of 0.7 μm. The purity of the minerals was determined to be in the range of 84-94% by X-ray fluorescence (see Table 3-1 on page 52). A high purity bitumen sample, which contained 99.5 wt% bitumen (determined by the Dean-Stark procedure), was collected from an oil sands operator in northern Alberta, Canada. (3-chloropropyl)triethoxysilane (3CTS) with a theoretical formula of $C_9H_{21}ClO_3Si$, purchased from Sigma-Aldrich, was used as the silanization agent and was prepared as a toluene solution at different concentrations. Hydrochloric acid (HCl) of analytical grade was purchased from Fisher Scientific and used to wash the quartz surface before silanization.

### 5.2.2. Preparation of silanized minerals

The quartz sample was silanized by 3CTS solution in toluene. The silanization process of different minerals was slightly different. Liu and Laskowsk's silanization process for quartz was closely followed [11]. The quartz was treated with 0.5 M HCl solution for 12 hours with magnetic stirring before silanization. The acid-treated quartz was collected by centrifugation at 20,000 RCF for 30 mins, and then the quartz was washed with DI water to remove the

remaining HCl followed by centrifugation. The acid-treated quartz was dried in a vacuum oven at 110℃ overnight. Afterwards, 20 g dried acid-treated quartz was treated with 0.005 M, 0.02 M, or 0.04 M 3CTS-toluene solution for a certain time, and the obtained silanized quartz samples were called Quartz 1, Quartz 2, and Quartz 3, respectively. The silanized quartz was washed with toluene repeatedly followed by centrifugation to remove the remaining 3CTS. The silanization process could be represented by the following reaction, i.e., the silanol groups of quartz were replaced by the silane groups of 3CTS in an organic solution [12].

$$\text{Surface-SiOH} + (C_2H_5O)_3Si(CH_2)_3Cl = \text{Surface-Si-O-}(CH_2)_3Si(C_2H_5O)_3 + HCl \quad (5.1)$$

As acid treatment could alter the clays, kaolinite and montmorillonite were not treated with acid before silanization [13]. Instead, the oven-dried kaolinite or montmorillonite was mixed with 200 mL 0.04 M 3CTS-in-toluene solution and stirred at 800 rpm with a magnetic stir bar for 24 hours. This was followed by toluene washing and centrifugation. The silanized minerals were air-dried in a fume hood overnight.

### 5.2.3. Preparation of bitumen-coated minerals

Bitumen-coated minerals were prepared by using a method that is typically used in oil sands research, i.e., by mixing the dried minerals with bitumen-toluene solution. In this work, the bitumen concentration in the toluene solution was fixed at 10 wt%, 30 wt%, and sometimes 50 wt%, and the mineral/bitumen-toluene solution ratio was 1 g/10 mL. The minerals were firstly dried in a vacuum oven at 110℃ overnight and then stored in a drying desiccator and cooled to room temperature. The dried mineral samples were then treated in the bitumen-toluene solutions. After 1 week of standing with 12-hours of agitation using a magnetic stir bar every second day, the suspension was centrifuged at 20,000 RCF for 30 min, and the recovered minerals were washed with toluene. The centrifugation and toluene washing were repeated 4-

5 times until the toluene phase was colorless. At that point, the free bitumen was considered removed. The bitumen-coated minerals were air-dried in a fume hood to remove the remaining toluene before use. Table 5-1 shows a list of sample names and the treatment conditions.

Table 5-1 Summary of sample designation.

| Sample label | Sample treatment |
|---|---|
| Q | Quartz |
| K | Kaolinite |
| M | Montmorillonite |
| R | Rutile |
| KT | Kaolinite treated with toluene only |
| MT | Montmorillonite treated with toluene only |
| B-T | Bitumen-toluene solution |
| QB10, QB30 | Quartz treated with 10 wt%, 30 wt% B-T solution |
| RB10, RB30, RB50 | Rutile treated with 10 wt%, 30 wt%, 50 wt% B-T solution |
| KB10, KB30 | Kaolinite treated with 10 wt%, 30 wt% B-T solution |
| MB10, MB30, MB50 | Montmorillonite in 10 wt%, 30 wt%, 50 wt% B-T solution |

### 5.2.4. Vacuum filtration

The filterability of mineral slurry was evaluated by a laboratory glass filter funnel setup. The filter medium used was P2 grade paper from Fisher Scientific with a pore size of up to 5 μm, and the filter area was 9.6 $cm^2$. The effective working negative pressure generated by the vacuum pump was 30-50 mbar depending on the samples used in the filtration process. The prepared mineral slurry with different solids content was stirred by a magnetic stir bar at 800 rpm for 10 mins, followed by treatment in an ultrasonic bath for 5 mins. During the ultrasonic treatment, no bitumen was observed on the surface of the slurry. After stirring for another 5 mins, 20 mL of the slurry was immediately transferred to the glass funnel with a syringe. The filtrate volume was recorded every 1 min, and a filtration curve was plotted showing filtrate volume versus time. The initial filtration rate (IFR), mL/min/$cm^2$, was obtained by the slope of the filtration curve for the first 5 data points and used to evaluate the filtration performance.

### 5.2.5. Characterization techniques

The wettability of the minerals was assessed by the static sessile drop method, which directly measured the water contact angle on pressed pellets with a FTA2000 contact angle goniometer equipped with an illumination system. The pellet was prepared by pressing 150 mg mineral sample in a 1 cm diameter die for 1 min at 40 MPa pressure by an ICL 12 Ton E-Z Press$^{TM}$ pellet presser. The FTA2000 image system could record the dynamic changes of water droplets on the pellet surface every 0.1 s, and the first unambiguous image of water droplet shape was used to determine the contact angle of the minerals. The average value of three measurements was reported as the final contact angle.

The elemental compositions of untreated and bitumen-coated minerals were measured by a Flash 2000 CHNS/O elemental analyzer. X-ray photoelectron spectroscopy (XPS) analysis was performed at nanoFAB at the University of Alberta with a Kratos Axis (Ultra) spectrometer with monochromatized Al Kα (hν=1486.69 eV). The core-level spectra were collected using a hemispherical electron-energy analyzer at a pass energy of 20 eV, and the survey spectrum with binding energies from 0 to 1100 eV was collected at a pass energy of 160 eV. High-resolution scans of C 1s, O 1s, N 1s, S 2p, Al 2p, and Si 2p electrons were taken at the pass energy of 20 eV to acquire the element concentration. Depth profiling of the bitumen-coated kaolinite was carried out by XPS Versa Probe III (PHI 5000). An $Ar^+$ ion beam was used to etch the bitumen-coated kaolinite surface at 1 kV to progressively remove the surface layer at a 60-second interval. The sputtering rate according to $SiO_2$ calibration is 0.8 nm per min with a rotation speed of 1 RPM. The elemental concentrations on the newly exposed surface during sputtering were collected and compared with the un-coated kaolinite surface. When the surface elemental concentrations were stabilized and became similar to the

un-coated kaolinite, the bitumen layer was considered removed. Relative bitumen layer thickness could be estimated approximately by the sputtering time and the etching rate (absolute bitumen layer thickness could not be ascertained because the etching rate of the bitumen layer was expected to be different from quartz). Shirley or linear background type was used by Casa XPS software to determine the peak model parameters such as the peak positions and widths. All the spectra were calibrated based on the binding energy value of C 1s at 284.8 eV.

The pore structures of filter cakes from untreated and bitumen-coated kaolinite were imaged by a non-destructive Zeiss Xradia 620 Versa X-ray microscope/nanoCT (XRM). The samples for XRM/nanoCT analyses were prepared by vacuum filtration, and the slurry was prepared following the same procedure for the vacuum filtration sample preparation. An aliquot of 20 mL kaolinite slurry, at 1 wt% solids content, was used in the filtration test, and each test was run for 30 mins. A small piece of filter cake after filtration was collected for XRM/nanoCT analysis. A wooden toothpick with glue on the head was used to dip a small piece of filter cake and mount it on the sample holder of the XRM for analysis. 1601 projections were collected with an exposure time of 4 s, and the 3D images were acquired by rotating the sample from -180° to +180° with a 40× objective lens and 0.5 μm pixel size. Each projection was operated at 60 kV X-ray voltage and 6.5 W power. The 3-D visualization, reconstruction, and composition analysis were performed by Dragonfly Pro software provided by Objective Research Systems (ORS).

## 5.3. Results and Discussion

### 5.3.1. Effects of bitumen coating on mineral surface hydrophobicity and filtration

#### 5.3.1.1. The contact angle of bitumen-coated minerals

Figure 5-1 shows the contact angle of untreated and bitumen-coated minerals. Quartz and kaolinite were treated with 10 wt% and 30 wt% bitumen-toluene solutions, and rutile and montmorillonite were treated with 10 wt%, 30 wt%, and 50 wt% bitumen-toluene solutions. As can be seen in Figure 5-1A, the quartz contact angle increased from 13° to more than 110° after the bitumen treatment, indicating that the bitumen coated the quartz surface and rendered it hydrophobic. Rutile (Figure 5-1B) and kaolinite (Figure 5-1C) also showed dramatic increase in contact angles after the bitumen-coating treatment. It was observed that 10 wt% bitumen-toluene solution was sufficient to make the mineral surfaces hydrophobic, and further increase of bitumen concentration to 30 wt% or 50 wt% could only further increase the contact angle slightly. For montmorillonite (Figure 5-1D), the bitumen-coating treatment did not significantly increase the surface hydrophobicity, and the contact angle was only slightly increased, indicating that the montmorillonite surface was still hydrophilic.

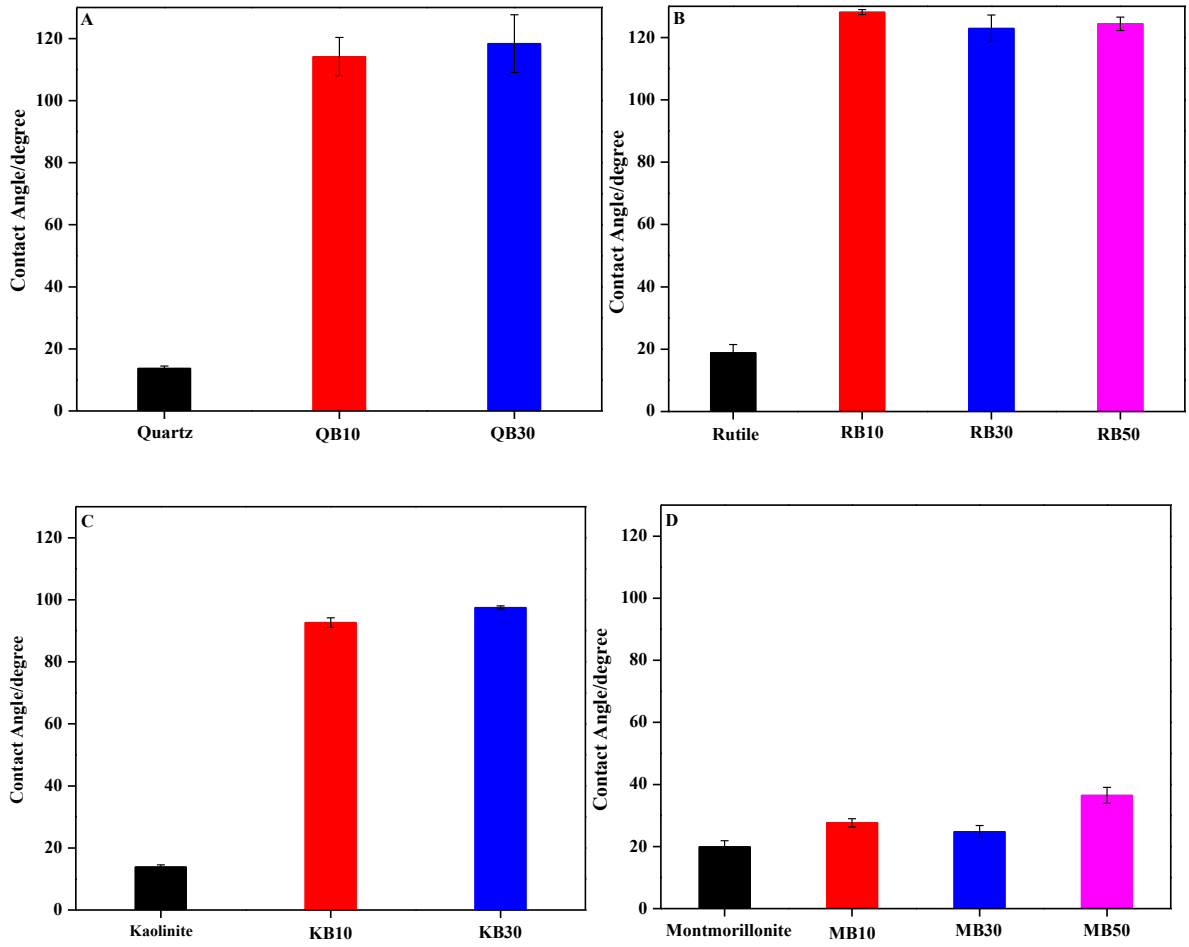


Figure 5-1 The contact angle of untreated and bitumen-coated minerals. A Quartz, B Rutile, C Kaolinite, and D Montmorillonite.

### 5.3.1.2. Filtration of bitumen-coated minerals

The filtration curves of bitumen-coated minerals at different bitumen concentrations are presented in Figure 5-2, and the initial filtration rate (IFR), determined from the filtration curves, was plotted as a function of bitumen concentration used in treating the minerals in Figure 5-3. As can be seen, the filtration rate of a 20 wt% quartz slurry was improved after treatment with 10 wt% bitumen-in-toluene solution. However, treating the quartz at a higher bitumen concentration (30 wt% bitumen-toluene) did not further improve its filtration. On the contrary, it in fact returned the filtration rate of the quartz to below the untreated state (Figure

5-3). Similarly, the bitumen-coating treatment increased the filtration rate of the 20 wt% rutile slurry; At the highest bitumen concentration used (50 wt% bitumen-toluene), there was a slight drop in the filtration rate of the rutile. Like quartz, the filterability of bitumen-coated kaolinite was also sensitive to the variation of bitumen concentration. When the kaolinite was treated with 10 wt% bitumen-toluene solution, almost half of the water in the 10 wt% kaolinite slurry passed through the filter within the first minute (Figure 5-2), resulting in a filtration rate of nearly 1 mL/min/cm$^2$ (Figure 5-3). However, the filtration rate dropped significantly when a higher bitumen concentration (30 wt% bitumen-toluene) was used to treat the kaolinite (Figures 5-2 and 5-3). Similar behavior was observed for montmorillonite, i.e., the filtration rate of the 1 wt% montmorillonite slurry was increased as the bitumen-toluene concentration was increased from 10 wt% to 30 wt%. However, when the bitumen-toluene concentration was increased to 50 wt%, the filtration of the 1 wt% montmorillonite slurry was decreased (Figure 5-2 and Figure 5-3).

Therefore, there seemed to be a "critical" bitumen concentration for each tested mineral to induce the highest filtration rate, beyond which the filtration rate started to decrease. This critical concentration was 10 wt% bitumen-toluene for quartz and kaolinite, and 30 wt% for rutile and montmorillonite. The different critical bitumen concentration seemed to be related to the specific surface area of the minerals. As shown in Chapter 3 (Table 3-2, page 57), the two non-clay minerals quartz and rutile had a BET specific surface area of 2.98 and 5.63 m$^2$/g, respectively, while the two clay minerals kaolinite and montmorillonite had a methylene blue titration specific surface area of 37.19 and 642.19 m$^2$/g, respectively. The rationale was that it was more accurate to describe the specific surface area of non-clay minerals using the BET method, and of clay minerals using methylene blue titration method. Therefore, the higher

"critical" bitumen concentration for rutile than for quartz was likely due to the higher specific surface area of rutile. The higher "critical" bitumen concentration for montmorillonite than kaolinite was also likely due to the higher specific surface area of the montmorillonite.

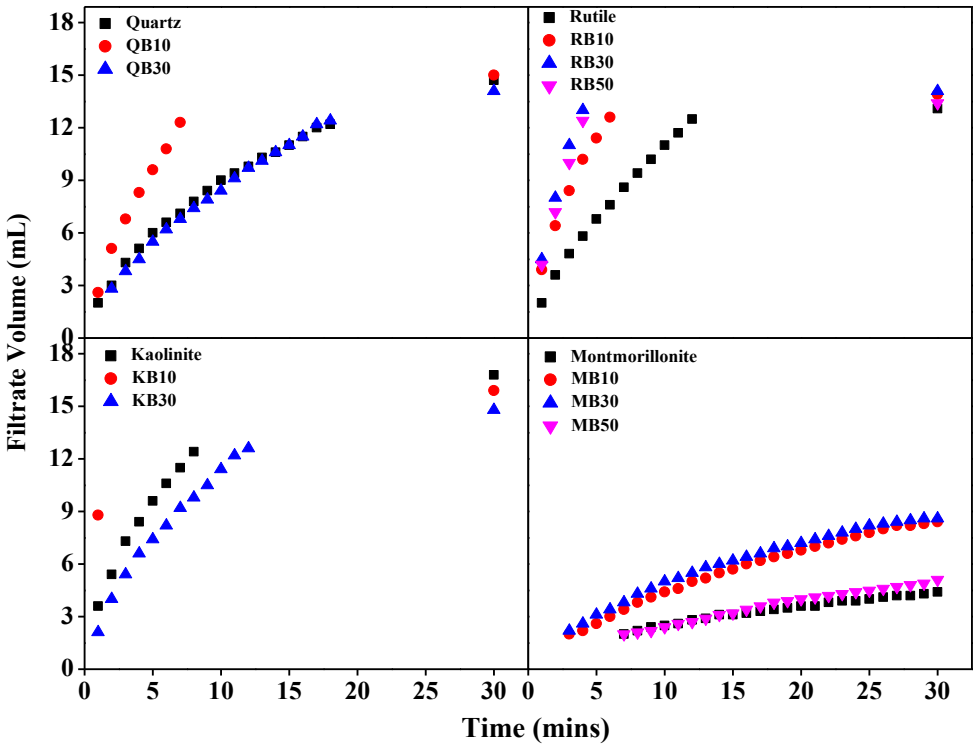


Figure 5-2 Vacuum filtration curves of untreated and bitumen-coated minerals. In the filtration tests, the quartz and rutile were 20 wt% solids, the kaolinite slurry was 10 wt% solids, and the montmorillonite slurry was 1 wt% solids.

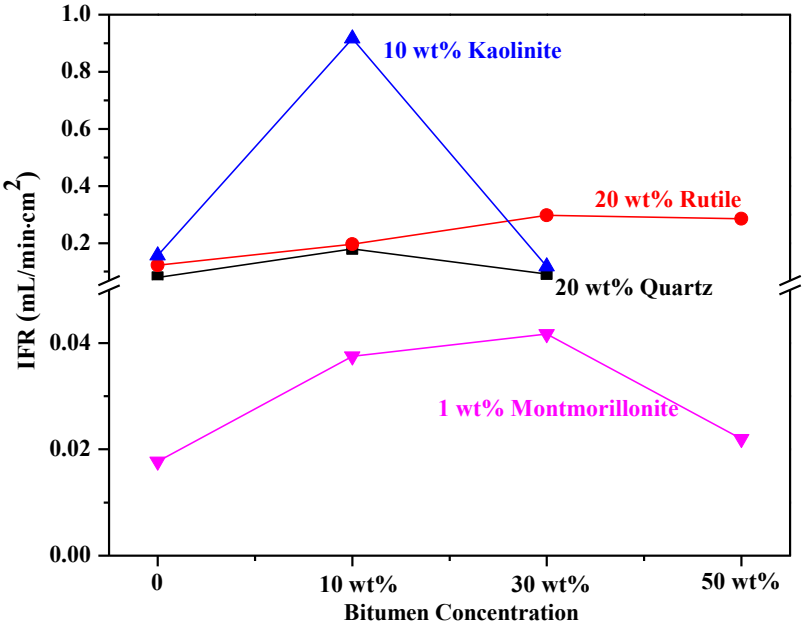


Figure 5-3 Initial filtration rate (IFR) as a function of bitumen-toluene concentration used in treating the tested minerals.

Comparison of Figure 5-1 with Figures 5-2 and 5-3 shows that the bitumen-coating treatment led to an increase in the contact angle of the treated minerals, more significantly for the non-clay and the non-swelling clay minerals, and less so for the swelling clay. The filtration rate of the bitumen-coated minerals was also increased, but the increase was not monotonous in lock step with the contact angle. For all the four tested minerals, Figure 5-3 shows that the filtration rate was the highest at some intermediate bitumen-toluene concentration. The filtration rates of the original untreated minerals and the minerals treated at high bitumen-toluene concentrations were both lower, despite the high contact angle of the minerals treated at the high bitumen-toluene concentrations.

Using QNM-AFM measurements, Chen et al. reported that the organic matters adsorbed on the fine solids in bitumen froth were patchy, soft and could not be washed off by toluene [14].

We hypothesize that such a patchy, soft and deformable adsorbed bitumen layer on the mineral surface could be mobilized by the pressure gradient in filtration. The mobilized bitumen could close off the pores of the filter cake, lowering the filtration rate. Therefore, it was possible that the observed "optimum" bitumen-toluene concentration that was used to treat the different minerals might be related to a "critical" thickness of the bitumen coating on the mineral surfaces. The possible conflicting effects of the bitumen coating, i.e., the bitumen-coating induced surface hydrophobicity which benefited filtration, and the thick deformable bitumen layer that could be mobilized to close off pores in filtration, were analyzed in the following sections.

### 5.3.2. Effects of surface hydrophobicity on the filterability of minerals

In order to decouple the effects of hydrophobicity and bitumen layer thickness on mineral filtration, the mineral surface was made hydrophobic by a single layer of silanization reagent to examine its effect on mineral filtration without the complication of a mobile deformable organic layer.

Three quartz samples, Quartz 1, Quartz 2, and Quartz 3, were obtained by treating the quartz sample in 3CTS-toluene solutions at concentrations of 0.005, 0.02, and 0.04 M, respectively. The images of the water droplets on the pressed quartz pellet surface are shown in Figure 5-4, from which the contact angle was determined to be 14°±3 (Quartz 1), 40°±6 (Quartz 2), 120°±8 (Quartz 3). As expected, the higher 3CTS concentration and/or longer treatment time led to higher contact angle and thus higher degree of quartz surface hydrophobicity.

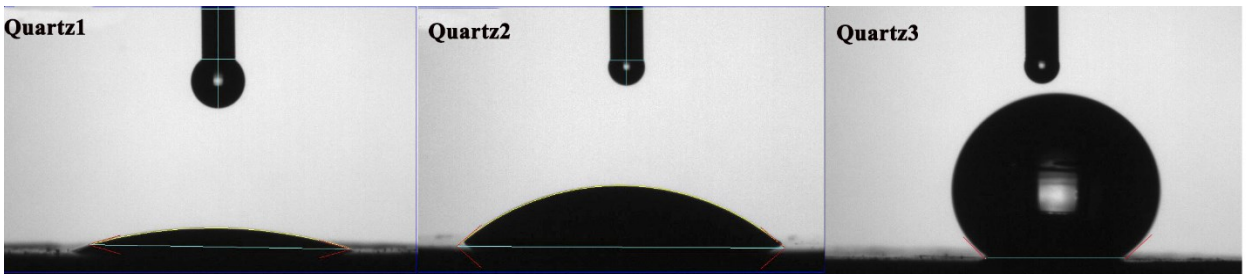


Figure 5-4 Water droplet images on the surface of quartz pellets. Quartz treated with 0.005 M (Quartz 1) and 0.02 M 3CTS (Quartz 2) in toluene for 30 mins, and with 0.04 M 3CTS (Quartz 3) for 24 hours.

Figure 5-5A shows the filtration curves of the silanized quartz samples and Figure 5-5B shows a comparison of the filtration rates of the silanized quartz with bitumen-coated quartz. As can be seen from Figure 5-5A, the three silanized quartz samples showed distinctly different filterability. The filtration rate followed the order Quartz 3 > Quartz 2 > Quartz 1, which matched the order of contact angle, clearly demonstrating the beneficial effect of surface hydrophobicity. According to the silanization reactions shown in Equation (5.1), the silanized quartz should have at most a single layer coating of the (propyl)triethoxysilane groups, and the coating layer should therefore be thin and immobile. The silanized quartz surface was considered as a "hard" surface compared with the soft layer of bitumen-coated minerals [17,18].

Figure 5-5B shows the initial filtration rate of the different quartz samples as a function of their contact angles. A straight line (line 1) could be fitted to the silanized quartz showing a monotonous increase of filtration rate with contact angle. However, it appeared that for the bitumen-coated quartz, the filterability of quartz was not related to contact angle. The contact angle of QB10 and QB30 was similar and at a high value of almost 120°, but the QB30 filtered much more slowly than QB10 (line 3). It can also be seen from line 2 that the contact angles

of untreated quartz, quartz treated with 3CTS (Quartz 2), and the QB30 increased from 14°±3 to almost 120°±8, but they had similar initial filtration rates.

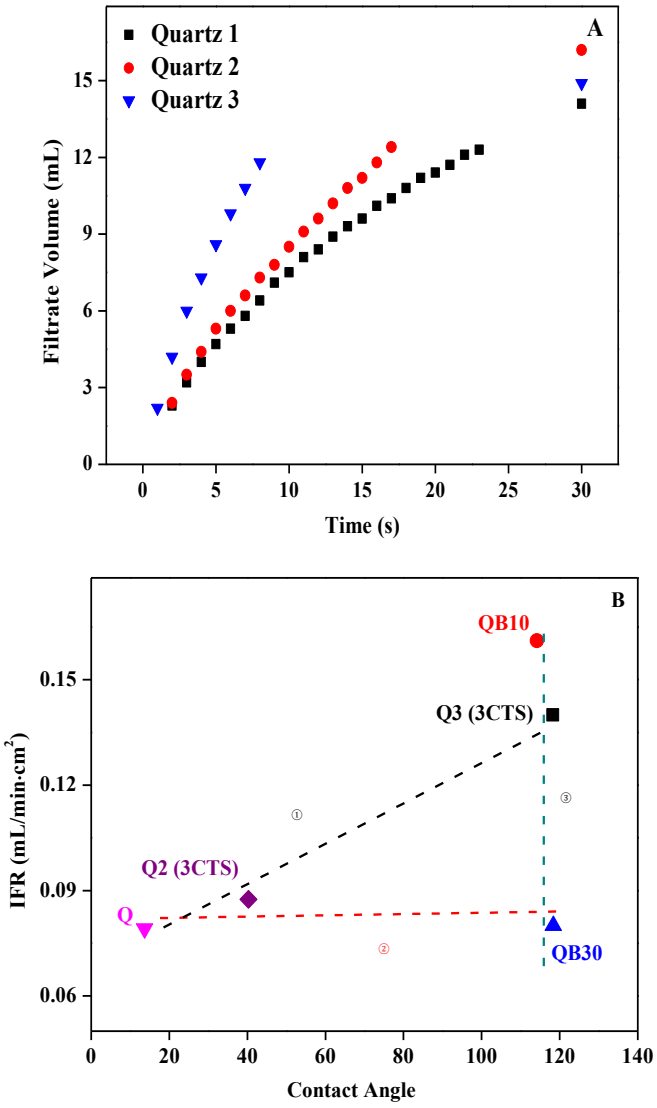


Figure 5-5 A Filtration curves of silanized quartz and B correlation between initial filtration rate (IFR) and contact angle of silanized and bitumen-coated quartz. In the filtration tests, the quartz slurry had a concentration of 20 wt% quartz.

Figure 5-6 shows the correlation (or lack thereof) between the filtration rate and measured contact angle for rutile, kaolinite, and montmorillonite. The different contact angles were

obtained by either silanization or bitumen-coating. As can be seen, the silanization of kaolinite and montmorillonite did not work as well as on quartz surface at the same treatment condition, likely because of the lack of silanol groups on these clay mineral surfaces or the relatively mild treatment conditions. There was also no apparent correlation between the filtration rate and the contact angle for any of the three minerals. The only general conclusion that could be drawn from Figure 5-6 was that at some low or intermediate bitumen-toluene concentrations that were used to treat the minerals, the filtration rates of all three minerals were increased, together with an increase in contact angle. At higher bitumen-toluene concentrations, the filtration rate was significantly decreased despite the high contact angle. This "optimum" bitumen-toluene concentration was not the same for all the minerals.

Therefore, it appears that the filtration performance was dependent on how much bitumen was used to treat the minerals. When a high bitumen concentration was used, the filtration rate was reduced despite the high contact angle. It was suspected that the "thick" bitumen layer could be mobilized under the pressure gradient during filtration to close off the pores in the filter cake. In order to verify this hypothesis, the untreated and bitumen-coated minerals were studied by different characterization techniques.

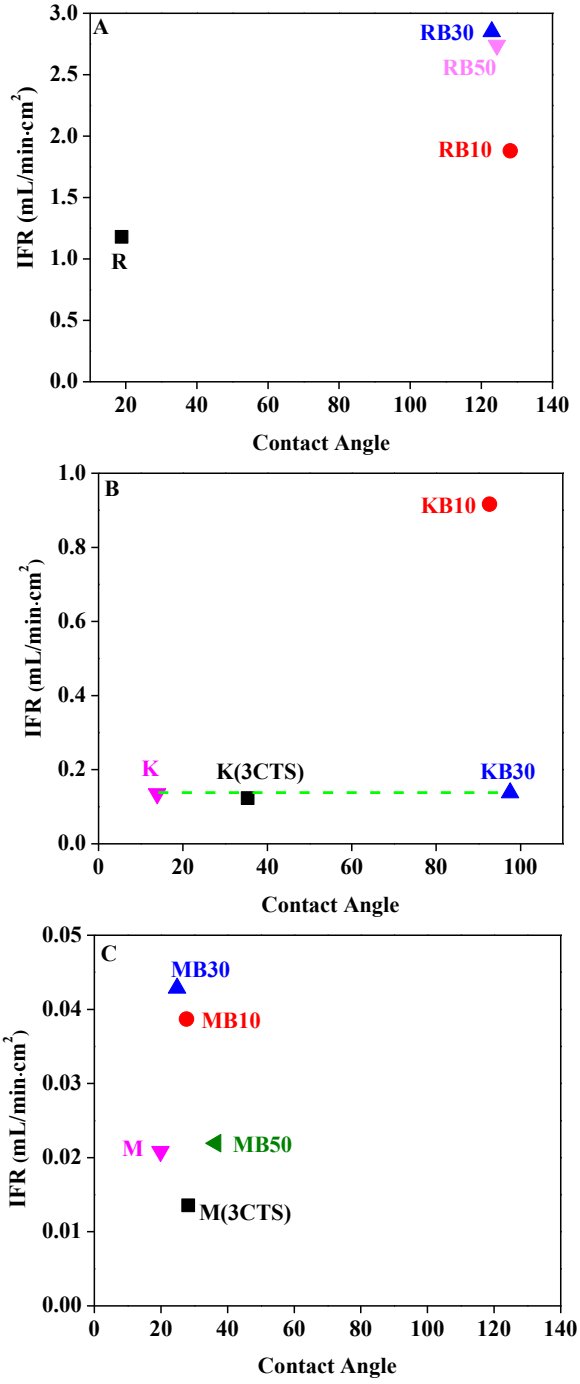


Figure 5-6 The correlation between initial filtration rate (IFR) and contact angle of (A) rutile, (B) kaolinite, and (C) montmorillonite. The "K (3CTS)" and "M(3CTS)" were kaolinite and montmorillonite treated in 0.04 M 3CTS-in-toluene solution for 24 hours.

### 5.3.3. Bitumen coating layer thickness

Different analytical techniques were used to obtain parameters that differentiated the bitumen coating layer thickness when the mineral samples were treated with toluene solutions with different bitumen concentrations. Most of the characterization analyses were performed on kaolinite.

#### 5.3.3.1. CHNS elemental analysis

Table 5-2 CHNS contents for minerals before and after bitumen-coating treatment.

| Sample | Content (%) | | | |
|---|---|---|---|---|
| | Nitrogen | Carbon | Hydrogen | Sulfur |
| | | Kaolinite | | |
| KT | 0.0035±0.0035 | 0.0370±0.0162 | 1.5427±0.0137 | 0.0231±0.0042 |
| KB10 | 0.0425±0.0001 | 2.8184±0.0019 | 1.7257±0.0053 | 0.3047±0.0011 |
| KB30 | 0.0217±0.0038 | 3.2280±0.1231 | 1.7077±0.0154 | 0.3609±0.015 |
| | | Montmorillonite | | |
| MT | 0.0063±0.0005 | 0.4747±0.0377 | 1.1517±0.0274 | 0.1506±0.0823 |
| MB10 | 0.0307±0.0761 | 1.9771±0.0006 | 0.9336±0.0366 | 0.0641±0.0121 |
| MB30 | 0.0480±0.0037 | 2.6267±0.0441 | 0.9701±0.0094 | 0.0290±0.0070 |
| MB50 | 0.0756±0.0169 | 2.8695±0.1227 | 1.3650±0.0556 | 0.0616±0.0197 |
| | | Quartz | | |
| Quartz | not detected | 0.0050±0.0020 | 0.0054±0.0009 | not detected |
| QB10 | not detected | 0.6514±0.0147 | 0.0732±0.0015 | 0.1116±0.0012 |
| QB30 | not detected | 1.1845±0.0307 | 0.1213±0.0024 | 0.1998±0.0031 |
| QB50 | not detected | 1.9726±0.0087 | 0.1954±0.0017 | 0.2963±0.0004 |
| | | Rutile | | |
| Rutile | not detected | 0.0060±0.0005 | 0.0120±0.0002 | not detected |
| RB10 | not detected | 1.0040±0.0150 | 0.1071±0.0015 | not detected |
| RB30 | not detected | 1.6723±0.0101 | 0.1673±0.0020 | 0.1486±0.0128 |
| RB50 | not detected | 2.1618±0.0052 | 0.2093±0.0009 | 0.4289±0.0022 |

Table 5-2 shows the total nitrogen, carbon, hydrogen, and sulfur contents for kaolinite, montmorillonite, quartz, and rutile before and after bitumen coating treatment. The bitumen-

coated minerals had higher carbon content than untreated one. Also, the carbon content increased with increasing bitumen-toluene concentration.

#### 5.3.3.2. X-ray photoelectron spectroscopy (XPS) surface analysis

Table 5-3 shows the surface elemental composition of kaolinite determined by the XPS survey scan. It can be seen that 22 to 29 at% of organic carbon was detected on bitumen-coated kaolinite surface. By comparison, pure kaolinite had a surface carbon concentration of 8.6 at%. The carbon, nitrogen, and sulfur concentration increased while the oxygen, aluminum, and silicon concentration decreased with the increase of bitumen concentration.

Table 5-3 Atomic concentration of elements on the surfaces of kaolinite and bitumen-coated kaolinite.

| Sample | Concentration (atom %) | | | | | |
|---|---|---|---|---|---|---|
| | O | C | Si | Al | N | S |
| Kaolinite | 67.60±0.15 | 8.58±0.40 | 13.26±0.31 | 10.57±0.23 | 0 | 0 |
| KB10 | 55.88±0.24 | 22.52±0.44 | 11.47±0.13 | 9.32±0.07 | 0.40±0.04 | 0.41±0.03 |
| KB30 | 51.32±0.14 | 28.79±0.09 | 10.54±0.05 | 8.14±0.05 | 0.67±0.09 | 0.56±0.07 |

#### 5.3.3.3. X-ray photoelectron spectroscopy (XPS) depth profile analysis

XPS depth profile analysis was performed on 10 wt% and 30 wt% bitumen-toluene solution treated kaolinite surface by etching the surface with $Ar^+$ beam at 1 kV to progressively remove the surface layer. The results of the depth profile analysis are shown in Figure 5-7.

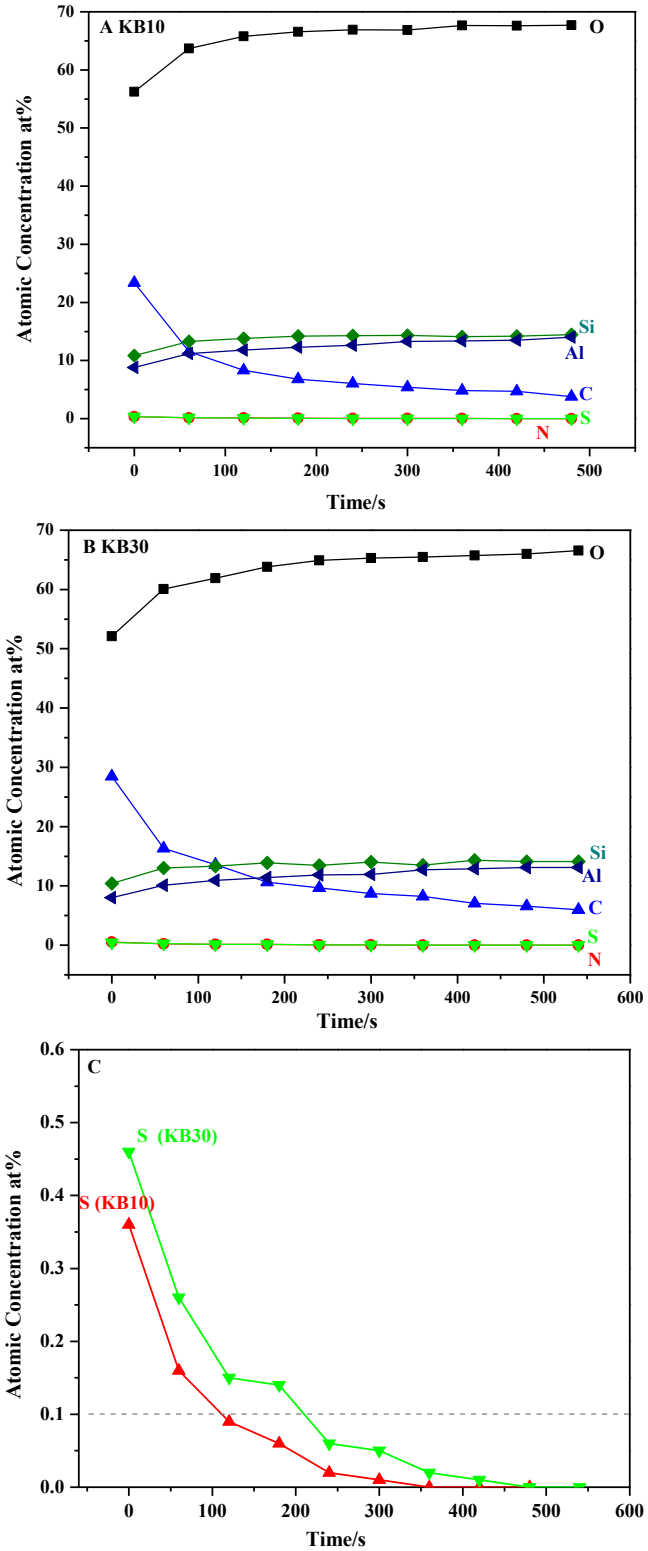


Figure 5-7 The atomic concentration of (A) KB10, (B) KB30, and (C) S concentration of KB10 and KB30 as a function of sputtering time.

As can be seen, the O, Al, Si contents increased, and the C and S contents decreased until the beam reached the kaolinite surface. As C, O, Si, Al were all observed on the untreated kaolinite surface, the S contents were selected to judge the presence of bitumen and the thickness of the bitumen coating layer. The depth profile of S is shown in Figure 5-7C. As can be seen, the KB30 had a higher S concentration before etching started. As etching went on, the S concentration of the KB10 reached less than 0.1 at% at 180 s. For the KB30 sample, the S atomic concentration reached less than 0.1 at% at 240 s. The results showed that the KB30 sample required more time than the KB10 to reach 0.1 at% S atomic concentration. The results clearly show that the KB30 sample had a thicker bitumen coating layer than the KB10 sample. The adsorbed bitumen could form a multilayer structure on kaolinite surface [17].

#### 5.3.3.4. X-ray microscopy/nanoCT (XRM) imaging

Figure 5-8 shows the pore distribution, 3-D pore networks, and the cross section images of kaolinite filter cakes. The porosity of the cakes from untreated kaolinite and bitumen-coated kaolinite were determined by the software. As can be seen, most of the pores were uniformly distributed in kaolinite (Figure 5-8 A1), with a porosity about 15 vol%. The pores in KB10 were mainly distributed in the uncoated kaolinite space while the bitumen-coated kaolinite showed lower pore distribution and smaller pore size than the untreated kaolinite. The total porosity of KB10 was about 28 vol%, which was higher than that of the other two kaolinite samples, consistent with the improved filterability of KB10. For KB30, the size of pores was smaller than pure kaolinite and KB10 and the pores were distributed in the uncoated kaolinite space, with a porosity of about 10 vol%.

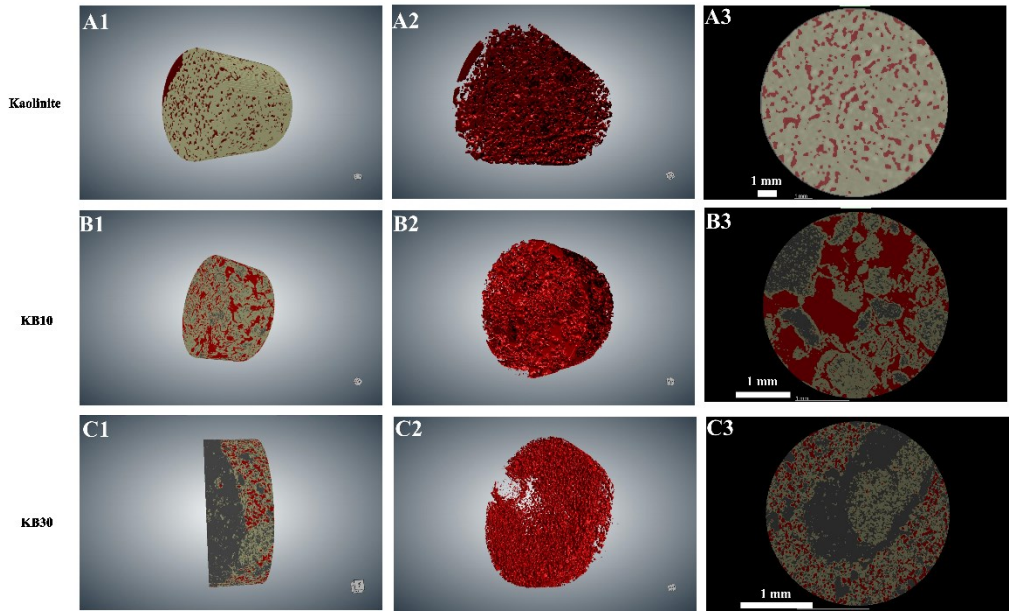


Figure 5-8 Left panel: XRM 3-D diffusion view; middle panel: The corresponding XRM 3-D diffusion views of pore networks; right panel: XRM cross sections. The red color represents the pores, the grey color represents bitumen or bitumen-covered kaolinite, and the beige color represents the bare kaolinite. Top row: kaolinite; middle row: K10; bottom row: K30.

#### 5.3.3.5. Discussion

The results described in section 5.3.3 pointed to higher carbon contents for minerals that were treated with higher concentration of bitumen-toluene, judging from both bulk CHNS elemental analyses and XPS mineral surface elemental concentration analyses. The XPS depth profile analysis also showed that the bitumen layer on KB30 (i.e., kaolinite treated in 30 wt% bitumen-toluene) was thicker than on KB10 (kaolinite treated in 10 wt% bitumen-toluene). On the other hand, the XPS mineral surface concentration analysis, and FTIR spectra (Appendix B) of KB30 and KB10 showed that the kaolinite substrate was still visible in both KB30 and KB10. Therefore, the bitumen coating on the mineral surface was not uniform and continuous, but patchy and discontinuous. For this reason, no attempt was made to calculate an "average"

thickness of the adsorbed bitumen layer on the mineral surface, although such an average thickness may be deduced from the bulk and surface carbon content data (Tables 5-2 and 5-3) as well as the XPS depth profile data (Figure 5-7c). The average thickness data might give a false “critical” thickness criterion to judge bitumen coating on filtration performance, which could be misleading.

Previous studies have also shown that bitumen (or asphaltene) coating on mineral surface was patchy and discontinuous [16,20]. Chen et al. [16] used a quantitative nanomechanical atomic force microscope (QNM-AFM) and were able to detect a patchy bitumen coating on clays from a bitumen froth sample even after 30 min ultrasonic treatment. Wang et al. [20] studied asphaltene adsorption on the same batch of kaolinite that had been put in contact with an asphaltene-toluene solution, then repeatedly dried and put in contact with a fresh asphaltene-toluene solution. They repeated this procedure four times. They observed that the cumulative amount of adsorbed asphaltene on the kaolinite was the same as when a different batch of kaolinite was contacted with a progressively higher concentration bitumen-toluene solution (i.e., how an adsorption isotherm was normally done). However, their XPS surface analysis of the kaolinite showed that the Si and Al concentrations remained constant during the repeated contacts with a fresh asphaltene solution. The results prompted them to suggest that the asphaltene tended to adsorb on the kaolinite surface that was already covered by asphaltene, rather than to fill the bare kaolinite surface. In other words, the asphaltene adsorption layer was very rough, with high “peaks” and deep “valleys” when more asphaltene was adsorbed. We suspect that this may be the case here when the kaolinite was treated with a higher concentration of bitumen (30 wt%) compared with the 10 wt%, i.e., the bitumen coating on the KB30 may be much rougher and only marginally thicker on average than KB10.

The XRM results in Figure 5-8 showed that the bitumen-coated kaolinite had low porosity and formed a tighter structure. So it was supposed that such a patchy bitumen layer with a higher degree of roughness could make it more likely to form an "inter-locking" structure due to the inter-penetration of the bitumen when the particles approached each other (Figure 5-9). This inter-locking structure would more readily block the drainage channels and pore space than a uniform bitumen coating, as schematically shown in Figure 5-9.

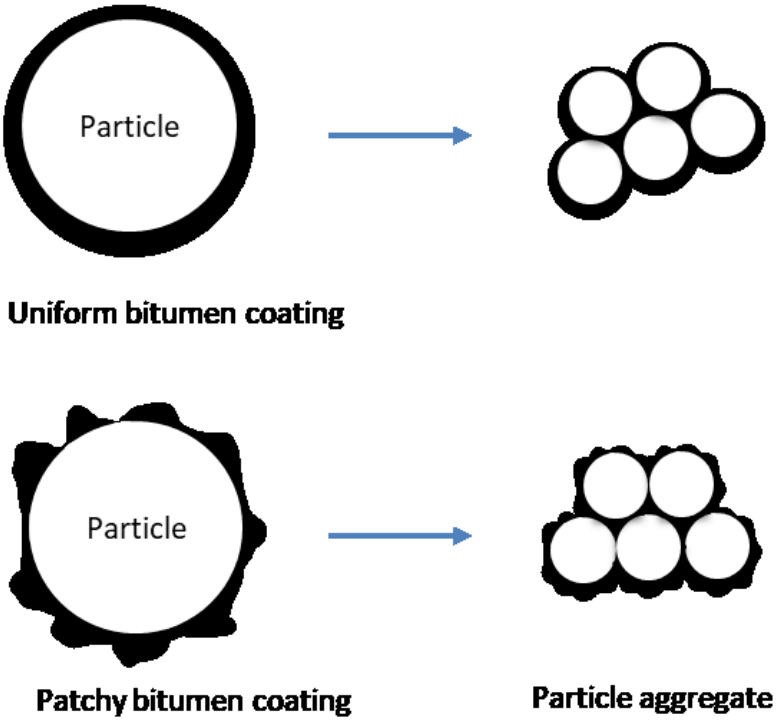


Figure 5-9 Schematic of particle aggregates with uniform bitumen coating (top) and patchy bitumen coating (bottom).

To form such pore-blocking inter-locking structures, one would not need a significant increase in the average thickness of the bitumen layer, but only need the bitumen layer to have a higher degree of roughness.

## 5.4. Conclusions

In this work, an attempt was made to decouple the effects of bitumen coating and hydrophobicity on the surface of a mineral on its filtration behavior. Two non-clay minerals (quartz, rutile), one non-swelling clay (kaolinite), and one swelling clay (montmorillonite) were used in the study. The mineral surface hydrophobicity was created by silanization or bitumen-coating. The bitumen coating thickness was studied by CHNS elemental analysis and XPS depth profile analysis, the filtration performance was studied by vacuum filtration, and the filter cakes were analyzed by X-ray microscope/nanoCT imaging. The major conclusions are:

(1) Silanization of quartz significantly increased its surface hydrophobicity and filtration rate. A linear relationship was observed between the filtration rate and contact angle of the silanized quartz.

(2) When quartz was coated by bitumen through the treatment in a bitumen-toluene solution, the contact angle of the quartz was also significantly increased. However, the filtration rate of the bitumen-coated quartz did not monotonically increase with contact angle or with bitumen concentration used in the bitumen-coating treatment. In fact, at high bitumen concentration, the filtration rate of the bitumen-coated quartz was significantly reduced to the level below untreated quartz, despite the high contact angle.

(3) The same phenomena were observed when rutile, kaolinite, and montmorillonite were subjected to similar bitumen-coating treatment. The “critical” bitumen concentration beyond which the filtration rate was reduced was different for the different minerals, but seemed to be related to the specific surface area of the tested minerals.

(4) CHNS elemental composition analysis and XPS depth profile analysis indicated that minerals treated at higher bitumen-toluene concentration had higher C, N, and S content, and thicker bitumen coating. X-ray microscope/nanoCT imaging analysis of the filter cake of kaolinite showed that the kaolinite treated with high concentration of bitumen had a higher proportion of bitumen-coated kaolinite, visible mineral-bitumen aggregates, and a lower porosity, which were likely the reasons for the significantly reduced filtration rate.

(5) It appeared that surface hydrophobicity indeed benefited the filtration of aqueous mineral slurries. However, when the surface hydrophobicity was induced by the coating of a deformable hydrocarbon material such as bitumen, the filtration rate could be adversely affected. This is likely because under the pressure gradient, the patchy and deformable bitumen layer could inter-penetrate to form an inter-locked structure to close off the pores in the filter cake and to lower filtration rate. This was probably one of the reasons why the oil sands tailings were more difficult to filter than typical mine tailings that do not contain residual bitumen.

**References**

[1] Government of Alberta. Alberta Environment and Parks Oil Sands Information Portal 2021. http://osip.alberta.ca/map/ (accessed November 24, 2021).

[2] Alberta Energy Regulation. Directive 085: Fluid Tailings Management for Oil Sands Mining Projects. 2017. https://doi.org/https://static.aer.ca/prd/documents/directives/Directive085.pdf.

[3] Beier N, Wilson W, Dunmola A, Sego D. Impact of flocculation-based dewatering on the shear strength of oil sands fine tailings. Can Geotech J 2013;50:1001–7. https://doi.org/10.1139/cgj-2012-0262.

[4] Amoah N. Large-Scale Tailings Filtration and Dry Stacking at Karara Magnetite Iron Ore Operation. Proc. Tailings Mine Waste 2019, Vancouver, BC: 2019, p. 15–32.

[5] Moreno J, Kendall S, Ortiz A. Dewatering options for management of fine gold tailings in Western Australian Goldfields. Paste 2018 21st Int Semin Paste Thick Tailings, 2018 11-13 April Perth 2018:413–24. https://doi.org/10.36487/ACG_REP/1805_34_MORENO.

[6] Leonida C. How to Make Filtered Tailings Feasible. Eng Min J 2020:1–10. https://doi.org/https://www.e-mj.com/features/how-to-make-filtered-tailings-feasible/.

[7] Loerke R, Tan X, Liu Q. Dewatering of Oil Sands Mature Fine Tailings by Dual Polymer Flocculation and Pressure Plate Filtration. Energy and Fuels 2017;31:6986–95. https://doi.org/10.1021/acs.energyfuels.7b00938.

[8] Pendharker S, Shende S, Jacob Z, Nazemifard N. Three-dimensional optical tomography of bitumen and clay association in oil sands tailings. Fuel 2017;207:262–7. https://doi.org/10.1016/J.FUEL.2017.06.107.

[9] Gumfekar SP, Rooney TR, Hutchinson RA, Soares JBP. Dewatering Oil Sands Tailings with Degradable Polymer Flocculants. ACS Appl Mater Interfaces 2017;9:36290–300. https://doi.org/10.1021/acsami.7b10302.

[10] Wang C, Harbottle D, Liu Q, Xu Z. Current state of fine mineral tailings treatment: A critical review on theory and practice. Miner Eng 2014;58:113–31. https://doi.org/10.1016/J.MINENG.2014.01.018.

[11] Liu Q, Laskowsk JS. The role of metal hydroxide at inmeral surfaces in dextrin

adsorption , I . studies on modified quartz samples. Int J Miner Process 1989;26:297–316. https://doi.org/https://doi.org/10.1016/0301-7516(89)90035-5.

[12] Barry A. Hydrophobicity, Hydrophilicity and Silane Surface Modification. Gelest Inc 2011;Morrisvill.

[13] Bendou S, Amrani M. Effect of hydrochloric acid on the structural of sodic-bentonite clay. J Miner Mater Charact Eng 2014;02:404–13. https://doi.org/10.4236/jmmce.2014.25045.

[14] Chen Q, Liu J, Thundat T, Gray MR, Liu Q. Spatially resolved organic coating on clay minerals in bitumen froth revealed by atomic force microscopy adhesion mapping. Fuel 2017;191:283–9. https://doi.org/10.1016/j.fuel.2016.11.091.

[15] McNamee CE, Tsujii Y, Ohshima H, Matsumoto M. Interaction Forces between Two Hard Surfaces in Particle-Containing Aqueous Systems. Langmuir 2004;20:1953–62. https://doi.org/10.1021/LA0357763.

[16] McNamee CE, Tsujii Y, Ohshima H, Matsumoto M. Interaction forces between two silica surfaces in an apolar solvent containing an anionic surfactant. Langmuir 2004;20:1953–62.

[17] Jouault N, Corvis Y, Cousin F, Jestin J, Le L. Asphaltene Adsorption Mechanisms on the Local Scale Probed by Neutron Reflectivity : Transition from Monolayer to Multilayer Growth above the Flocculation Threshold † 2009:3991–8.

# CHAPTER 6 Conclusions, Contributions, and Recommendations

## 6.1. Summary and Conclusions

The extremely slow solid-liquid separation of Alberta oil sands tailings is the major challenge faced by the Alberta oil sands industry today. This leads to the accumulation of large amount of mature fine tailings requiring several hundreds of square kilometers of land to contain. The slow solid-liquid separation means that about a quarter of warm process water cannot be recycled, and needs to be replenlished with fresh water from the Athabasca River. This not only causes high fresh water demands, at about 3-4 bbl of fresh water per bbl of produced bitumen, but also high energy consumption and high green house gas (GHG) emission due to the need to heat the fresh river water to about 50°C. Therefore, the three major environmental problems caused by the Alberta oil sands operation, i.e., large tailings pond areas which pose threats to migrating birds and local eco-system, the high fresh water consumption, and the high energy consumption and GHG emission, are all rooted in the extremely slow solid-liquid separation of the oil sands tailings. If the oil sands tailings could be rapidly dewatered so that the warm process water is recycled and the tailings solids reclaimed, then the three major environmental problems associated with the Alberta oil sands operations would not be an issue anymore.

There has been significant advances in the past several years on the adoption of pressue filtration technologies in the mining industry, not only for dewatering mineral concentrates but also mine tailings. This is driven by the need to rapidly recycle process water to lower fresh water consumption, and to mitigating the tremendous risks of impounding large volumes of unconsolidated fluid fine tailings. Many of the reported adoption of pressure filtration in typical hardrock mining tailings dewatering are successful, generating filter

cakes that contain >=85 wt% solids, well over the plastic limit of the tailings sludge so that they can be reclaimed immediately.

In the Alberta oil sands industry, there has not been an extensive study on using filtration as a dewatering method for the oil sands tailings. Most of the past studies have been focused on testing different coagulants and flocculants to speed up the gravitational or centrifugal sedimentation of the tailings. However, it is known that relying on sedimentation alone, it would not be possible to dewater the oil sands tailings to achieve the required solid content to reach the plastic limit for reclamation. For example, Syncrude has shown that even after polymer flocculation and centrifugal sedimentation, the oil sands tailings can only be dewatered to about 55 wt% solids, far from the plastic limit.

Inspiried by the increasingly widespread adoption in the mine tailings treatment, the oil sands industry has recently conducted a pilot testing campaign to use commercial filter press to filter the oil sands tailings. The results showed the filter cakes containing >= 60 wt% solids could be routinely produced and although this did not meet plastic limit, the filter cakes were found to be reclaimable. Therefore, the Alberta oil sands tailings clearly demonstrated properties that are different from the typical mine tailings, and one of which was the fact that the oil sands tailings contain residual bitumen. However, the pilot tests showed that the filter press would be uneconomical to use to filter the oil sands tailings, because in order to generate the filter cakes ready for reclamation, the required dosages of coagulants and flocculants were too high.

It was under such a background that the present study was carried out. The objective of this study was not to attempt to establish the solid content in filter cakes that could be achieved under different process conditions. The objective of this study was to fundamentally exmine

the filtration behaviors of the Alberta oil sands tailings, particularly how the different components in the oil sands tailings responded to the filtration. Such a fundamental study would provide guidance to implement the pressure filtration technology to Alberta oil sands tailings dewatering.

At the outset, it was recognized that the fine mineral solids and residual bitumen in the Alberta oil sands tailings are the two contributing factors to the low filterability of oil sands tailings. To decouple the effects of different minerals and residual bitumen, the filtration behaviors of six different mineral samples, rutile ($d_{50}$= 0.7 μm), quartz ($d_{50}$ = 3.6 μm), kaolinite ($d_{50}$ = 4.1 μm), illite ($d_{50}$ = 2.8 μm), illite–smectite ($d_{50}$ = 2.7 μm), and montmorillonite ($d_{50}$ = 2.8 μm), were investigated by vacuum filtration and capillary suction time (CST) measurements to identify the minerals that were responsible for the difficult filtration of oil sands tailings. The effects of bitumen on the oil sands tailings filtration was investigated separately considering that the residual bitumen could exist in the tailings as bulk free bitumen, bitumen-in-water emulsion, and bitumen coated on mineral surfaces. Various instrumental characterization techniques, such as particle size analysis, CHNS elemental composition ana;ysis, X-ray diffraction, X-ray fluorescence, scanning electron microscope, Fourier transform infrared spectrometry, X-ray photoelectron spectroscopy, and X-ray microscope/nanoCT imaging, were employed to characterize the minerals and their association with bitumen. The main conclusions of this study were:

(1) Particle size was not the primary factor that affected the filtration behavior of the six tested minerals. The rutile sample had the smallest particle size of all six tested mineral samples, with a submicron medium size of 0.7 μm, yet it had the highest filtration rate. The

other five mineral samples had similar medium particle sizes but showed very different filtration rates.

(2) The filtration rate was distinctly different for the different types of minerals. The swelling clays (montmorillonite, illite–smectite) were much more difficult to filter than the non-swelling clays (kaolinite, illite), which in turn was more difficult to filter than the non-clay minerals (quartz, rutile). Since the particle sizes were mostly similar, this conclusion was not masked by particle size effect. Also, the presence of a small amount of swelling clays in a mineral mixture was found to significantly affect the filtration behavior of the mineral mixture. The filtration rate decreased with an increase in the effective volume fraction of mineral solids in the aqueous mineral slurries. The tested minerals and mineral mixtures clearly fall into two different bands, with swelling clays in one band, and the non-clay and non-swelling clays in the other band. This banded division clearly showed the different filtration behavir of the swelling clays.

(3) The bulk bitumen, in the form of bitumen froth, only lowered the filter cake solids content slightly; the bitumen-in-water emulsion was found to have no discernable effect on the filtration process. However, the bitumen adsorbed on minerals surface demonstrated very different effects depending on the amount of adsorbed bitumen. At low bitumen coating density, the filterability of all treated minerals was improved, more so for the non-clay minerals (quartz, rutile) and non-swelling clay (kaolinite), and less so for the swelling clay (montmorillonite). At high bitumen coating density, the filterability of the coated minerals was reduced. There seemed to be an optimum quantity of adsorbed bitumen that resulted in the maximum filtration rate. This optimum quantity was different for the different minerals.

(4) X-ray microscope/nanoCT imaging analysis of the filter cake of kaolinite showed that the kaolinite treated with high concentration of bitumen had a higher proportion of bitumen-coated kaolinite, visible mineral-bitumen aggregates, and a lower porosity, which were likely the reasons for the significantly reduced filtration rate of the kaolinite at high bitumen coating.

(5) Mineral surface hydrophobicity benefited the filtration of aqueous mineral slurries. This was clearly demonstrated by the filtration behavior of quartz after different degrees of silanization. However, when the surface hydrophobicity was induced by the coating of a deformable hydrocarbon material such as bitumen, the filtration rate could be adversely affected. This is likely because under the pressure gradient, the patchy and deformable bitumen layer could inter-penetrate to form an inter-locked structure to close off the pores in the filter cake and to lower filtration rate. This was probably one of the reasons why the oil sands tailings were more difficult to filter than typical mine tailings that do not contain residual bitumen.

(6) Consistent with the hypothesis that the mineral filtration was governed by the effective volume fraction of the mineral solids, it was found that treatment of a swelling clay by acid or multivalent metal ions could significantly improve its filtration behavior. This was attributed to a reduction in the electrical double layer thickness, which in turn reduced the effective volume fraction of the mineral solids. Indeed, the multivalent metal ions are known to significantly compress the electrical double layer. Acid treatment of the swelling clay led to the release of the interlayer metal ions (through cation exchange with $H^+$) which became available to compress the electrical double layer.

Therefore, chemicals that can compress the mineral surface electrical double layer, and chemicals that can modulate the mineral surface bitumen coating, are expected to be able

improve the pressure filtration performance of the Alberta oil sands tailings. Also, since the swelling clays are known to be contained mainly in the ultrafine particle size fraction of the oil sands tailings, it would be possible to lower chemical dosage and cost if only the fine and ultrafine fractions of the oil sands tailings are treated with the chemicals to maximize their effects without wasting them on the coarse particles.

### 6.2. Orginal Contributions

This PhD dissertation research was a fundamental study aimed at understanding the filtration behaviors of different components of Alberta oil sands tailings. It was built on accumulated knowledge of oil sands tailings dewatering reported in the open literature in the past several decades. Based on the author's reading of the literature, the following were considered the original contributions of this thesis work:

(1) Identified swelling clays such as illite-smectite and montmorillonite as the most difficult minerals to filter, and the presence of a small amount of swelling clays in a mineral mixture could significantly affect its filtration behavior. Therefore, the swelling clays likely account for the difficulty of oil sands tailings filtration.

(2) Discovered that bitumen-coating on mineral surface did not monotonously improve the mineral's filtration from an aqueous slurry. The bitumen coating could render the mineral surface hydrophobic which benefited its filtration from an aqueous slurry. However, since bitumen was deformable and adsorbed on mineral surface as a patchy and discontinuous coating, at relatively high adsorption density, the patchy and discontinuous bitumen coating could form an inter-locking structure under the pressure gradient, which could block the water drainage channels and pores, and lower filtration rate.

These findings are privide insightful guidance to the treatment of oil sands tailings. Rather than blindly trialing different chemicals, these findings suggest that the oil sands industry could focus on two aspects to more effectively treat the tailings for pressure filtration. The first approach is to use chemicals that could compress the electrical double layers so that the effective volume fractions of the fine solids, particularly the swelling clays, could be reduced. Granted, coagulants have been used in the tailings treatment in general, but this research points out that the function of the coagulants is to target specifically the electrical double layer of the swelling clays. Therefore, the tailings may be segregated into coarse and fine fractions, for example, by the use of hydrocyclones, and then only the fine fraction is treated with coagulants. This is because the swelling clays are known to be concentrated in the fine fraction. The second approach is to use chemicals that could thin the bitumen layer on the mineral surface to reduce the inter-locking structure induced by the bitumen layer coated on the minerals surface. These may sometimes involve the use of dispersants during tailings filtration, which is counter-intuitive from conventional reasoning.

### 6.3. Suggestions for Future Work

This study revealed swelling clays as the most difficult to filter of all the minerals samples tested. Swelling clays are known to be present in oil sands tailings in various quantities, but the average swelling clay content in the oil sands tailings has not be definitely reported. A further study needs to be carried out to quantify the concentration of swelling clays in oil sands tailings and correlate it to the filtration behavior.

The swelling clays was identified as the most difficult filtered solids of all tested minerals, but how the presence of swelling clays make other minerals unfilterable is unknown. This will

require further study so that effective methods can be found to mitigate the detrimental effects of the swelling clays on oil sands tailings filtration.

Different chemicals and polymers have been tested to treat the oil sands tailings, but most of the reported studies mainly concerned the settling rates of the oil sands tailings, and very little of the reported work has targeted the improvement of oil sands tailings filtration. Future work should focus on finding suitable chemical additives that can target ultrafine fractions to compress the electrical double layer and to modulate the adsorbed bitumen layer to maintain a porous filter cake under the filtration pressure gradient.

**Bibliography**

Alberta Energy Regulator. Alberta Energy Regulator 2016/17 Annual Report. 2017. https://doi.org/https://static.aer.ca/prd/documents/reports/AER2016-17AnnualReport.pdf.

Masliyah JH, Czarnecki J, Xu Z. Handbook on Theory and Practiceon Bitumen Recovery from Athabasca Oil Sands. 2011. https://doi.org/https://doi.org/10.7939/r3-nr43-8t34.

Hande AB. Accelerated Dewatering and Drying Treatment of Oil Sands Tailings by Electrical Resonant Auto-Transformer 2014:59–61.

Alberta Environment and Parks. OSIP - Data Library 2015. http://osip.alberta.ca/library/Dataset/Details/542 (accessed April 4, 2015).

Fennell J, Arciszewski TJ. Current knowledge of seepage from oil sands tailings ponds and its environmental influence in northeastern Alberta. Sci Total Environ J 2019. https://doi.org/10.1016/j.scitotenv.2019.05.407.

Finkel ML. The impact of oil sands on the environment and health. Curr Opin Environ Sci Heal 2018;3:52–5. https://doi.org/10.1016/J.COESH.2018.05.002.

Environmental defence. One trillion litres of toxic waste and growing: Alberta's tailings ponds. n.d.https://doi.org/https://d36rd3gki5z3d3.cloudfront.net/wp-content/uploads/2017/06/AlbertaTailingsPondsReportFINAL.pdf?x78791.

Timoney K. Environmental and Health Impacts of Canada's Oil Sands Industry 2010. https://doi.org/http://www.youtube.com/watch?v=nReBw5IzaCM.

Small CC, Cho S, Hashisho Z, Ulrich AC. Emissions from oil sands tailings ponds: Review of tailings pond parameters and emission estimates. J Pet Sci Eng 2015;127:490–501.

https://doi.org/10.1016/J.PETROL.2014.11.020.

Taylor BEng T, Jamieson W, Grant A. Fugitive Emissions from Tailings Facilities in the Athabasca Oil Sands Region Summary of national emissions database, current scientific knowledge, and regulatory frameworks ENVS 4405: Air Quality. 2021. https://doi.org/https://www.canada.ca/content/dam/eccc/documents/pdf/npri-/academic challenge/Fugitive%20Emissions%20from%20Tailings%20Facilities%20in%20the%20Athabasca%20Oil%20Sands%20Region.pdf.

Government of Alberta P. Annual Emissions Inventory Report Standard and Guidance Document: 2018 and 2019 Emissions Inventory Years. 2018. https://doi.org/https://open.alberta.ca/dataset/7f234172-a595-47b0-b8f9-4b3739bbcfda/resource/6c1cc270-ba68-4fff-8b12-f2b8eb6dfe73/download/aeir-standard-aug2018.pdf.

Environmental defence. Report: Alberta's Tailings Ponds： One Trillion Litres of Toxic Waste and Growing 2022. https://doi.org/https://environmentaldefence.ca/report/albertas-tailings-ponds/.

Proskin S, Sego D, Alostaz M. Oil Sands MFT Properties and Freeze-Thaw Effects. J Cold Reg Eng 2012;26:29–54. https://doi.org/10.1061/(asce)cr.1943-5495.0000034.

Matthews JG, Shaw WH, MacKinnon MD, Cuddy RG. Development of Composite Tailings Technology at Syncrude. Int J Surf Mining, Reclam Environ 2002;16:24–39. https://doi.org/10.1076/ijsm.16.1.24.3407.

Sobkowicz J. Oil Sands Tailings Technology Deployment Roadmap. vol. 2. 2012.

Revington, Adrian Peter  et al. Process for flocculating and dewatering oil sands mature fine tailings. 9,909,07, 2018.

Zhu Y, Tan X, Liu Q. Dual polymer flocculants for mature fine tailings dewatering. Can J Chem Eng 2017;95:3–10. https://doi.org/10.1002/cjce.22628.

Loerke R, Tan X, Liu Q. Dewatering of Oil Sands Mature Fine Tailings by Dual Polymer Flocculation and Pressure Plate Filtration. Energy and Fuels 2017;31:6986–95. https://doi.org/10.1021/acs.energyfuels.7b00938.

Osacky M, Geramian M, Ivey DG, Liu Q, Etsell TH. Mineralogical and chemical composition of petrologic end members of Alberta oil sands. Fuel 2013;113:148–57. https://doi.org/10.1016/j.fuel.2013.05.099.

Ignasiak TM. Separation and characterization of clay from Athabasca asphaltene 1983;62:353–62.

Botha L, Soares JBP. The Influence of Tailings Composition on Flocculation. Can J Chem Eng 2015;93:1514–23. https://doi.org/10.1002/cjce.22241.

Kaminsky HAW, Etsell TH, Ivey DG, Omotoso O. Distribution of clay minerals in the process streams produced by the extraction of bitumen from athabasca oil sands. Can J Chem Eng 2009;87:85–93. https://doi.org/10.1002/cjce.20133.

Cloutis EA, Gaffey MJ, Moslow TF. Characterization of minerals in oil sands by reflectance spectroscopy 1994.

Omotosoa O, Mikulaa R, Urquhartb S, Sulimmab H, Stephensc P. Characterization of Clays from Poorly Processing Oil Sands using Synchrotron Techniques. Clay Sci 2006;12:88–93.

Gupta SK, Gartley MG. XRD analysis of illite-smectite interstratification in clays from oil sands ores. Adv. X-ray Anal., vol. 62, 1999, p. 22–31.

Osacky M, Geramian M, Dyar MD, Sklute EC, Valter M, Ivey DG, et al. Characterisation of petrologic end members of oil sands from the athabasca region, Alberta, Canada. Can J Chem Eng 2013;91:1402–15. https://doi.org/10.1002/cjce.21860.

Poon HY, Cossey HL, Balaberda A lynne, Ulrich AC. The role of carbonate mineral dissolution in turbidity reduction in an oil sands end pit lake. Chemosphere 2021;271:129876. https://doi.org/10.1016/j.chemosphere.2021.129876.

Liu X, Yan W, Stenby EH, Thormann E. Release of Crude Oil from Silica and Calcium Carbonate Surfaces: On the Alternation of Surface and Molecular Forces by High- and Low-Salinity Aqueous Salt Solutions. Energy and Fuels 2016;30:3986–93. https://doi.org/10.1021/acs.energyfuels.6b00569.

COSIA. Tailings clay chanllenge. 2017. https://doi.org/https://cosia.ca/sites/default/files/attachments/COSIA%20Challenge%20Tailings%20-%20Tailings%20Clay%20Challenge_0.pdf.

Mohammad Ali Hooshiar Fard. Characterization of Clay Minerals in the Athabasca Oil Sands in Water Extraction and Nonaqueous Solvent Extraction Processes. University of Alberta, 2011.

Kotlyar LS. Effect of Particle Size on the Flocculation Behaviour of Ultra-Fine Clays in Salt Solutions. Clay Miner 1998;33:103–7. https://doi.org/10.1180/claymin.1998.033.1.10.

Kotlyar LS, Deslandes Y, Sparks BD, Kodama H, Schutte R. Characterization of colloidal

solids from Athabasca fine tails. Clays Clay Miner 1993;41:341–5. https://doi.org/10.1346/CCMN.1993.0410309.

Kotylar LS, Sparks BD, Schutte R. Effect of salt on the flocculation behavior of nano particles in oil sands fine tailings. Clays Clay Miner 1996;44:121–31. https://doi.org/10.1346/CCMN.1996.0440111.

Schoonheydt RA, Johnston CT. Chapter 3 Surface and Interface Chemistry of Clay Minerals. Handb. Clay Sci. Clay Sci., vol. 1, 2006, p. 87–113. https://doi.org/10.1016/S1572-4352(05)01003-2.

Many CM. Chapter 15 - trioctahedral 1:1 clay minerals. Chem. Clay Miner., 1962, p. 159–67.

Brigatti MF, Galan E, Theng BKG. Chapter 2 Structures and Mineralogy of Clay Minerals. Handb. Clay Sci., vol. 1, 2006, p. 19–86. https://doi.org/10.1016/S1572-4352(05)01002-0.

Środoń J. Chapter 12.2 Identification and Quantitative Analysis of Clay Minerals. Handb. Clay Sci. Clay Sci., vol. 1, 2006, p. 765–87. https://doi.org/10.1016/S1572-4352(05)01028-7.

Geramian M, Osacky M, Ivey DG, Liu Q, Etsell TH. Effect of Swelling Clay Minerals (Montmorillonite and Illite-Smectite) on Nonaqueous Bitumen Extraction from Alberta Oil Sands. Energy and Fuels 2016;30:8083–90. https://doi.org/10.1021/acs.energyfuels.6b01026.

Pham Thi，Hang, G. W. Brindley. Methylene Blue Absorption by Montmorillonites. Determinations of Surface Areas and Exchange Capacities with Different Initial Cation Saturations (Clay-Organic Studies XIX). Isr J Chem 1970;8:409–15. https://doi.org/10.1002/ijch.197000047.

Chen Q, Liu Q. Bitumen Coating on Oil Sands Clay Minerals: A Review. Energy and Fuels 2019;33:5933–43. https://doi.org/10.1021/acs.energyfuels.9b00852.

Kuh SE, Kim DS. Effects of surface chemical and electrochemical factors on the dewatering characteristics of fine particle slurry. J Environ Sci Heal - Part A Toxic/Hazardous Subst Environ Eng 2004;39:2157–82. https://doi.org/10.1081/ESE-120039382.

Senft D, Masala S, Nik Klohn Crippen Berger R, Scott Martens C, Esposito G, Eaton T. Comparison of particle size distributions obtained by laser diffraction and sieve-hydrometer methods for oil sand tailings. Geotech. Conf., 2011.

Beier N, Wilson W, Dunmola A, Sego D. Impact of flocculation-based dewatering on the shear strength of oil sands fine tailings. Can Geotech J 2013;50:1001–7. https://doi.org/10.1139/cgj-2012-0262.

Kaminsky H, Etsell T, Ivey DG, Omotoso O. Fundamental particle size of clay minerals in athabasca oil sands tailings. Clay Sci 2006;12:217–22. https://doi.org/10.11362/jcssjclayscience1960.

Kotlyar LS, Sparks BD, Woods J, Capes CE, Schutte R. Biwetted ultrafine solids and structure formation in oil sands fine tailings. Fuel 1995;74:1146–9. https://doi.org/10.1016/0016-2361(95)00064-C.

Tu Y, O'Carroll JB, Kotlyar LS, Sparks BD, Ng S, Chung KH, et al. Recovery of bitumen from oilsands: gelation of ultra-fine clay in the primary separation vessel. Fuel 2005;84:653–60. https://doi.org/10.1016/J.FUEL.2004.03.020.

Majid A, Argue S, Boyko V, Pleizier G, L'Ecuyer P, Tunney J, et al. Characterization of sol-

gel-derived nano-particles separated from oil sands fine tailings. Colloids Surfaces A Physicochem Eng Asp 2003;224:33–44. https://doi.org/10.1016/S0927-7757(03)00266-8.

Mercier PHJ, Patarachao B, Kung J, Kingston DM, Woods JR, Sparks BD, et al. X-ray Diffraction (XRD)-Derived Processability Markers for Oil Sands Based on Clay Mineralogy and Crystallite Thickness Distributions. Energy and Fuels 2008;22:3174–93. https://doi.org/10.1021/EF8002203.

Murray H. Structure and composition of the clay minerals and their physical and chemical. Clay Miner., 1997, p. 7–31.

Omotoso OE, Mikula RJ. High surface areas caused by smectitic interstratification of kaolinite and illite in Athabasca oil sands. Appl Clay Sci 2004;25:37–47. https://doi.org/10.1016/j.clay.2003.08.002.

Rao SR. Flocculation and dewatering of Alberta oil sands tailings. Int J Miner Process 1980;7:245–53. https://doi.org/10.1016/0301-7516(80)90020-4.

Liu J, Xu Z, Masliyah J. Role of fine clays in bitumen extraction from oil sands. AIChE J 2004;50:1917–27. https://doi.org/10.1002/aic.10174.

Osacky M, Geramian M, Liu Q, Ivey DG, Etsell TH. Surface properties of petrologic end-members from alberta oil sands and their relationship with mineralogical and chemical composition. Energy and Fuels 2014;28:934–44. https://doi.org/10.1021/ef402150z.

Basnayaka L, Subasinghe N, Albijanic B. Influence of clays on fine particle filtration. Appl Clay Sci 2018;156:45–52. https://doi.org/10.1016/J.CLAY.2018.01.008.

Ottley DJ. Gravity Concentration In Modern Mineral Processing. 1986.

https://doi.org/10.1007/978-94-009-4476-3_11.

Wright HJL, Kitchener JA. The problem of dewatering clay slurries: Factors controlling filtrability. J Colloid Interface Sci 1976;56:57–63. https://doi.org/10.1016/0021-9797(76)90146-6.

D.R.， Nagaraj, P.， Somasundaran, L.， McAllister. Subsidence of suspensions of phosphatic slime and its major constituents. Int J Miner Process 1977;4:111–29. https://doi.org/https://doi.org/10.1016/0301-7516(77)90020-5.

J.V.， O'Gorman, J.A.， Kitchener. The flocculation and de-watering of kimberlite clay slimes. Int J Miner Process 1974;1:33–49. https://doi.org/https://doi.org/10.1016/0301-7516(74)90025-8.

Camp FW. Processing athabasca tar sands — tailings disposal. Can J Chem Eng 1977;55:581–91. https://doi.org/10.1002/cjce.5450550516.

Kessick MA. Structure and properties of oil sands clay tailings. J Can Pet Technol 1979:49–52. https://doi.org/10.2118/79-01-01.

Sworska A, Laskowski JS, Cymerman G. Flocculation of the Syncrude fine tailings Part I. Effect of pH, polymer dosage and Mg2+ and Ca2+ cations. Int J Miner Process 2000;60:143–52. https://doi.org/10.1016/S0301-7516(00)00012-0.

Babu DR, Cormack DE. Effect of low-temperature oxidation on the composition of Athabasca bitumen. Fuel 1984;63:858–61. https://doi.org/10.1016/0016-2361(84)90080-2.

Meyer R. The Petroleum System- Status of Research and Methods. 2003.

Gray MR. Upgrading oilsands bitumen and heavy oil. 2015.

Adams JJ. Asphaltene adsorption, a literature review. Energy and Fuels 2014;28:2831–56. https://doi.org/10.1021/ef500282p.

Gray MR, Jokuty P, Yeniova H, Nazarewycz L, Wanke SE, Achia U, et al. The relationship between chemical structure and reactivity of alberta bitumens and heavy oils. Can J Chem Eng 1991;69:833–43. https://doi.org/10.1002/CJCE.5450690404.

Gray MR, Tykwinski RR, Stryker JM, Tan X. Supramolecular assembly model for aggregation of petroleum asphaltenes. Energy and Fuels 2011;25:3125–34. https://doi.org/10.1021/ef200654p.

Pernyeszi T, Patzkó Á, Berkesi O, Dékány I. Asphaltene adsorption on clays and crude oil reservoir rocks. Colloids Surfaces A Physicochem Eng Asp 1998;137:373–84. https://doi.org/10.1016/S0927-7757(98)00214-3.

Bensebaa F, Kotlyar LS, Sparks BD, Chung KH. Organic coated solids in Athabasca bitumen: Characterization and process implications. Can J Chem Eng 2000;78:610–6. https://doi.org/10.1002/cjce.5450780402.

Chen Q, Liu J, Thundat T, Gray MR, Liu Q. Spatially resolved organic coating on clay minerals in bitumen froth revealed by atomic force microscopy adhesion mapping. Fuel 2017;191:283–9. https://doi.org/10.1016/j.fuel.2016.11.091.

Kotlyar LS, Ripmeester JA, Sparks BD, Montgomery DS. Characterization of oil sands solids closely associated with Athabasca bitumen. Fuel 1988;67:808–14. https://doi.org/10.1016/0016-2361(88)90155-X.

Zhou J, Li H, Zhao L, Chow R. Role of Mineral Flotation Technology in Improving Bitumen

Extraction from Mined Athabasca Oil Sands: I. Flotation Chemistry of Water-Based Oil Sand Extraction †. Can J Chem Eng 2018;96:1986–99. https://doi.org/10.1002/cjce.23139.

Xiaoli Tan QL. Two-stage chemicals treatment for tailings slurry dewatering. Final Proj Rep 2016.

Scott J., Dusseault MB, Carrier WD. Behaviour of the clay/bitumen/water sludge system from oil sands extraction plants. Appl Clay Sci 1985;1:207–18. https://doi.org/10.1016/0169-1317(85)90574-5.

Azizov I, Dudek M, Øye G. Studying droplet retention in porous media by novel microfluidic methods. Chem Eng Sci 2022;248:117152. https://doi.org/10.1016/J.CES.2021.117152.

Klein C, Harbottle D, Alagha L, Xu Z. Impact of fugitive bitumen on polymer-based flocculation of mature fine tailings. Can J Chem Eng 2013;91:1427–32. https://doi.org/10.1002/cjce.21863.

Suthaker NN, Scott. JD. Measurement of hydraulic conductivity in petroleum sand tailings slurries. Can Geotech J 1996;33:642–53.

Chalaturnyk RJ, Scott JD, Özüm B. Management of oil sands tailings. Pet Sci Technol 2002;20:1025–46. https://doi.org/10.1081/LFT-120003695.

Li H, Zhou J, Chow R, Adegoroye A, Najafi AS. Enhancing treatment and geotechnical stability of oil sands fine tailings using thermo-sensitive poly(n-isopropyl acrylamide). Can J Chem Eng 2015;93:1780–6. https://doi.org/10.1002/CJCE.22276.

Reis LG, Oliveira RS, Palhares TN, Spinelli LS, Lucas EF, Vedoy DRL, et al. Using

acrylamide/propylene oxide copolymers to dewater and densify mature fine tailings. Miner Eng 2016;95:29–39. https://doi.org/10.1016/j.mineng.2016.06.005.

Vajihinejad V, Guillermo R, Soares JBP. Dewatering Oil Sands Mature Fine Tailings (MFTs) with Poly(acrylamide-co-diallyldimethylammonium chloride): Effect of Average Molecular Weight and Copolymer Composition. Ind Eng Chem Res 2017;56:1256–66. https://doi.org/10.1021/acs.iecr.6b04348.

Gumfekar SP, Vajihinejad V, Soares JBP. Advanced Polymer Flocculants for Solid–Liquid Separation in Oil Sands Tailings. Macromol Rapid Commun 2019;40:1–18. https://doi.org/10.1002/marc.201800644.

Kotlyar LS, Sparks BD, Woods JR, Raymond S, Le Page Y, Shelfantook W. Distribution and types of solids associated with bitumen. Pet Sci Technol 1998;16:1–19. https://doi.org/10.1080/10916469808949769.

Zhu Y. Cationic and Anionic Dual Polymer Pairs for Mature Fine Tailings Flocculation and Dewatering 2015.

Loerke RS. Pressure Filtration of Mature Fine Tailings. University of Alberta, 2016.

Salou M, Si B, Jada A. Study of the stability of bitumen emulsions by application of DLVO theory 1998;142:9–16.

Darcovich K, Kotlyar LS, Tse WC, Ripmeester JA, Capes CE, Sparks BD. Wettability Study of Organic-Rich Solids Separated from Athabasca Oil Sands. Energy and Fuels 1989;3:386–91. https://doi.org/10.1021/ef00015a023.

Ivanova NO, Xu Z, Liu Q, Masliyah JH. Surface forces in unconventional oil processing.

Curr Opin Colloid Interface Sci 2017;27:63–73. https://doi.org/10.1016/j.cocis.2016.09.013.

Sendner C, Horinek D, Bocquet L, Netz RR. Interfacial Water at Hydrophobic and Hydrophilic Surfaces : Slip , Viscosity , and Diffusion 2009;25:10768–81. https://doi.org/10.1021/la901314b.

Fleys M. Water behavior in hydrophobic porous materials. Comparison between Silicalite and Dealuminated zeolite Y by Molecular Dynamic Simulations. Worcester Polytechnic Institute, 2003.

Hripko R, Vajihinejad V, LopesMotta F, Soares JBP. Enhanced Flocculation of Oil Sands Mature Fine Tailings Using Hydrophobically Modified Polyacrylamide Copolymers. Glob Challenges 2018;2:1700135. https://doi.org/10.1002/gch2.201700135.

Zhang D, Thundat T, Narain R. Flocculation and dewatering of mature fine tailings using temperature-responsive cationic polymers. Langmuir 2017;33:5900–9. https://doi.org/10.1021/acs.langmuir.7b01160.

Gumfekar SP, Rooney TR, Hutchinson RA, Soares JBP. Dewatering Oil Sands Tailings with Degradable Polymer Flocculants. ACS Appl Mater Interfaces 2017;9:36290–300. https://doi.org/10.1021/acsami.7b10302.

Younes GR, Proper AR, Rooney TR, Hutchinson RA, Gumfekar SP, Soares JBP. Structure Modifications of Hydrolytically-Degradable Polymer Flocculant for Improved Water Recovery from Mature Fine Tailings. Ind Eng Chem Res 2018;57:10809–22. https://doi.org/10.1021/acs.iecr.8b02783.

Chen Q. Organically-Modified Clay Minerals in Oil Sands: Characterization and Effect of

Hydrothermal Treatment. University of Alberta, 2017.

Condie DJ, Veal CJ. Modeling the Vacuum Filtration of Fine Coal : Part 2. Filtaration&Separation 1997;2:957–63.

Clarke TP. Oil sands hot water extraction process. US 4240897, 1980. https://doi.org/https://www.osti.gov/biblio/6555796.

Avagyan AB. Environmental building policy by the use of microalgae and decreasing of risks for Canadian oil sand sector development. Environ Sci Pollut Res 2017;24:20241–53. https://doi.org/10.1007/s11356-017-9864-x.

Farrow JB, Johnston RRM, Simic K, Swift JD. Consolidation and aggregate densification during gravity thickening. Chem Eng J 2000;80:141–8. https://doi.org/10.1016/S1383-5866(00)00083-6.

Liu D, Edraki M, Berry L. Investigating the settling behaviour of saline tailing suspensions using kaolinite, bentonite, and illite clay minerals. Powder Technol 2018;326:228–36. https://doi.org/10.1016/J.POWTEC.2017.11.070.

Mikula RJ, Kasperski KL, Burns RD, MacKinnon MD. Nature and fate of oil sands fine tailings. Suspens Fundam Appl Pet Ind 1996;251:677–723.

Li Y, Chen Y, Xia W, Xie G. Filtration of kaolinite and coal mixture suspension: Settling behavior and filter cake structure analysis. Powder Technol 2021;381:122–8. https://doi.org/10.1016/J.POWTEC.2020.12.050.

Liu D, Edraki M, Fawell P, Berry L. Improved water recovery: A review of clay-rich tailings and saline water interactions. Powder Technol 2020;364:604–21.

https://doi.org/10.1016/J.POWTEC.2020.01.039.

Sabah E, Yüzer H, Çelik MS. Characterization and dewatering of fine coal tailings by dual-flocculant systems. Int J Miner Process 2004;74:303–15. https://doi.org/10.1016/J.MINPRO.2004.03.001.

Onuaguluchi O, Eren Ö. Recycling of copper tailings as an additive in cement mortars. Constr Build Mater 2012;37:723–7. https://doi.org/10.1016/J.CONBUILDMAT.2012.08.009.

Adeyinka OB, Samiei S, Xu Z, Masliyah JH. Effect of particle size on the rheology of athabasca clay suspensions. Can J Chem Eng 2009;87:422–34. https://doi.org/10.1002/cjce.20168.

Majid A, Ripmeester JA. Characterization of unextractable organic matter associated with heavy minerals from oil sand. Fuel 1986;65:1714–27. https://doi.org/10.1016/0016-2361(86)90275-9.

Besra L, Sengupta DK, Roy SK. Particle characteristics and their influence on dewatering of kaolin, calcite and quartz suspensions. Int J Miner Process 2000;59:89–112. https://doi.org/10.1016/S0301-7516(99)00065-4.

Forbes E, Chryss A. Fundamentals of clays: Surface and colloid science, and rheology. Clays Miner. Process. Value Chain, 2017, p. 81–110. https://doi.org/10.1017/9781316661888.004.

Bleam WF. Clay Mineralogy and Clay Chemistry. Soil Environ. Chem., 2012, p. 85–116. https://doi.org/10.1016/b978-0-12-415797-2.00003-0.

Madsen FT, Muller-vonmoos MAX. The Swelling Behaviour of Clays. Appl Clay Sci

1989;4:143–56. https://doi.org/https://doi.org/10.1016/0169-1317(89)90005-7.

Osacky M, Geramian M, Ivey DG, Liu Q, Etsell TH. Influence of nonswelling clay minerals (illite, kaolinite, and chlorite) on nonaqueous solvent extraction of bitumen. Energy and Fuels 2015;29:4150–9. https://doi.org/10.1021/acs.energyfuels.5b00269.

Eberl DD, Velde B. Beyond the Kubler Index. Clay Miner 1989;24:571–7. https://doi.org/10.1180/claymin.1989.024.4.01.

Kahr G, Madsen FT. Determination of the cation exchange capacity and the surface area of bentonite, illite and kaolinite by methylene blue adsorption. Appl Clay Sci 1995;9:327–36. https://doi.org/10.1016/0169-1317(94)00028-O.

Chen Q, Stricek I, Gray MR, Liu Q. Interface Science Influence of hydrophobicity distribution of particle mixtures on emulsion stabilization. J Colloid Interface Sci 2017;491:179–89. https://doi.org/10.1016/j.jcis.2016.12.045.

Bergaya F, Lagaly G, Vayer M. CATION AND ANION EXCHANGE. Handb. Clay Sci., vol. 1, 2006, p. 979–1001. https://doi.org/10.1016/S1572-4352(05)01036-6.

Foster MD. The relation between composition and swelling in clays. Clays Clay Miner 1954;3:205–20. https://doi.org/10.1346/ccmn.1954.0030117.

Dolinar B, Macuh B. Determining the thickness of adsorbed water layers on the external surfaces of clay minerals based on the engineering properties of soils. Appl Clay Sci 2016;123:279–84. https://doi.org/10.1016/J.CLAY.2015.12.029.

Lim HM, Misni M. Colloidal and rheological properties of natural rubber latex concentrate. Appl Rheol 2016;26:1–10. https://doi.org/10.3933/ApplRheol-26-15659.

Liang H, Guan D, Yang L, Zhang L, Song Y, Zhao J. Multi-scale characterization of shell thickness and effective volume fraction during gas hydrates formation: A kinetic study. Chem Eng J 2021;424:130360. https://doi.org/10.1016/J.CEJ.2021.130360.

Prestidge C, Tadros TF. Viscoelastic properties of aqueous concentrated polystyrene latex dispersions containing grafted poly(ethylene oxide) chains. J Colloid Interface Sci 1988;124:660–5. https://doi.org/10.1016/0021-9797(88)90204-4.

Doroszkowski A. The physical chemistry of dispersion. Second Edi. Woodhead Publishing Ltd; 1999. https://doi.org/10.1533/9781855737006.198.

Siddique T, Kuznetsov P, Kuznetsova A, Arkell N, Young R, Li C, et al. Microbially-accelerated consolidation of oil sands tailings. Pathway I: Changes in porewater chemistry. Front Microbiol 2014;5:1–11. https://doi.org/10.3389/fmicb.2014.00106.

Bendou S, Amrani M. Effect of hydrochloric acid on the structural of sodic-bentonite clay. J Miner Mater Charact Eng 2014;02:404–13. https://doi.org/10.4236/jmmce.2014.25045.

COSIA. Technical Guide for Fluid Fine Tailings Management. 2012. https://doi.org/https://cosia.ca/uploads/documents/id7/TechGuideFluidTailingsMgmt_Aug2012.pdf.

COSIA. Innovative Solutions for Sustainable Oil. 2020. https://doi.org/https://cosia.ca/sites/default/files/2021-06/2020COSIA_AnnualReport.pdf.

Alam N, Ozdemir O, Hampton MA, Nguyen A V. Dewatering of coal plant tailings: Flocculation followed by filtration. Fuel 2011;90:26–35. https://doi.org/10.1016/J.FUEL.2010.08.006.

Xu Y, Dabros T, Kan J. Filterability of oil sands tailings. Process Saf Environ Prot 2008;86:268–76. https://doi.org/10.1016/j.psep.2008.04.005.

Mercier PHJ, Ng S, Moran K, Sparks BD, Kingston D, Kotlyar LS, et al. Colloidal Clay Gelation: Relevance to Current Oil Sands Operations. Pet Sci Technol 2012;30:915–23. https://doi.org/10.1080/10916466.2010.495959.

Kotylar LS, Sparks BD, Schutfe R. Effect of Salt on the Floculation Behavior of Nano Particles in Oil Sands Fine Tailings 1996;44:121–31. https://doi.org/10.1346/CCMN.1996.0440111.

Loeber L, Muller G, Morel J, Sutton O. Bitumen in colloid science: a chemical, structural and rheological approach. Fuel 1998;77:1443–50. https://doi.org/10.1016/S0016-2361(98)00054-4.

Chalaturnyk RJ, Scott JD, Özüm B. Management of oil sands tailings. Pet Sci Technol 2002;20:1025–46. https://doi.org/10.1081/LFT-120003695.

Guzma J, Isquierdo F, Carbognani L, Vitale G, Scott CE, Pereira-almao P. X-ray Photoelectron Spectroscopy Analysis of Hydrotreated Athabasca Asphaltenes. Energy & Fuels 2017;31:10706–17.

Baillie RA, Malmberg EW. Removal of clay from the water streams of the hotwater process by flocculation. 3,487,003, 1969.

Xu K, Zhu P, Huh C, Balhoff MT. Microfluidic Investigation of Nanoparticles Role in Mobilizing Trapped Oil Droplets in Porous Media. Langmuir 2015;31:13673–9. https://doi.org/10.1021/acs.langmuir.5b03733.

Majid A, Sparks BD. Role of hydrophobic solids in the stability of oil sands fine tailings. Fuel 1996;75:879–84. https://doi.org/10.1016/0016-2361(96)00015-4.

Pendharker S, Shende S, Jacob Z, Nazemifard N. Three-dimensional optical tomography of bitumen and clay association in oil sands tailings. Fuel 2017;207:262–7. https://doi.org/10.1016/J.FUEL.2017.06.107.

Liu J, Wang J, Huang J, Cui X, Tan X, Liu Q, et al. Heterogeneous Distribution of Adsorbed Bitumen on Fine Solids from Solvent-Based Extraction of Oil Sands Probed by AFM 2017. https://doi.org/10.1021/acs.energyfuels.7b00396.

Liu J, Zhou Z, Xu Z, Masliyah J. Bitumen-clay interactions in aqueous media studied by zeta potential distribution measurement. J Colloid Interface Sci 2002;252:409–18. https://doi.org/10.1006/jcis.2002.8471.

Wang D, Tao H, Wang K, Tan X, Liu Q. The filterability of different types of minerals and the role of swelling clays in the filtration of oil sands tailings. Fuel 2022;316:123395. https://doi.org/10.1016/J.FUEL.2022.123395.

Government of Alberta. Alberta Environment and Parks Oil Sands Information Portal 2021. http://osip.alberta.ca/map/ (accessed November 24, 2021).

Alberta Energy Regulation. Directive 085: Fluid Tailings Management for Oil Sands Mining Projects. 2017. https://doi.org/https://static.aer.ca/prd/documents/directives/Directive085.pdf.

Beier N, Wilson W, Dunmola A, Sego D. Impact of flocculation-based dewatering on the shear strength of oil sands fine tailings. Can Geotech J 2013;50:1001–7. https://doi.org/10.1139/cgj-2012-0262.

Amoah N. Large-Scale Tailings Filtration and Dry Stacking at Karara Magnetite Iron Ore Operation. Proc. Tailings Mine Waste 2019, Vancouver, BC: 2019, p. 15–32.

Moreno J, Kendall S, Ortiz A. Dewatering options for management of fine gold tailings in Western Australian Goldfields. Paste 2018 21st Int Semin Paste Thick Tailings, 2018 11-13 April Perth 2018:413–24. https://doi.org/10.36487/ACG_REP/1805_34_MORENO.

Leonida C. How to Make Filtered Tailings Feasible. Eng Min J 2020:1–10. https://doi.org/https://www.e-mj.com/features/how-to-make-filtered-tailings-feasible/.

Wang C, Harbottle D, Liu Q, Xu Z. Current state of fine mineral tailings treatment: A critical review on theory and practice. Miner Eng 2014;58:113–31. https://doi.org/10.1016/J.MINENG.2014.01.018.

Liu Q, Laskowsk JS. The role of metal hydroxide at inmeral surfaces in dextrin adsorption , I . studies on modified quartz samples. Int J Miner Process 1989;26:297–316. https://doi.org/https://doi.org/10.1016/0301-7516(89)90035-5.

Barry A. Hydrophobicity, Hydrophilicity and Silane Surface Modification. Gelest Inc 2011;Morrisvill.

McNamee CE, Tsujii Y, Ohshima H, Matsumoto M. Interaction Forces between Two Hard Surfaces in Particle-Containing Aqueous Systems. Langmuir 2004;20:1953–62. https://doi.org/10.1021/LA0357763.

McNamee CE, Tsujii Y, Ohshima H, Matsumoto M. Interaction forces between two silica surfaces in an apolar solvent containing an anionic surfactant. Langmuir 2004;20:1953–62.

Jouault N, Corvis Y, Cousin F, Jestin J, Le L. Asphaltene Adsorption Mechanisms on the

Local Scale Probed by Neutron Reflectivity : Transition from Monolayer to Multilayer Growth above the Flocculation Threshold † 2009:3991–8.

Nandiyanto ABD, Oktiani R, Ragadhita R. How to read and interpret FTIR spectroscope of organic material. Indones J Sci Technol 2019;4:97–118. https://doi.org/10.17509/ijost.v4i1.15806.

Madejová J. FTIR techniques in clay mineral studies. Vib Spectrosc 2003;31:1–10. https://doi.org/10.1016/S0924-2031(02)00065-6.

Oelichmann J. Surface and depth-profile analysis using FTIR spectroscopy. Fresenius Z Anal Chem 1989;333:353–9.

## Appendices

## Appendix A: Morphology of the Dried Mineral Suspension

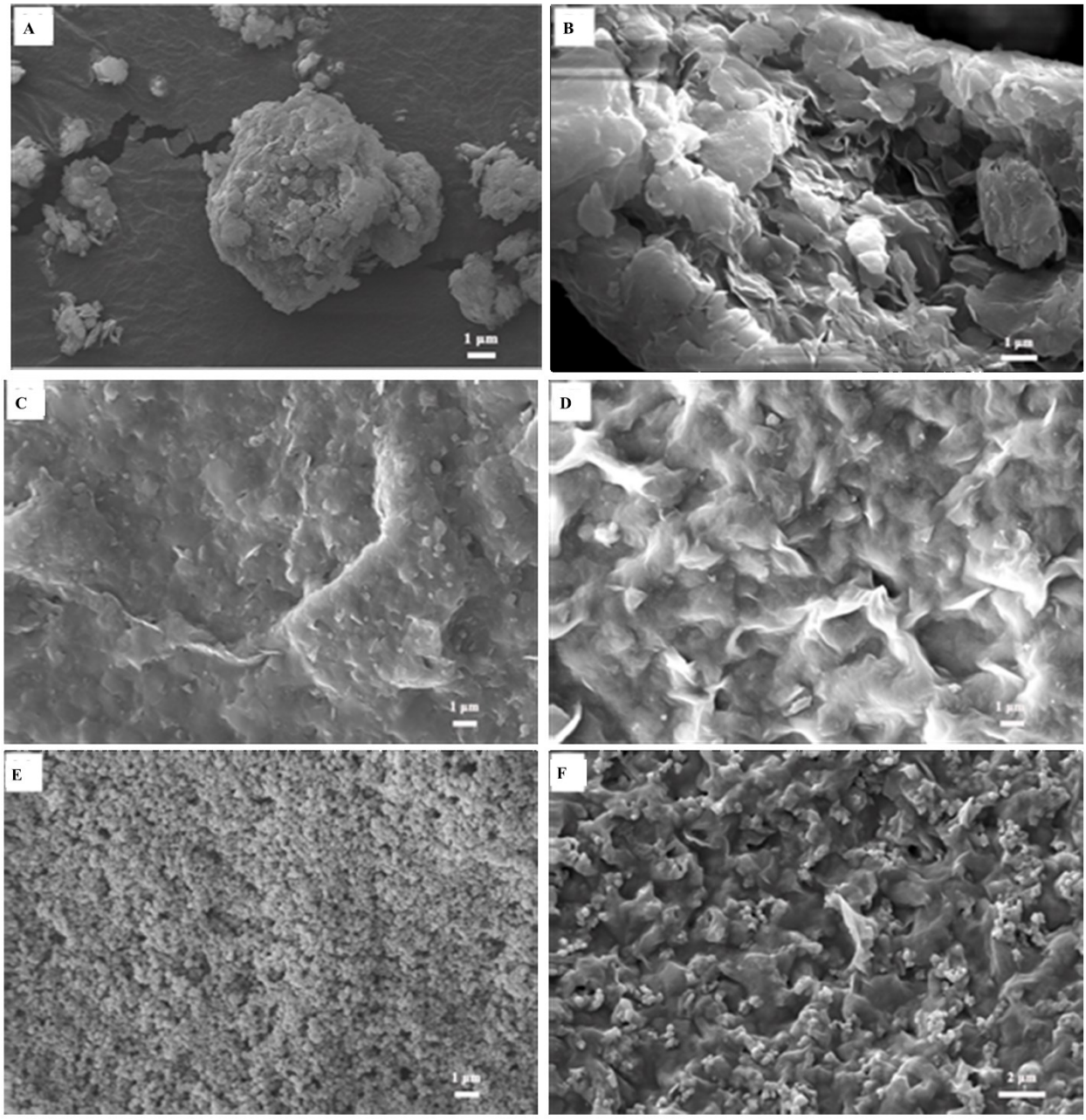

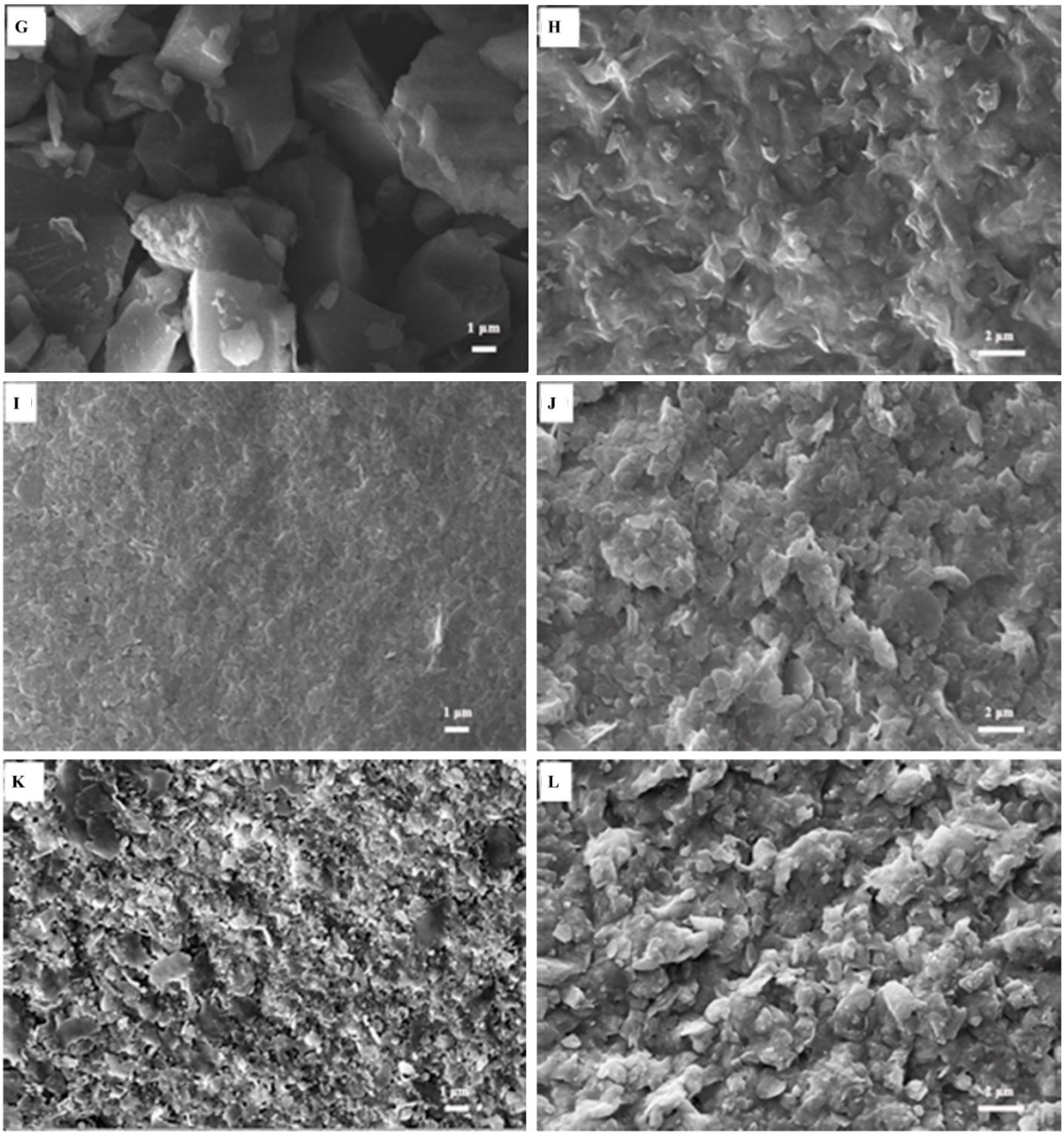


Figure 1. The SEM images of original dry (A) illite-smectite and (B) montmorillonite particles and dried suspensions of (C) illite-smectite, (D) montmorillonite, (E) rutile, (F) rutile mixed with montmorillonite, (G) quartz, (H) quartz mixed with montmorillonite, (I) kaolinite, (J) kaolinite mixed with montmorillonite, (K) illite, (L) illite mixed with montmorillonite. The samples for images (C) to (L) were prepared by mixing with water and then air-dryingin a

fume hood. Magnification: 5000x (except the orginal dry montmorillonite which was 7000x). All mineral mixtures were prepared at 3 parts montmorillonite and 7 parts other minerals.

The SEM images of the original dry illite-smectite and montmorillonite, and air-dried suspensions of minerals are shown in Figure 1. Figures 1A and 1B show the morphology of the original illite-smectite and montmorillonite, and Figure 1B and 1C show the mineral suspensions after air-drying (wetted mineral morphology) of illite-smectite and montmorillonite, respectively. As can be seen, the wetted illite-smectite and montmorillonite morphology were gel-like and formed a sealed structure that seemed impermeable to water. This sealed structure could explain why the montmorillonite was so difficult to filter. Figures 1E and 1F show the morphology of rutile alone (Figure 1E) and as a 7:3 mixture with montmorillonite (Figure 1F). As can be seen from Figure 1e, despite the small particle size, the rutile sample showed a honeycomb structure with apparent passageways for water. However, when rutile was mixed with montmorillonite (at a 7:3 weight ratio) and submerged in water, a sealed structure similar to montmorillonite was formed (Figure 1F). The 10 wt% solids mixture of rutile and montmorillonite, at a weight ratio of 7:3, had slightly higher IFR than the 3 wt% solids montmorillonite slurry. Considering that the 10 wt% solids rutile and montmorillonite mixture (7:3) slurry had the same montmorillonite concentration (i.e., 3 wt%), we speculate that the slightly better filtration of the mixture was due to the rutile particles that were dispersed in the gel-like montmorillonite to create passageways for water. Unlike rutile, quartz did not have a uniform spherical shape, and most quartz particles showed characteristic trapezohedral shape with large gaps (Figure 1G). Interestingly, even the trapezohedral quartz could be fully sealed by montmorillonite without any passageways for water at a weight ratio of 7:3, as shown in Figure 1h. Both the kaolinite and illite show a plate-like appearance in

water (Figures 1I and 1K). The kaolinite/montmorillonite and illite/montmorillonite mixtures (Figure 1J and 1L) were less gel-like compared to the pure montmorillonite (Figure 1D). However, the kaolinite and illite plates seemed to have been “glued” together more tightly by montmorillonite, so there were no passageways for water. This plate-like appearance was similar to the SEM images of the fine fractions in MFT [1].

Overall, the mixtures of mineral samples with montmorillonite showed similar gel-like structures and filterability as illite-smectite and montmorillonite, which could explain why montmorillonite could decrease the filterability of rutile, quartz, kaolinite, and illite dramatically. Correlating the SEM images with the filterability results, we can see again that particle size was not a primary factor to control the filterability of the mineral slurry, but the type of the mineral was. When swelling clays such as montmorillonite were present in the slurry, they would form a gel-like structure and seal the water passageways, making other mineral solids unfilterable.

## Appendix B: Fourier Transform Infrared Spectroscopy (FTIR) Spectra

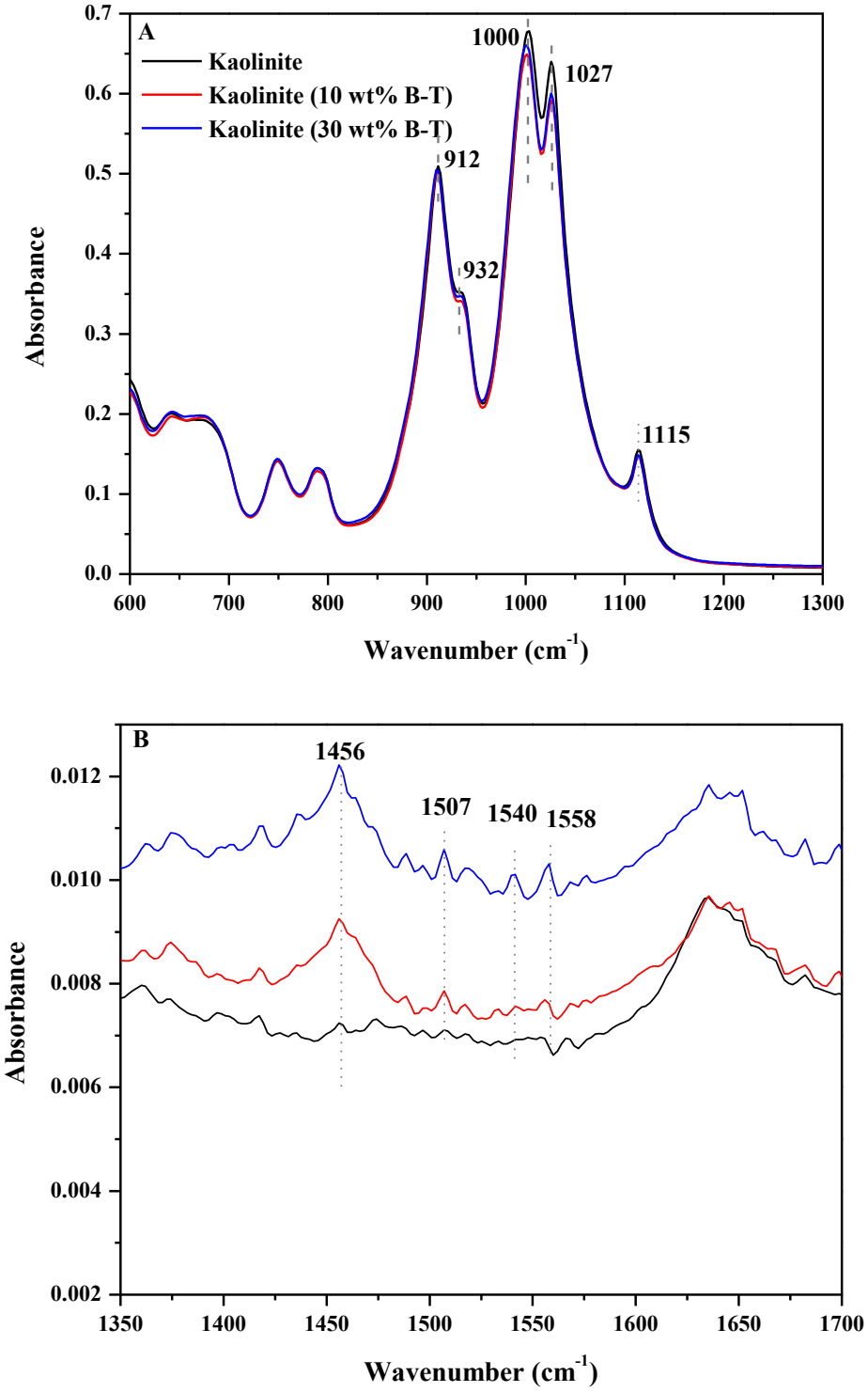

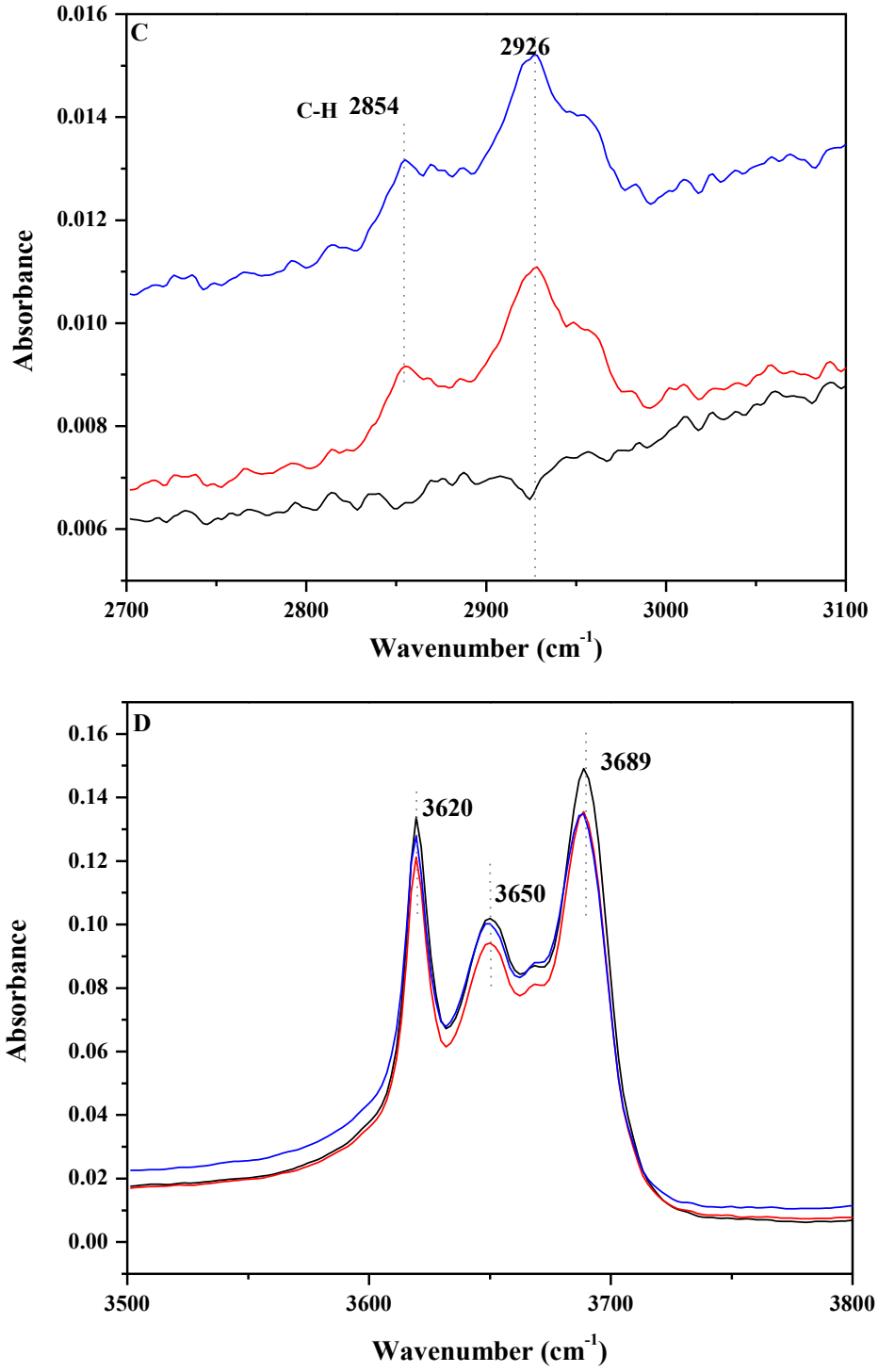


Figure 2. FTIR spectra (A) 600-1300 $cm^{-1}$, (B) 1350-1700 $cm^{-1}$ (C) 2700-3100 $cm^{-1}$, (D) 3500-3800 $cm^{-1}$ of kaolinite, kaolinite treated with 10 wt% and 30 wt% bitumen-toluene (B-T) solutions.

The FTIR spectra of kaolinite, kaolinite treated at 10 wt% and 30 wt% bitumen-in-toluene solutions are present in Figure 2 in the spectral range of 600-3800 $cm^{-1}$. The spectrum of kaolinite shows absorption bands at 3620 $cm^{-1}$ (Figure 2D) which was assigned to the inner OH groups between the tetrahedral and octahedral sheets [2] tied to Al site. The absorption bands at 3689 $cm^{-1}$ and 3650 $cm^{-1}$ (Figute 2D) which represent the OH in-phase symmetric and out-of-plane stretching vibration, are attributed to the hydrogen bonds with the oxygen of the Si-O-Si bonds [3]. The absorption bands observed at 912 $cm^{-1}$ and 932 $cm^{-1}$ (Figure 2A) are assigned to the bending vibrations of inner and inner-surface OH groups, respectively, and the most intensive bands at 1000 and 1027 $cm^{-1}$ (Figure 2A) were attributed to the Si-O stretching in the tetrahedral sheets [4–6]. The characteristic bands of kaolinite were also detected in the bitumen treated kaolinite samples, indicating that the kaolinite surface was not fully covered with bitumen, and there were "bare" kaolinite surfaces for both 10 wt% and 30 wt% bitumen-in-toluene treated kaolinite. Furthermore, the FTIR spectrum of kaolinite treated with 30 wt% bitumen-in-toluene solution showed lower absorption intensity than the 10 wt% bitumen-in-toluene treated kaolinite at 3689 $cm^{-1}$ (Figure 2D), 1000 $cm^{-1}$ and 1027 $cm^{-1}$ (Figure 2A). This was taken to indicate that the 30 wt% bitumen treated kaolinite had thicker bitumen coating and/or more surface bitumen coverage than the 10 wt% bitumen treated kaolinite sample.

The spectra of bitumen adsorbed on the kaolinite surface can be observed in Figures 2B and C. The two absorption bands at 2854 $cm^{-1}$ and 2926 $cm^{-1}$ (Figure 2C) were due to the asymmetric and symmetric stretches of C–H in methyl, methylene and methyne, and the bending vibration of the same groups are found at 1456 $cm^{-1}$ [2] (Figure 2B). It can be seen that the relative intensity of C-H peaks for different bitumen concentrations was almost the same. Therefore, it is possible that the bitumen interacted with the kaolinite layer by layer. And even with 30 wt%

bitumen solution treatment, the bitumen was not evenly spread over the entire surface but coated on the surface in discrete patches. So the decreased absorbance at 3689 $cm^{-1}$ for 30 wt% bitumen-in-toluene solution treated kaolinite was possibly due to the thicker bitumen layer than the 10 wt% treated one.

## Appendix C: Scanning Electron Microscopy (SEM) with Energy Dispersive X-Ray (EDX)

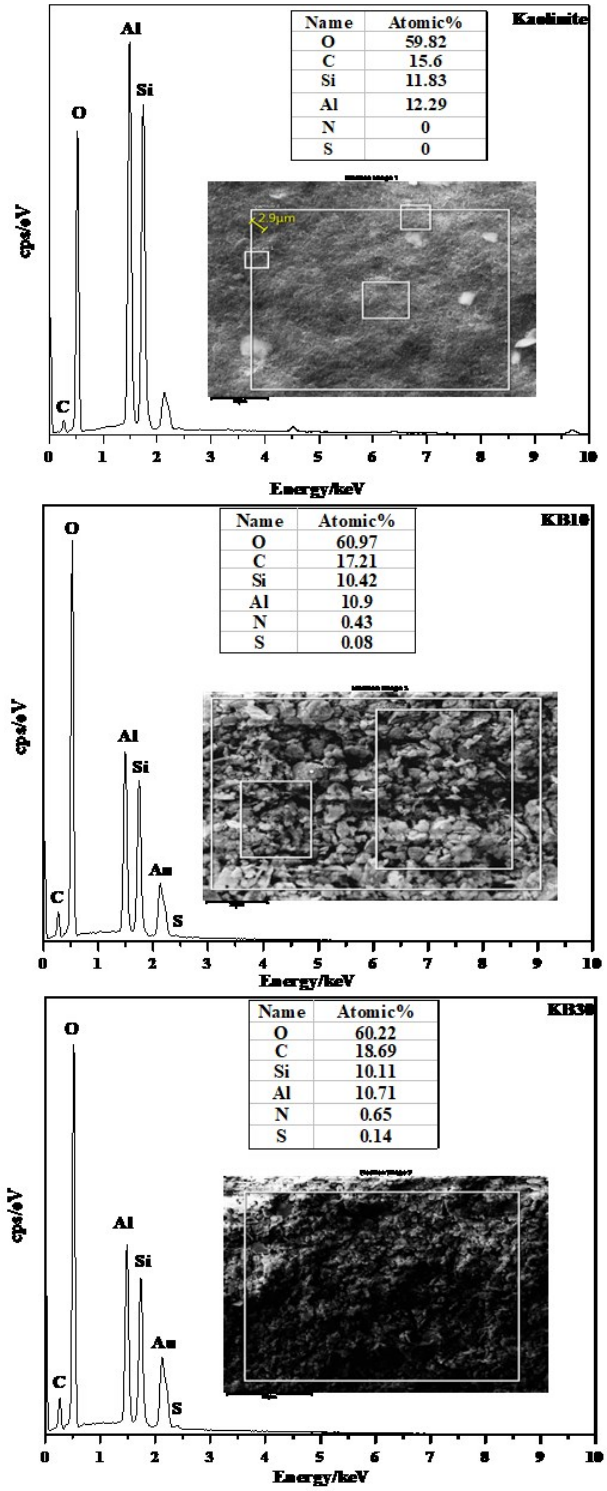


Figure 3. EDX spectra and atomic concentration of (a) kaolinite, kaolinite treated with (b) 10 wt% and (c) 30 wt% bitumen-toluene solution.

The bitumen-coating treated kaolinite had higher oxygen and carbon contents, and lower silicon and aluminum contents than the untreated kaolinite. As well as that the 30 wt% bitumen-treated kaolinite was detected with more carbon, nitrogen, sulfur than the 10 wt% bitumen-treated one. It was possible because the thick bitumen-coated layer and/or more kaolinite surface was covered with bitumen for the 30 wt% treated one.

**References**


[1] Adeyinka OB, Samiei S, Xu Z, Masliyah JH. Effect of particle size on the rheology of athabasca clay suspensions. Can J Chem Eng 2009;87:422–34. https://doi.org/10.1002/cjce.20168.

[2] Nandiyanto ABD, Oktiani R, Ragadhita R. How to read and interpret FTIR spectroscope of organic material. Indones J Sci Technol 2019;4:97–118. https://doi.org/10.17509/ijost.v4i1.15806.

[3] Madejová J. FTIR techniques in clay mineral studies. Vib Spectrosc 2003;31:1–10. https://doi.org/10.1016/S0924-2031(02)00065-6.

[4] Osacky M, Geramian M, Ivey DG, Liu Q, Etsell TH. Mineralogical and chemical composition of petrologic end members of Alberta oil sands. Fuel 2013;113:148–57. https://doi.org/10.1016/j.fuel.2013.05.099.

[5] Bendou S, Amrani M. Effect of hydrochloric acid on the structural of sodic-bentonite clay. J Miner Mater Charact Eng 2014;02:404–13. https://doi.org/10.4236/jmmce.2014.25045.

[6] Oelichmann J. Surface and depth-profile analysis using FTIR spectroscopy. Fresenius Z Anal Chem 1989;333:353–9.